Data Fusion for Ground Target Tracking in GSM Networks

Vom Fachbereich Elektrotechnik und Informatik der
Universität Siegen
zur Erlangung des akademischen Grades

Doktor der Ingenieurwissenschaften
(**Dr.-Ing.**)

genehmigte Dissertation

von

M.E. Miao Zhang

1. Gutachter: Prof. Dr.-Ing. habil. O. Loffeld
2. Gutachter: Prof. Dr. rer. nat. C. Ruland
Vorsitzender: Prof. Dr. H. Bessai

Tag der mündlichen Prüfung: 7.12.2010

Acknowledgments

I would like to take this opportunity to express my sincere gratitude to all the people who have supported and encouraged me during my Ph.D. study.

My first thank goes to Prof. Dr.-Ing. habil. Otmar Loffeld for supervising me in this thesis work. He encouraged me to pursue my ideas and supported me with valuable discussions. His comprehensive knowledge and experience in estimation theory was very insightful for me. I am specially grateful to Dr.-Ing. Stefan Knedlik, the team leader of my research group. From him I learned how to write academic documents and how to present my work. He supported me to attend a variety of conferences in my field to present my work and discuss with professional people. Moreover, he also helped me a lot in applying for scholarships. His suggestions of not only the work but also the other matters are very useful. I also want to thank Prof. Dr. rer. nat. Christoph Ruland, an expert in communication, for being my second supervisor. The discussion with him helped me in understanding the communication field.

I would like to thank my colleagues, Pakorn Ubolkosold, Gustave Franck Tchere, Seyed Eghbal Ghobadi, Jinshan Ding, Zhen Dai, Junchuan Zhou, and Ezzaldeen Edwan. Their encouragement and attention to me have supported me and helped me with various issues. My thanks also go to other colleagues in the Center for Sensor Systems (ZESS), University of Siegen. The secretaries, Silvia Niet-Wunram, Renate Szabó, Ira Dexling and Katharina Haut, were always friendly and patient to help me to solve problems. Amaya Medrano Ortiz was very passionate to organize activities and help us. The members in the navigation group have shared a lot of knowledge and experience in the field of navigation with me. Other nice colleagues have given me a lot of valuable assistances in various ways.

Finally, I want to thank my parents for firmly supporting me in these years. Their unconditional love and support has been a great source of inspiration to me.

Kurzfassung

Die Ortung in Mobilfunknetzen ist ein faszinierendes Forschungsgebiet. Der in großem Umfang genutzte Mobilfunkstandard für digitale Netze Global System for Mobile communications (GSM) kann auch zur Positionsbestimmung erfolgreich eingesetzt werden. Eine der bedeutenden Anwendungen bezüglich der Ortung von Mobilstationen (MS), d.h. von Mobilfunkendgeräten, ist das sogenannte Ground-Target-Tracking, also die Zielverfolgung derselben. Im Falle eines GSM-basierten Ortungssystems, das auf den aktuellen GSM-Spezifikationen basiert, müssen viele Schwierigkeiten überwunden werden, um die Position genau schätzen zu können. Zum einen liegen - da die Signale im Wesentlichen unter Berücksichtigung der Anforderungen hinsichtlich der Kommunikation (und nicht der Ortung) entworfen wurden - die Ergebnisse der Ortung in GSM-Netzwerken nur in einer groben Auflösung vor, und im Falle einer nicht ausreichend hohen Anzahl von verfügbaren Messwerten treten Mehrdeutigkeiten bei der Positionsschätzung auf. Zum anderen führt das Ziel entsprechend dem Gelände, dem Straßenverlauf und dem Verkehr oft Bewegungsänderungen durch. In dieser Arbeit werden deshalb Datenfusionsansätze verfolgt, die redundante Messwerte aus verschiedenen Quellen berücksichtigen, um eine verbesserte Genauigkeit der Positionsschätzung zu erzielen.

Im Mittelpunkt der Arbeit steht die Zustandsschätzung unter Berücksichtigung der Messwerte aus dem GSM-Netzwerk und von a priori Information zum Straßenverlauf. Es wird ein Datenfusionsansatz eingeführt, mit dem die Fusion der Messwerte aus den Verfahren Time-of-Arrival (TOA) und Received-Signal-Strength (RSS) möglich wird, um einen verbesserten Positionsschätzwert zu erhalten. Es wird dabei ein Extended-Kalman-Filter (EKF) eingesetzt. Die theoretisch beste erzielbare Genauigkeit mit dem Datenfusionsansatz wird in Form der posterior Cramér-Rao lower bound (PCRLB) abgeleitet. Die PCRLB wird herangezogen um die Vorteile des Datenfusionsansatzes zu zeigen und dient als Benchmark für den Vergleich verschiedener Verfahren. Die Information über den Straßenverlauf wird in den Schätzprozess in Form einer Pseudomessung integriert. Simulationen

sowohl in linearen als auch in nichtlinearen Fällen zeigen die Vorteile dieses Ansatzes, der die Randbedingungen durch den Straßenverlauf einbezieht. Weiterhin wird das Problem der Unsicherheit bei der Auswahl der Bewegungsart im Multiple-Model (MM) - Ansatz betrachtet und gelöst. Insbesondere wird ein sogenannter Adaptive-Road-Constraint-Interacting-Multiple-Model (ARC-IMM) - Schätzer, der die Straßen-information in einen MM-Ansatz mit variabler Struktur integriert, vorgeschlagen. Es wird gezeigt, dass dieser Schätzer effizient und robust ist, und eine wesentlich verbesserte Positionsschätzung liefert.

Abstract

Positioning in mobile cellular networks is an exciting research area. The Global System for Mobile communications (GSM) network, as a widely used mobile communication standard around the world, has shown the potential to provide position information. Ground target tracking is a significant application of finding the position of a mobile station (MS). However, a GSM positioning system based on current specifications faces many difficulties to yield an accurate position estimate. Since the signals are designed by communication needs rather than positioning, the resolution of the measurements in GSM networks for positioning is coarse. The ambiguities of the position estimate arise when there are not a sufficient number of measurements available. Moreover, due to the restriction of terrain, road and traffic, the ground target often maneuvers. Therefore, data fusion approaches, which integrate redundant information from different sources, are applied in this work to obtain improved position estimation accuracy.

This work focuses on the state estimation problem of the MS's position given the measurements from the GSM networks and *a priori* road information. A data fusion solution, which integrates time of arrival (TOA) and received signal strength (RSS) measurements using an extended Kalman filter (EKF), is proposed to provide an improved position estimate. The theoretical best achievable performance, posterior Cramér-Rao lower bound (PCRLB), is derived for the data fusion approach. The PCRLB is used to demonstrate the benefits of the fusion approach and applied as a benchmark to compare different estimators. The road constraint is incorporated into the estimation process as a pseudomeasurement. Simulations of the linear and nonlinear road segments prove the advantages of the road-constrained approach. Moreover, the motion mode uncertainty problem is considered and solved by a multiple model (MM) approach. In particular, an adaptive road-constrained interacting MM (ARC-IMM) estimator, which incorporates the road information into a variable structure MM mechanism, is proposed and demonstrated to be effective and robust to provide a significantly improved position estimate.

Contents

List of Figures

List of Tables

Nomenclatures

Symbols

(x, y)	Position of the mobile station in x and y directions
(x_i, y_i)	Position of the i^{th} base station in x and y directions
$[\cdot]^T$	Transpose
$\arg\max$	Argument that maximizes
$\arg\min$	Argument that minimizes
$\bar{\bar{\mathbf{x}}}$	Conditional mean of $\mathbf{x}$ given the measurement $\mathbf{z}$
$\boldsymbol{\lambda}$	Multiplier vector to form a Lagrangian
$\ddot{x}, \ddot{y}$	Acceleration in x and y directions
Δ	The corresponding distance of one bit time
$\delta(\cdot)$	Kronecker (discrete) delta function
$\mathrm{diag}(\cdot), \mathrm{diag}[\cdot]$	Diagonal or block-diagonal matrix
$\dot{x}, \dot{y}$	Velocity in x and y directions
$\mathbb{E}\{\cdot\}$, $\mathbb{E}[\cdot]$	Expectation
$\hat{\mathbf{x}}$	State estimate
$\hat{\mathbf{x}}^+$	Updated state estimate
$\hat{\mathbf{x}}^-$	Predicted state estimate
$\Lambda(\boldsymbol{\xi})$	Likelihood function
$\mathbf{F}$	State transition matrix
$\mathbf{f}[\cdot]$	State transition function vector
$\mathbf{G}$	Noise gain matrix
$\mathbf{h}(\cdot), \mathbf{h}[\cdot]$	Vector of measurement functions
$\mathbf{I}$	Identity matrix
$\mathbf{J}$	Fisher information matrix
$\mathbf{P}^+$	Updated state error covariance matrix
$\mathbf{P}^-$	Predicted state error covariance matrix
$\mathbf{Q}$	Process noise covariance matrix
$\mathbf{R}$	Measurement error covariance matrix
$\mathbf{r}$	Residual vector
$\mathbf{S}$	Covariance matrix of the residual
$\mathbf{v}$	Measurement noise vector

$\mathbf{w}$	Process noise or driving noise vector
$\mathbf{X}(k)$	State vector including the states in all time step till k
$\mathbf{z}$	Measurement vector
$\mathbf{Z}(k)$	Measurement vector including the measurements in all time step till k
$\mathcal{B}$	Set of base stations
$\mathcal{N}\big(\mathbf{x}; \bar{\mathbf{x}}, \mathbf{P}\big)$	Probability density function of a Gaussian random vector with mean $\bar{\mathbf{x}}$ and covariance $\mathbf{P}$
$\mathcal{N}(\bar{\mathbf{x}}, \mathbf{P})$	pdf of a Gaussian random vector with mean $\bar{\mathbf{x}}$ and covariance $\mathbf{P}$
$\mathcal{N}(\bar{x}, \sigma^2)$	pdf of a Gaussian random variable with mean $\bar{x}$ and variance σ^2
$\nabla_{\boldsymbol{\xi}}$	Gradient with repect to $\boldsymbol{\xi}$
$\tilde{\mathbf{x}}$	Constrained state estimate
$\tilde{d}$	Distance between a mobile station and a base station in km
$\tilde{f}$	Frequency in MHz
$\triangleq$	Equal by definition
$\|\|\cdot\|\|$	Norm of a vector
a_t, a_n	Tangential acceleration, normal acceleration
d	Distance between a mobile station and a base station
f	Frequency
$f_{\mathbf{x}}(\boldsymbol{\xi})$	Probability density function
$f_{\mathbf{z}\|\mathbf{x}}(\boldsymbol{\zeta}\|\boldsymbol{\xi})$	Conditional probability density function
$f_{\mathbf{z},\mathbf{x}}(\boldsymbol{\zeta}, \boldsymbol{\xi})$	Joint probability density function
L	Lagrangian
L_P	Propagation loss
T_b	Time per bit, bit period
$tr[\cdot]$	Trace
$v_{i,TOA}$	TOA measurement noise from the i^{th} base station
$z_{i,TOA}$	TOA measurement from the i^{th} base station

Acronyms

2G	second generation
3G	third generation
AGPS	assisted GPS
AOA	angle of arrival
ARC-IMM	adaptive road-constrained interacting multiple model
AVL	automatic vehicle location
BER	Bit Error Rate
BS	base station

BTS	base transceiver station
CA	nearly constant acceleration
CDF	cumulative density function
CDMA	Code Division Multiple Access
CGALIES	Coordinate Group on Access to Location Information by Emergency Services
CGI	Cell Global Identification
COST-WI	COST 231-Walfisch-Ikegami-Model
CRLB	Cramér-Rao lower bound
CT	coordinated turn
CV	nearly constant velocity
E-CID	enhanced cell identity
EKF	extended Kalman filter
EOTD	enhanced observed time difference
FCC	Federal Communications Commission
FIM	Fisher information matrix
GDOP	geometric dilution of precision
GNSS	Global Navigation Satellite Systems
GPRS	General Packet Radio Service
GPS	Global Positioning System
GSM	Global System for Mobile communications
GTD	Geometric Time Difference
HDOP	horizontal dilution of precision
ILS	iterated least squares
IMM	interacting multiple model
INS	Inertial Navigation System
ITS	intelligent transport system
LMU	location measurement unit
LOS	line-of-sight
LS	least squares
MAP	maximum a posteriori
ML	maximum likelihood
MM	multiple model
MMSE	minimum mean square error
MS	mobile station
NLOS	non-line-of-sight
OTD	Observed Time Difference
PCRLB	posterior Cramér-Rao lower bound
pdf	probability density function
PDOP	position dilution of precision
RMSE	root mean square error

RSS	received signal strength
RTD	Real Time Difference
SNR	signal-to-noise ratio
TA	Timing Advance
TDMA	Time Division Multiple Access
TDOA	time difference of arrival
TDOP	time dilution of precision
TOA	time of arrival
UMTS	Universal Mobile Telecommunications System
VDOP	vertical dilution of precision
VS-IMM	variable structure interacting multiple model
WLS	weighted least squares

Chapter 1

Introduction

1.1 Motivation

Firstly driven by the requirement of localizing emergency calls, positioning in mobile cellular networks has become an exciting research area over the past few years. As a widely used mobile communication standard around the world, the *Global System for Mobile communications* (GSM) network has shown the potential to provide position information. Besides emergency assistance, a reliable estimate of a *mobile station*'s (MS) position has been found very useful for many applications. For the GSM itself, the estimator can assist the network to dynamically optimize its resource assignment. There are many commercial services based on the knowledge of the MS's position, such as fraud protection, asset tracking, mobile yellow pages, location-sensitive billing, and so on. In particular, ground target tracking is also an important task of finding the position of a MS in the applications like *automatic vehicle location* (AVL), *intelligent transport system* (ITS), and *fleet management*.

There are two basic categories of methods for determining a MS's position, handset-based solution and network-based solution. The handset-based solution relies on the use of a handset that includes a specialized chipset capable of calculating its own position like a *Global Positioning System* (GPS) receiver. The network-based solution uses the attributes of the radio signals exchanged between the MS and multiple *base transceiver stations* (BTSs) to determine the MS's location. The most popular proposed measurements in this category include *time of arrival* (TOA), *time difference of arrival* (TDOA), *angle of arrival* (AOA), and *received signal strength* (RSS).

However, a GSM positioning system based on current specifications faces many difficulties to yield an accurate position estimate for ground target

tracking applications. The resolution of the measurements in GSM networks related to positioning is coarse. The ambiguities of the position estimate arise when there are not a sufficient number of measurements available. Moreover, due to the restriction of terrain, road and traffic, the ground target may frequently start, accelerate, decelerate, stop, or turn on the road, i.e., the state to be estimated may change dramatically. Therefore, it is difficult to obtain an accurate position estimate when relying on just a single type of measurements. In this research work, we use data fusion solutions for ground target tracking applications, which integrate two or more types of measurements, to provide position estimation with better accuracy, reliability and coverage.

1.2 Previous Research

The research of mobile positioning was motivated by the requirement of the *Federal Communications Commission* (FCC) in the United States for locating emergency 911 calls. The FCC adopted such accuracy and reliability requirements first in 1996 and they were revised in the Third Report and Order [1] in 1999. In the report [2], the status of main technologies for determining a caller's position was addressed. The emergency call number in Europe is 112 and localizing emergency calls, i.e., Enhanced 112, was demanded to be in the new telecommunications regulatory framework in 2000. The report by the *Coordinate Group on Access to Location Information by Emergency Services* (CGALIES) [3] suggests relevant implementations to enhance the emergency services in Europe with location information. It is mentioned that the location accuracy has different requirements in different stages of the emergency helps like call routing, dispatching and call finding. When the caller is unable to provide location information and the location estimate is the only available information source, the desired location accuracy should be 10 m - 150 m for urban areas, 10 m - 500 m for suburban areas, rural areas and motorways. In response of the location requirement for wireless communication services, many efforts in the research field have been made on different issues and challenges for mobile positioning in wireless communication networks. The fundamentals and algorithms of position location technologies were described in [4]. The unique challenges and some proposed approaches for each of the major wireless standards were presented in [5]. Some overviews and surveys can be found in [6–11].

With respect to different standards of communication networks, specific solutions and issues have been considered. Caffery *et al.* [12] investigated

the positioning methods in *Code Division Multiple Access* (CDMA) cellular networks and the problems encountered. The wireless location in CDMA networks can further refer to [13]. In [14], the ability of deriving position information from GSM networks was examined by Drane *et al.*, the features of GSM signals relevant to positioning were analyzed, and the arising issues were also discussed. Further, Zhao [15] focused on the standardization of mobile positioning for 3G[1] systems. The QUALCOMM company also reported their investigation of location technologies for GSM and the next generation communication networks of *General Packet Radio Service* (GPRS) and *Universal Mobile Telecommunications System* (UMTS) [16, 17].

However, the basic mobile positioning methods based on the measurements from the communication networks, no matter which wireless standard is concerned, includes TOA, TDOA, AOA and RSS. These approaches are also the basis of radio location systems, which locate a mobile station by measuring the radio signals traveling between the mobile station and a set of fixed stations. Silventoinen *et al.* [18] presented the approaches of using already existing measurements in GSM networks for positioning, *Timing Advance* (TA, a TOA measurement) and *Observed Time Difference* (OTD). Spirito *et al.* [19] focused on three network-based location methods using *Cell Identity* (CI), TA, and RSS measurement in GSM networks. Caffery *et al.* [20] considered two methods of radio location, TOA obtained from the code tracking loop in the CDMA receiver and AOA assumed to be made with an antenna array. In [21], Pent *et al.* proposed a trilateration based method using TA in a GSM network and some experimental results were given in [22]. In [23] two *least squares* (LS) algorithms were developed, which use TOA measurements received at three or more base stations. A method of hyperbolic positioning of GSM mobile station was presented in [24, 25]. The location based on the measurement of the propagation loss between the mobile terminal and the fixed base stations derived from RSS measurements was discussed in [26, 27]. Hellebrandt *et al.* [28, 29] presented the method of using the RSS from GSM networks to estimate the position and velocity of the mobile station, where a LS based approach and an *extended Kalman filter* (EKF) based approach is employed, respectively. In [30], a method based on the differences of downlink signal attenuations was proposed, which does not require a known and accurate path loss modeling.

The above research work have shown that it is difficult to obtain an accurate position estimate relying on a single kind of existing measurements from wireless communication networks due to the high measurement errors. Therefore, data fusion approaches have been proposed to integrate differ-

[1]Third generation

ent types of measurements in order to achieve a more accurate and robust position. In [31], a data fusion architecture was proposed for the enhanced accuracy of position estimate within wireless networks, which can be used to include different complementary and redundant position related measurements. McGuire *et al.* [32] explored the fusion of power and time measurements obtained from CDMA networks at low cost. A hybrid TDOA and AOA location scheme was proposed in [33] to achieve high location accuracy and low cost of the mobile receiver. In [34], the performance improvement of a TDOA location system utilizing the AOA measurements over a TDOA only system was evaluated. Other hybrid systems in the literature include TDOA and TOA [35], signal attenuation difference of arrival and TDOA [36], TDOA and Doppler [37], and so on. By using the data fusion approaches, the estimation accuracy can be improved compared with using a single type of measurements, the advantages of both types of measurements will be utilized, and the estimation results are more robust to the noisy measurements.

It is well known that the dynamic information of the mobile station with respect to the time can be used to predict the mobile's position into the next time instant and incorporating it correctly using a recursive filter, e.g., Kalman filter, can greatly facilitate the position estimation. Cartrein *et al.* [38] analyzed the performance of a tracking algorithm based on Kalman filter using data from a field trial, which shows the estimation improvement by using Kalman filter. McGuire *et al.* [39] proposed a model-based dynamic filter based on the accurate model of mobile station motion. The motion model includes a kinematic state space model describing the physical rules governing the terminal motion and a control model, which describes the user decisions concerning the mobile's motion. In [40], Zaidi *et al.* presented two algorithms based on RSS measurements for real-time tracking of the mobile's location. In particular, the second algorithm was able to track mobility with adequate accuracy when there are less measurements, and this problem was also discussed using the concept of observability. However, relatively few studies have been reported on the dynamic estimation problem for mobile positioning. More research on this topic, especially for different scenarios of ground target tracking, should be conducted.

1.3 Research Area and Main Assumptions of the Thesis

1.3.1 Research Area

Data fusion is defined as the fusion of multiple and a diversity of measurements, technologies or systems simultaneously to form hierarchical and overlapping levels of processing. It can provide aggregate properties, robust measurements and more accurate estimation because if there is redundant information available from independent sources then higher precision and reliability in the estimation can be achieved. As shown in Fig. 1.1, a data fusion system for ground target tracking in GSM networks mainly consists of source preprocessing, object refinement, situation refinement, and process refinement. The focus of this work is in the stage of object refinement. In

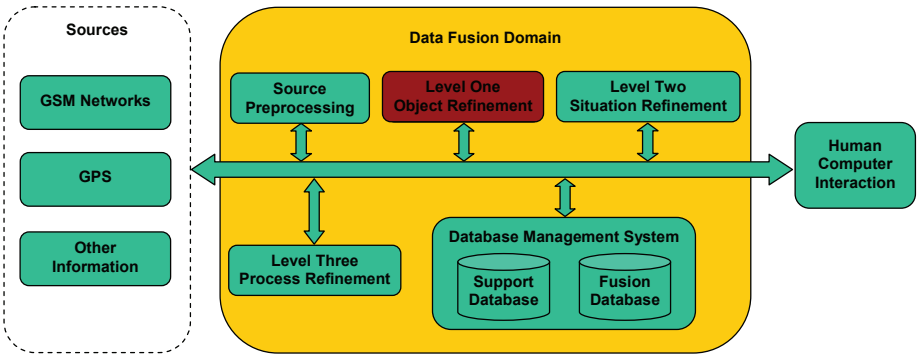

Figure 1.1: A data fusion system for ground target tracking

other words, it aims to find a better estimation solution when integrating redundant information from different sources to obtain the most reliable and accurate estimate of the MS's position, velocity, or other attributes. To realize this goal, our work consists of the following parts:

- ***Measurement part***: According to whether the position estimate is obtained directly from the received signals or from intermediate parameters, such as TOA, TDOA, AOA, and RSS, the positioning can be divided into *direct positioning* and *two-step positioning*. In this work, the two-step positioning is considered for the sake of low complexity, where some position related parameters are extracted firstly from the received signals, and then the position and velocity of the MS are

estimated from these intermediate parameters as shown in Fig. 1.2.

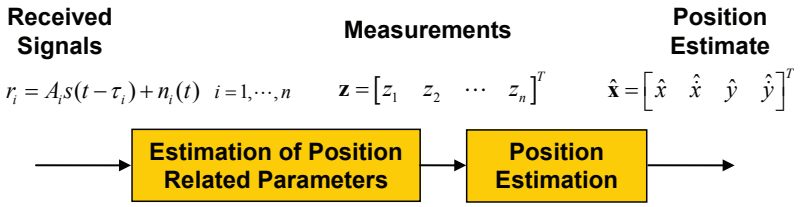

Figure 1.2: Two-step positioning

Our work focuses on the second step to obtain the position estimate from the pre-estimated parameters. Measurement models are built and measurement errors are modeled according to GSM standards. After investigating different measurements from the network, i.e., TOA, TDOA, AOA, and RSS, a data fusion method of integrating two different types of measurements in GSM networks, namely TOA and RSS, by using an EKF to estimate the MS's position is proposed. The data fusion method yields an improved positioning accuracy compared with the methods employing only TOA measurements or only RSS measurements. This approach can also be easily applied to other combinations of the network-based measurements. However, this thesis does not present it.

- ***Estimation part***: Depending on whether the target motion with respect to time is considered, the position estimation can be divided into *static estimation* and *dynamic estimation*. We focus on the problem of ground target tracking, which is a dynamic estimation problem. Since the measurements are usually nonlinear, i.e., there is a nonlinear mapping of the states into the observation space, the EKF is the basic estimator applied in this work. The theoretical estimation accuracy is a very important issue because it predicts the best achievable performance before designing any estimator and provides a benchmark of assessing the estimation algorithms. Therefore, the *posterior Cramér-Rao lower bound* (PCRLB) for the proposed data fusion approach is derived. The bound shows the basic principle of the data fusion approach, that is, information is additive. In addition, the bound can be used to analyze the performance of the data fusion. It shows that, theoretically, the data fusion approach yields a better accuracy and is more robust than using a single kind of measurements. Moreover, the

performance of different estimators can be also evaluated by comparing the results with the corresponding PCRLBs.

- ***Target part***: For the dynamic estimation problem, the dynamic model is very important since the estimator works well when the dynamic model matches the real motion of the target, otherwise the estimator will not provide an accurate estimate. Different dynamic models are studied, such as *nearly constant velocity* (CV) model, *nearly constant acceleration* (CA) model, *coordinated turn* (CT) model, and so on. Different movements of the ground target are simulated and estimators are examined under different scenarios. Moreover, the ground target maneuvers quite often, which is different from other types of targets, e.g., air targets. Hence, the motion mode uncertainty should be considered. It is well known that the *multiple model* (MM) method is a powerful approach for maneuvering target tracking under motion mode uncertainty. An *interacting multiple model* (IMM) estimator is developed for our problem, and the estimation results of three different simulated scenarios are evaluated.

- ***Road information part***: The resolution of the measurements in GSM networks related to positioning is coarse according to the GSM specifications. Thus, additional information about the target should be incorporated, and the road restriction is such a promising *a priori* information. Taking advantage of the road knowledge for tracking ground targets can be regarded as a constrained state estimation problem. The main approaches which address the solution to this problem are pseudomeasurement approach and projection approach. These two approaches are investigated and compared. For our problem, the road constraint is incorporated into an EKF as a pseudomeasurement, by which the uncertainty of the constraint can be applied. The approach is tested not only for uniform motions but also for maneuver motions. Moreover, nonlinear equality constraints are fundamentally different from linear equality constraints. The benefits of applying the nonlinear road constraint using the proposed approach are also demonstrated. In particular, incorporating the road constraint into a *variable structure IMM* (VS-IMM) greatly improves the estimation accuracy for maneuvering target tracking, which we propose as an *adaptive road-constrained IMM* (ARC-IMM) estimator.

1.3.2 Main Assumptions of the Thesis

Since the second step of the positioning is mainly concerned (see Fig. 1.2), i.e., estimating the MS's position from some position-related parameters in GSM networks, some assumptions on these measurements, i.e., the parameters, should be made.

- The base stations and the mobile station lie in the same plane. This will hold approximately true for most networks except for regions with extremely hilly topologies or high-rise buildings. Therefore, the positioning in this thesis is in two-dimensional space.

- The measurements are assumed to be corrupted by additive Gaussian noises, which are also assumed in most of the literature in mobile positioning. The main rationales of this assumption are: First, the time measurement in wireless networks is computed using correlation techniques. When the effective bandwidth and the *signal-to-noise ratio* (SNR) are sufficiently large and there is *line-of-sight* (LOS) signal, the additive Gaussian assumption of the measurement noise holds. Second, if the time interval used to obtain the measurement is large, the central limit theorem can be motivated to approximate the measurement error by a Gaussian distribution. The third is for simplicity of analysis. The Gaussian assumption is the least informative distribution with a given variance, the theoretical bound calculated under Gaussian assumption still holds for the estimation using EKF. The details of the error modeling will be presented in Chapter 2.

- The multipath and *non-line-of-sight* (NLOS) error are assumed to be identified and mitigated before the position estimation since they can be done in the first step of the positioning (see Fig. 1.2). The mitigation approaches are not discussed in this thesis. However, the effect of multipath and NLOS propagation and general approaches are introduced in Chapter 2.

- The measurements from different *base transceiver stations* (BTSs) and different types of measurements are assumed to be uncorrelated. This can be easily justified in the GSM network, which is a *Time Division Multiple Access* (TDMA) system, since each measurement is made at a different BTS using a different time slot.

1.4 Thesis Contributions

Most of the research in mobile positioning focuses on the static position estimation. In this thesis, we are specifically concerned with the target tracking applications, which are a dynamic estimation problem, using the available position related measurements from GSM networks and will discover the principle behind the data fusion approaches. The main contributions of this thesis are summarized as follows:

- Two kinds of measurements, TA and RSS from GSM networks, are integrated using an EKF to track the position of a mobile station set in a vehicle.
- The theoretical performance of ground target tracking using GSM networks is evaluated by the PCRLB. The benefits of the above mentioned data fusion approach are demonstrated in terms of the PCRLB.
- An approach of incorporating the road information into a conventional EKF as a pseudomeasurement for target tracking in GSM networks is proposed, which is the extension of constrained state estimation in mobile positioning. The benefits of the proposed road-constrained approach are demonstrated in both of linear and nonlinear road segments.
- An IMM estimator is designed for tracking maneuvering targets in GSM networks since it can better estimate the changing dynamics of a target than a conventional EKF.
- A novel adaptive approach considering the various possible target dynamics on changing road segments, an *adaptive road-constrained IMM* (ARC-IMM) estimator, is proposed, which incorporates the road information into a *variable structure IMM* (VS-IMM) mechanism to improve the estimation performance.

1.5 Structure of the Thesis

The following part of the thesis is organized as:

Chapter 2 introduces the fundamentals of positioning using GSM networks and provides a basic understanding of the research background. The measurements from GSM networks, TOA, TDOA, AOA and RSS, are modeled and the estimation techniques are presented. The main error sources,

multipath and NLOS propagation, are discussed and general mitigation approaches are introduced. The hearability problem of the BTSs on the MS is addressed. Moreover, the accuracy criteria and their connections are described.

Chapter 3 presents the proposed data fusion approach of integrating two different types of measurements, and the simulation results are given to show the improved positioning results compared with using a single type of measurements. In addition, the PCRLB for the data fusion approach is derived in this chapter and the performance is analyzed in terms of PCRLB to prove the benefits of the data fusion approach from a theoretical point of view.

Chapter 4 addresses the issue of incorporating the road information into the estimation process. The projection and pseudomeasurement approaches are introduced and compared. Simulations of a linear road and of a nonlinear road are implemented and the estimation results are analyzed.

Chapter 5 deals with the motion mode uncertainty problem. First an IMM estimator is designed and the simulation results show that the estimation accuracy during the non-maneuvering period is improved. Next, the proposed ARC-IMM estimator is presented. The simulation results depict the significant improvement of the tracking performance.

Chapter 6 provides a conclusion of the work. The main contributions are highlighted and some suggestions for the future work are also given.

Chapter 2

Mobile Station Positioning Using GSM Networks

GSM was first developed as an European digital mobile telephone standard and is now the most widely used mobile communication standard in the world. The GSM network has the potential to provide position information. In this chapter, the fundamentals of MS positioning using GSM networks are introduced. First, an overview of the GSM network is given and the important terms related to the positioning are explained. Then the radio propagation environment is described in Section 2.2 to provide an understanding of the complex radio propagation mechanisms. Most importantly, the positioning techniques and measurements in GSM networks are introduced and modeled in Section 2.3. There are basically two categories of positioning techniques, i.e., handset-based and network-based solutions. Considering that the network-based solutions do not require great modifications on the MS and networks, they are mainly introduced and employed in this thesis, including *time of arrival* (TOA), *time difference of arrival* (TDOA), *angle of arrival* (AOA), and *received signal strength* (RSS) measurements. The most important error sources for mobile positioning are multipath and *non-line-of-sight* (NLOS) propagation. Section 2.3.5 and 2.3.6 discuss the error modeling and general mitigation approaches. Another practical issue, hearability problem, is introduced in Section 2.3.7. Based on the measurement models obtained, the problem of position estimation is addressed in Section 2.4. The static estimation problem can be also called parameter estimation. Depending on modeling the parameters as nonrandom unknown constants or random variables, then non-Bayesian or Bayesian estimators are applied. On the other hand, the dynamic estimation problem is referred to as state estimation, which will be presented in the next chapter. The accuracy criteria to evaluate the positioning accuracy are described in Section 2.5.

2.1 Overview of GSM Networks

The GSM network was firstly deployed in 1991 and is now the most popular standard for mobile communications in the world. GSM is used by over 3 billion people across more than 219 countries and territories.[2] Its ubiquity makes international roaming very common between mobile phone operators, which enables the users to travel freely with their mobile phones in many parts of the world. This is realized by the *handover* procedure, which is the process of automatically transferring a call in progress to a different cell so that the call could be continued even when a MS crosses the border of one cell into another.

A GSM network is a cellular network. A *cell* is a certain limited area which is reached by one transmitter or a small collection of transmitters at a single base site, and the cell size is determined by the power of the transmitter. There are five different cell sizes in GSM networks, *macro*, *micro*, *pico*, *femto* and *umbrella* cells. The most often used cells for this work are macro and micro cells. Macro cells can be regarded as cells where the base station antenna is installed on a mast or a building above the average roof top level. Micro cells are cells whose antenna height is under the average roof top level, which are typically used in urban areas.

Most 2G[3] GSM networks operate in the 900 MHz or 1800 MHz bands. GSM 900 uses two 25 MHz blocks of the radio frequency spectrum, *uplink* (MS to BTS) and *downlink* (BTS to MS). Each block is divided into 125 frequency channels of 200 kHz. GSM employs a *Time Division Multiple Access* (TDMA) scheme on each frequency channel, dividing it into *time slots* of 577 μs. Eight time slots are gathered to form a *frame* and frames are grouped into *multiframes* and *superframes*. GSM defines *logical channels*, which are mapped onto the predefined time slots, to carry different information, e.g., the broadcast channels are to transmit system parameters. The messages contained in the various logical channels are fitted into the time slots using a *burst* structure.

In the GSM network, the position of the MS is roughly known by its presence in a cell using *Cell Global Identification* (CGI), which is a parameter available for all MSs. It is the identity number associated with a cell, which is designated by the network operator. The operator knows the coordinates of each cell site, and therefore the MS can be located in the position of the BTS controlling the call. This method is limited in precision to several hundred

[2]Source: http://www.gsmworld.com/technology/index.htm last visited on 20/7/2009
[3]Second generation

meters at best and a number of kilometers in many cases, which depends on the size of the cell. Additionally, in most cases each cell is divided into 120 degree sectors, with three base transceiver subsystems in each cell and each base transceiver subsystem has a 120 degree antenna. Through dividing the cell into different sectors, the MS can be estimated in a fraction of the cell. Moreover, the accuracy can be further improved with the use of a parameter, *Timing Advance* (TA), which is needed in a GSM network to avoid overlapping of multiple connections. The TA can be used to estimate the distance from MS to BTS and define a circle centered at the BTS. This approach is called *enhanced cell identity* (E-CID) as shown in Fig. 2.1, which is simple to be implemented with very crude location estimation.

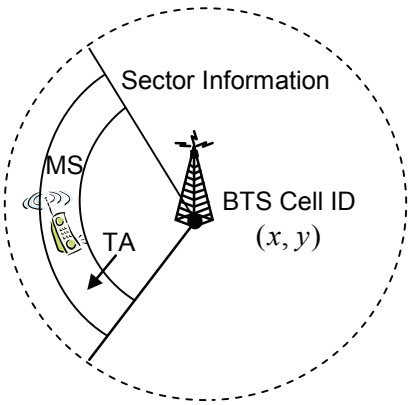

Figure 2.1: Enhanced cell identity

2.2 Radio Propagation

The radio signals transmit in free space based on Friis formula as follows

$$\frac{P_R}{P_T} = G_T G_R \left(\frac{\lambda}{4\pi d}\right)^2 \tag{2.1}$$

where P_T indicates the power supplied to the transmitting antenna, G_T is the power gain of the transmitter antenna, P_R denotes the power available at the receiving antenna, G_R stands for the power gain of the receiver antenna, λ indicates the wavelength and d is the distance between the transmitter and the receiver (see Fig. 2.2). The propagation loss L_P is defined as P_T/P_R

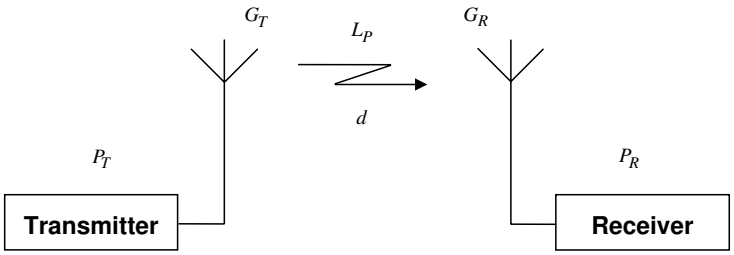

Figure 2.2: Propagation loss in free space

and usually expressed in decibel $10\log_{10}(P_T/P_R)$. For unity-gain (isotropic) antennas the propagation loss is

$$L_P = 32.44 + 20\log_{10}\tilde{f} + 20\log_{10}\tilde{d} \tag{2.2}$$

where L_P denotes the propagation loss in dB, $\tilde{f}$ stands for the frequency in MHz, $\tilde{f} = f/1$ MHz, and $\tilde{d}$ indicates the distance in km, $\tilde{d} = d/1$ km.

However, in a real environment the propagation mechanisms are very complex and diverse which may cause the propagation loss to differ from the free space case, because of reflection, diffraction, scattering, etc. [41] (as shown in Fig. 2.3). These three mechanisms result in three nearly independent phenomena of the radio propagation: *path loss* variation with distance, slow log-normal *shadowing*, and fast *multipath fading* [42]. Therefore, free

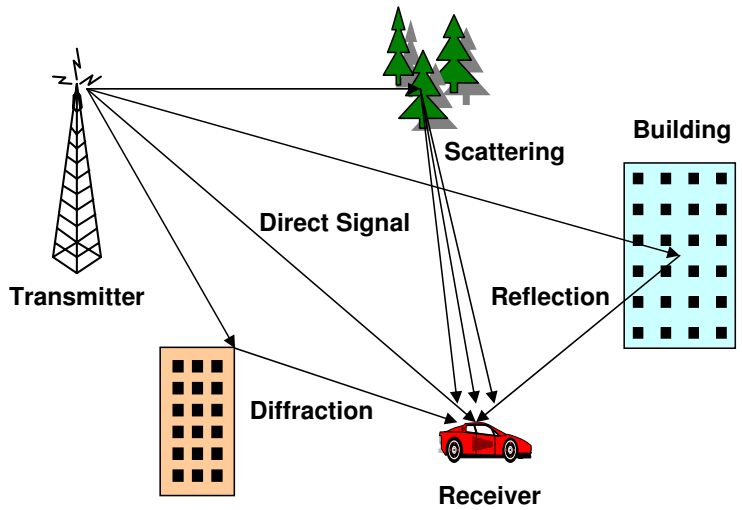

Figure 2.3: Propagation mechanisms

space propagation does not apply in the mobile radio environment and the propagation loss depends not only on the distance and wavelength, but also on the antenna height of the MSs and the *base stations* (BSs), and the local terrain characteristics. The simplest propagation loss model [42] assumes that

$$L_P = K + 10\beta \log_{10} \tilde{d} + \epsilon \tag{2.3}$$

where the parameters K and β are propagation constants. β is called path loss exponent which indicates the rate at which the path loss increases with distance and strongly depends on the cell size and local terrain characteristics. β is usually determined by empirical measurements, and it is equal to 2 in free space (see Eq. 2.2), it ranges from 3 to 4 in a typical urban macrocellular environment, and from 2 to 8 in a microcellular environment. Moreover, the surrounding environment may be greatly different at two different locations having the same d, which results in a log-normal distributed shadowing error. It is represented by the parameter ϵ, which is a zero-mean Gaussian random variable (in dB).

2.3 Positioning Techniques and Measurements from GSM Networks

There are a variety of technologies available to provide position estimates in GSM networks, and they can be loosely grouped into two basic classes depending on where the position information are mainly obtained: handset-based solutions and network-based solutions. The handset-based solution relies on the use of a handset that includes a specialized chipset capable of calculating its own position, e.g., a GPS receiver. *Assisted GPS* (AGPS) is such a solution which uses a terrestrial cellular network to improve GPS receiver performance by providing satellite constellation information directly to the GPS receiver. This approach offers the greatest accuracy compared with network-based solutions. However, embedding a GPS receiver into mobile devices leads to increased cost, size, and power consumption. It could also require the replacement of millions of mobile handsets that are already on the market. In addition, the location uncertainty can be quite small in cases where at least four GPS satellites are in view and where the GPS satellites are well distributed. In less ideal operating conditions, however, such as in urban environments as well as inside buildings, the GPS handset may have significant problems in providing accurate location information.

On the other hand, the network-based solution uses the attributes of the

radio signals exchanged between the MS and multiple BTSs to determine the MS's location. We will introduce the most important measurements from GSM networks including TOA, TDOA, AOA, and RSS in the following subsections.

2.3.1 Time of Arrival

By measuring the propagation time that a signal takes to travel between a BTS and a MS, the distance between them can be calculated. This requires that the BTS and the MS are well synchronized (e.g., 1 μs of timing error results in a 300 m position error). To avoid the synchronization problem, measuring the round trip time, i.e., the signal is transmitted from a source to a destination and then echoed back to the source, is more often utilized. Geometrically, assuming that the MS and the BTS are on the same plane, one TOA measurement provides a circle, centered at the BTS, on which the MS must lie. Using at least three BTSs to resolve ambiguities in two dimensions, the intersection of circles provides the MS's position, shown in Fig. 2.4.

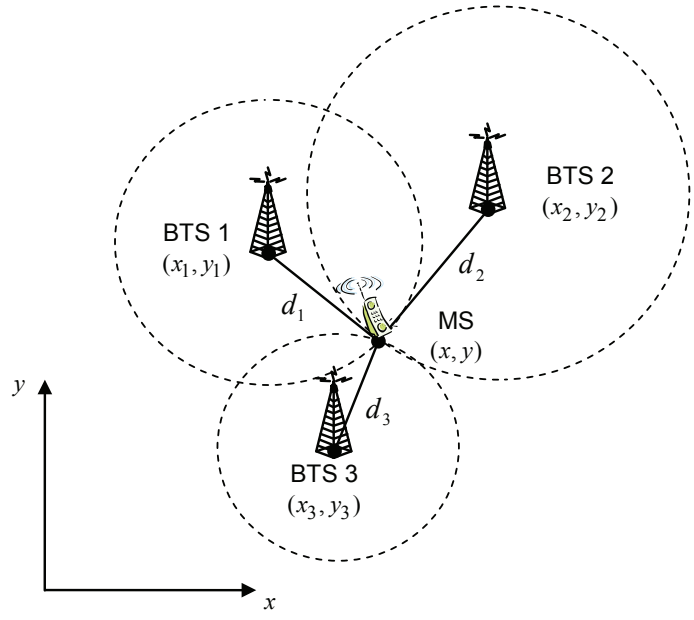

Figure 2.4: Time of arrival

TA represents a TOA measurement in the GSM system. TA is a parameter that a particular BTS sends to each MS according to the perceived

round trip propagation delay BTS-MS-BTS. Then the MS advances its timing by this amount to compensate the propagation delay in order to avoid user time slot overlap and maintain the frame alignment, especially when the MS is far away from the BTS. TA is rounded to the nearest integer bit period, and the time per bit is $T_b = 48/13$ μs. The corresponding distance $\Delta = c \cdot T_b \approx 1108$ m, where $c = 3 \times 10^8$ m/s is the speed of light. Then the distance between a BTS and a MS can be calculated as $d = \mathrm{TA} \cdot \Delta/2$. Therefore, the measurement of TA can be formulated as the distance between one MS and a certain BTS.

It should be noticed that under current GSM specifications, the TA is only taken in the current serving BTS. It is estimated by the serving BTS only when the MS is in connected mode, i.e., the MS is communicating with the serving BTS using a dedicated channel. As a consequence, TA can only be measured by sequentially forcing the communication to be handed over from one BTS to another until all BTSs have been accessed. However, this artificially forced handovers to suboptimal BTSs can degrade call quality and reduce system capacity.

Error Model

Let (x, y) denote the position of the MS, $\mathcal{B} = 1, 2, \cdots, n$ be the set of the BTSs, and (x_i, y_i) be the position of the i^{th} BTS. Assuming that a *line-of-sight* (LOS) signal between the i^{th} BTS ($i = 1, 2, \cdots, n$) and the MS exists, then the TOA measurement from the i^{th} BTS ($i = 1, 2, \cdots, n$) is formulated as distance with noise

$$z_{i,TOA} = \sqrt{(x - x_i)^2 + (y - y_i)^2} + v_{i,TOA} \tag{2.4}$$

where the measurement noise $v_{i,TOA}$ is usually, in most of the literature on mobile positioning [7, 10, 43, 44], assumed to be a zero-mean white Gaussian noise

$$v_{i,TOA} \sim \mathcal{N}(0, \sigma^2_{i,TOA}) \tag{2.5}$$

Without loss of generality, the subscript "TOA" is used instead of "TA". In fact, in GSM networks, the time measurements are averages of propagation delays estimated during periods longer than the typical coherence time of the mobile radio channel [45]. Therefore, it is reasonable to assume the time delay in LOS propagation is a zero-mean white Gaussian variable using the central limit theorem. On the other hand, in wireless networks, the time measurement is computed using correlation techniques. When the effective bandwidth and the *signal-to-noise ratio* (SNR) are sufficiently large, the

additive Gaussian assumption of the measurement noise in Eqs. (2.4) and (2.5) holds and $\sigma_{i,TOA}$ depends on the bandwidth and SNR [10, 46].

According to the GSM standard [47], the assessment error of TA due to noise and interference is less than 1/2 bit period, i.e., 1/2 T_b, for stationary MS and for MS moving at a speed of up to 500 km/h the additional error shall be less than 1/4 bit period. Thus, the error of the distance of one trip, due to noise and interference, is uniformly distributed in the range $[-E, +E]$, where $E = \Delta/4 + \chi \cdot \Delta/8$ in which χ varies from 0 to 1 accounting for the speed of MS. In literature [21], a uniform distribution for the error is given with the standard deviation

$$\sigma_{TA} = \frac{\Delta}{2}\sqrt{\frac{1}{6}\left[\left(1+\frac{\chi}{4}\right)^2 + \left(\frac{\chi}{4}\right)^2\right]} \tag{2.6}$$

which is derived from the above specification. Then the author used a Gaussian distribution with the standard deviation in Eq. (2.6) to approximate the statistics of the TA measurement error in the EKF for estimation. A field experiment was executed in [22], by which the rational of the Gaussian assumption usually used in EKF was verified with the comparison of the real TA measurement error statistics in GSM networks and the Gaussian assumption. It is also shown that the standard deviation of the measurement errors is in the level of few hundreds of meters and varies in different environments like rural and urban areas. Other explanations for the Gaussian assumption can be found in [48, 49]. For the simplicity of research and analysis, we use the error model in Eqs. (2.4) and (2.5) in the following chapters and the standard deviation in Eq. (2.6) derived from the GSM specifications for simulations.

The error model in Eq. (2.4) assumes unbiased measurements. However, in practice there are often biases within the time measurements, which arise from *non-line-of-sight* (NLOS) propagation, hardware calibration, and multipath propagation [48]. Assuming that the statistics of possible biases is known or estimated prior to the position estimation, it is equivalent to assume zero-mean measurement errors. The details of the NLOS and multipath propagation will be discussed in Section 2.3.5 and 2.3.6.

2.3.2 Time Difference of Arrival

Instead of the absolute time measurements, time difference measurements can be used to define hyperbolas, with foci at the BTSs, on which the MS must lie. The intersection of hyperbolas provides the location of the MS. For

a two dimensional scenario, at least two TDOA measurements are required, i.e., three BTSs, to uniquely define a position as shown in Fig. 2.5.

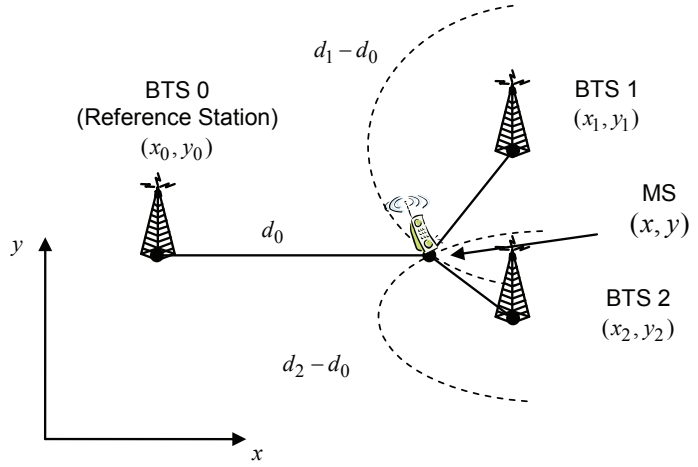

Figure 2.5: Time difference of arrival

There are two ways to calculate the TDOA measurement (refer to [10, 46] and the references therein). One method is to calculate the difference of two TOAs received at two BTSs. Another approach is to estimate the TDOA by correlating the received signals at different BTSs. In GSM networks, the TDOA approach is called *enhanced observed time difference* (EOTD), which is based on the first kind of TDOA technique. There are three parameters: *Observed Time Difference* (OTD), *Real Time Difference* (RTD), and the TDOA, which is termed *Geometric Time Difference* (GTD=RTD-OTD). They are used in GSM networks to improve the efficiency of handovers. If a burst is transmitted by BTS a (BTS b) at the instant $t_{T_{x_a}}$ ($t_{T_{x_b}}$) and received by the MS at instant $t_{R_{x_a}}$ ($t_{R_{x_b}}$), then

$$\text{RTD} = t_{T_{x_b}} - t_{T_{x_a}} \tag{2.7}$$

$$\text{OTD} = t_{R_{x_b}} - t_{R_{x_a}} \tag{2.8}$$

$$\text{GTD} = \text{RTD} - \text{OTD} = (t_{R_{x_a}} - t_{T_{x_a}}) - (t_{R_{x_b}} - t_{T_{x_b}}) \tag{2.9}$$

The TDOA measurement is modeled as the difference of the distances multiplied with a factor of the speed of light. First choosing a reference BTS from the set of BTSs $\mathcal{B}$, which has position (x_0, y_0), then the i^{th} TDOA measurement of the rest $n-1$ BTSs ($i = 1, 2, \cdots, n-1$) relative to the reference BTS is given by

$$z_{i,TDOA} = \sqrt{(x - x_i)^2 + (y - y_i)^2} - \sqrt{(x - x_0)^2 + (y - y_0)^2} + v_{i,TDOA} \tag{2.10}$$

Similar to the assumptions of TOA measurement errors, the measurement noise in Eq. (2.10) is usually assumed to be a zero-mean white Gaussian noise with standard deviation $\sigma_{i,TDOA}$ in LOS situation [7, 10, 24, 25, 43, 44]

$$v_{i,TDOA} \sim \mathcal{N}(0, \sigma^2_{i,TDOA}) \tag{2.11}$$

In [24], a value of the EOTD standard deviation in GSM networks is given according to the specifications in GSM networks for OTD and RTD

$$\sigma_{i,TDOA} = \sqrt{\frac{5}{12}}\Delta \tag{2.12}$$

where Δ is the corresponding distance of one bit period $\Delta = c \cdot T_b$.

RTDs are measured by ad hoc *location measurement units* (LMUs) installed through the network and OTDs are measured by the MS. In GSM-based systems, an MS performs OTD measurements either in connected mode or in idle mode (i.e., the MS is turned on but no two-way communication takes place). OTD measurements are made without forcing a handover. An important issue using TDOA is that the systems need to be synchronized.

2.3.3 Angle of Arrival

Using directive antennas or antenna arrays BTSs measure the AOA of a signal that is transmitted by the MS. There are three steps in the processing [50]. First the channel impulse response for each element of the antenna array is estimated from the signal received at the BTS. Then the AOA is extracted from the impulse responses. After that, simple geometric relationships are used to form the position estimate based on the AOA measurements and the known positions of the BTSs, or filtering techniques can be used to estimate the MS's position. For two-dimensional positioning, a minimum of two BTSs is required as shown in Fig. 2.6. Assuming a LOS signal, the AOA measurement at i^{th} BTS ($i = 1, 2, \cdots, n$) can be written as

$$z_{i,AOA} = \arctan\left(\frac{y - y_i}{x - x_i}\right) + v_{i,AOA} \tag{2.13}$$

where $v_{i,AOA}$ is assumed to be a zero-mean white Gaussian noise [10, 43, 46].

$$v_{i,AOA} \sim \mathcal{N}(0, \sigma^2_{i,AOA}) \tag{2.14}$$

Currently, it is possible to use the rough sector information (e.g., 120° for a three-sector antenna). By using an antenna array for 3G mobile networks, the AOA accuracy can be improved.

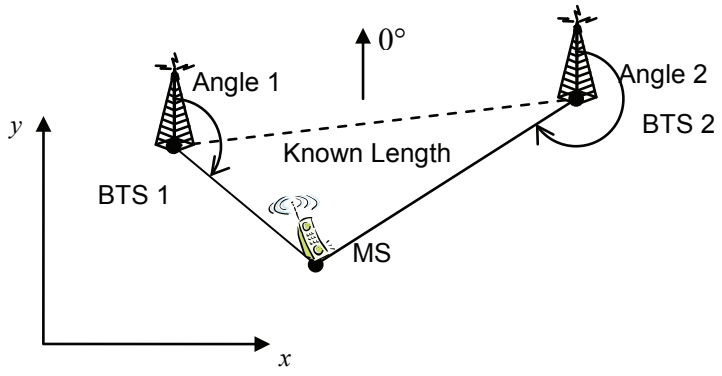

Figure 2.6: Angle of arrival

The advantages of AOA are that it requires only two BTSs to obtain the position in two dimensions, and there is also no time synchronization between BTSs required. However, the BTSs need to be equipped with complex hardware to obtain an accurate AOA. When the MS is far away from the BTS, the AOA measurement accuracy degrades.

2.3.4 Received Signal Strength

As introduced in Section 2.1, the propagation loss between a MS and a certain BTS derived from a RSS measurement is a logarithmic function of the distance between the stations. Therefore, if the propagation losses from three or more BTSs are available, we can estimate the MS's position in two dimensions based on trilateration techniques. The RSS measurement from the i^{th} BTS ($i = 1, 2, \cdots, n$) is generally formulated as

$$z_{i,RSS} = K + 10\beta \log_{10}\left(\sqrt{(\tilde{x} - \tilde{x}_i)^2 + (\tilde{y} - \tilde{y}_i)^2}\right) + v_{i,RSS} \tag{2.15}$$

where K and β are propagation constants depending on the environment characteristics, and the 'tilde' notations denote the positions of the MS and BTSs normalized by 1 km. It is well known that the attenuation of the signal strength is caused by three factors: path loss, fast multipath fading, and slow log-normal shadowing. Usually the fast fading effect can be removed by averaging the received power over a time interval. Therefore, the RSS measurement noise $v_{i,RSS}$ is assumed to be a zero-mean white Gaussian noise representing the shadowing

$$v_{i,RSS} \sim \mathcal{N}(0, \sigma^2_{i,RSS}) \tag{2.16}$$

The above propagation model can either be empirical or theoretical, or a combination of these two. The empirical models are based on measurements, whereas the theoretical models are derived from the fundamental principles of radio wave propagation phenomena.

The *COST 231-Walfisch-Ikegami-Model* (COST-WI) [51] is an empirical path loss model based on extensive measurement campaigns in European cities, which has been used extensively in typical suburban and urban environments. The model considers several parameters to describe the character of the urban environment, as shown in Fig. 2.7. The environment parameters

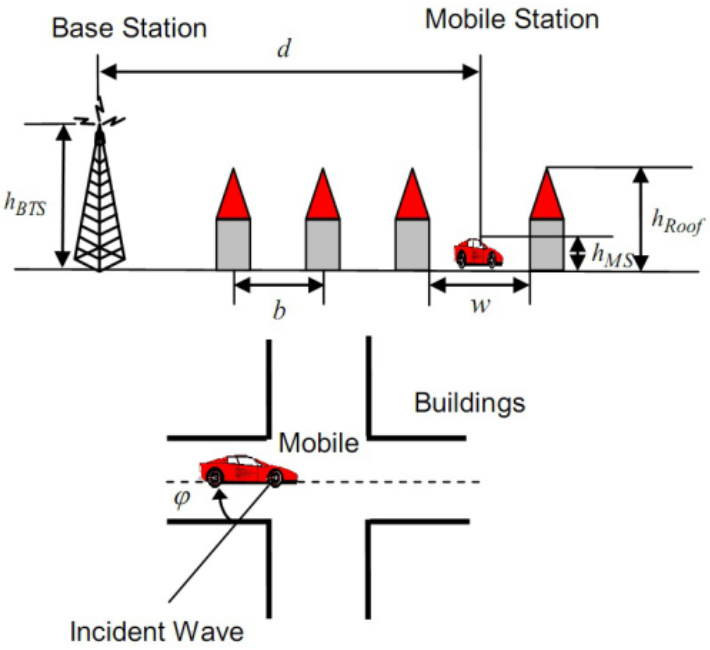

Figure 2.7: Definition of the parameters in the COST 231-WI model

are assumed as a typical small cell in urban environments, in which the cell range is less than 1-3 km and the antenna is sited above the median but below the maximum height of the surrounding roof tops [52]. Assuming that the environment parameters are as follows:

- Building separation $b = 40$ m; Widths of the roads $w = 20$ m;
- Heights of buildings $h_{Roof} = 15$ m; Heights of BTSs $h_{BTS} = 17$ m;
- Road orientation with respect to the direct radio path $\varphi = 90°$

in a LOS situation, the propagation loss is given by

$$L_P = 42.64 + 26 \log_{10}\left(\sqrt{(\tilde{x} - \tilde{x}_i)^2 + (\tilde{y} - \tilde{y}_i)^2}\right) + 20 \log_{10} \tilde{f} + v_{i,RSS} \quad (2.17)$$

where $\tilde{f}$ is the frequency normalized by 1 MHz, $\tilde{f} = f/1$ MHz. With $f =$ 900 MHz, the above equation becomes

$$L_P = 101.724 + 26 \log_{10}\left(\sqrt{(\tilde{x} - \tilde{x}_i)^2 + (\tilde{y} - \tilde{y}_i)^2}\right) + v_{i,RSS} \quad (2.18)$$

The transmission loss in the NLOS situation, which is composed of free space loss, multiple screen diffraction loss, and roof-top-to-street diffraction and scatter loss, based on these parameters is given by

$$\begin{aligned} L_P \approx\ & 33.49 + 20 \log_{10}(\Delta \tilde{h}_{MS}) \\ & + \left[26 + 0.7(\tilde{f}/925 - 1)\right] \log_{10}(\tilde{f}) + 38 \log_{10}(\tilde{d}) + v_{i,RSS} \end{aligned} \quad (2.19)$$

where $\Delta \tilde{h}_{MS} = \Delta h_{MS}/1$ m and $\Delta h_{MS} = h_{Roof} - h_{MS}$ is the height difference between the MS and the buildings, $\tilde{f}$ indicates the signal frequency in MHz, $\tilde{f} = f/1$ MHz, and $\tilde{d}$ denotes the distance between MS and BTS in km, $\tilde{d} = d/1$ km $= \sqrt{(\tilde{x} - \tilde{x}_i)^2 + (\tilde{y} - \tilde{y}_i)^2}$. Further, we assume the heights of mobiles $h_{MS} = 1.5$ m, and the frequency $f = 900$ MHz. Thus the path loss can be formulated as

$$L_P = 132.85 + 38 \log_{10} \tilde{d} + v_{i,RSS} \quad (2.20)$$

where $v_{i,RSS}$ is the measurement noise with the mean error in the range of ± 3 dB and the standard deviation about 4-8 dB [51].

2.3.5 Multipath Propagation

A radio signal transmitting through the complex wireless environment may arrive at the MS or BTS as multiple versions with different amplitude, phase and time delay due to the presence of reflecting objects and scatterers. The multiple radio waves combine vectorially at the receiver antenna to give a resultant signal which can be large or small depending upon whether the incoming waves combine constructively or destructively. This causes a rapid fluctuation of the envelope of the received signal over a short period of time or travel distance, which is called the phenomenon of fast fading to distinguish them from the much longer-term variation in mean level which is known as slow fading.

Multipath results in the rapid changes of the signal strength and also of the time dispersion. In a digital receiver, this is normally translated into an impact on the *Bit Error Rate* (BER). In wireless positioning, the BER is no longer concerned, whereas the first replica of the delay is under consideration [43]. In [53], for the time measurements the author follows a ML estimation of multipath delays, which is modeled as a vector $\boldsymbol{\tau} = \begin{bmatrix}\tau_1 & \tau_2 & \cdots & \tau_N\end{bmatrix}^T$

$$\hat{\tau}_i = \tau_i + \xi_i \tag{2.21}$$

where τ_i denotes the time delay of the i^{th} multipath signal received at one receiver, $\hat{\tau}_i$ is the estimate of the time delay and $\boldsymbol{\xi} = \begin{bmatrix}\xi_1 & \xi_2 & \cdots & \xi_N\end{bmatrix}^T$ stands for a multivariate Gaussian random variable. The usual approach to deal with the multipath effect is to detect and only use the first arrival signal (LOS or NLOS) for positioning [54]. For time-based and angle-based positioning approaches, the multipath problem can be reduced to the positioning of a single path. In [53], the author claims that the second and later arrived signals can also provide position information and the enhancement of accuracy depends on the strength of the multipath components and the variance of the related NLOS delays [53, 55].

2.3.6 None-line-of-sight Propagation

Due to reflection and diffraction, the signal may travel excess path lengths of the order of hundreds of meters and there might be no direct path from the BS to the MS. This problem is called NLOS problem, which is a critical issue for mobile positioning.

Assume that there are m NLOS measurements, and the corresponding BTSs are denoted by the set of NLOS BTSs $\mathcal{B}^{NLOS} = 1, 2, \cdots, m$. For the time-based and angle measurements, the NLOS error is usually modeled as an additive bias [10, 43, 44, 56–58]. For simplicity of analysis, the NLOS error is assumed to be Gaussian distributed in order to provide an understanding of the effect of NLOS on the location precision [44]. Since the Gaussian distribution is the least informative distribution for a given variance, the lower bound calculated based on Gaussian assumption will still hold for the estimation [7]. Some realistic models for the NLOS error include Gamma distribution [44], distributions based on certain scatter models [59], and the distribution from measurements [60]. Gaussian mixtures can be also used for approximating the distribution of the NLOS error [7]. The specific error model for each type of measurement based on Gaussian distribution is as follows:

TOA:

$$z_{i,TOA}^{NLOS} = \sqrt{(x-x_i)^2+(y-y_i)^2} + b_i + v_{i,TOA} \tag{2.22}$$

where b_i indicates the positive bias induced from the NLOS propagation, and $v_{i,TOA}$ is assumed to be a zero-mean white Gaussian noise such that formula $v_{i,TOA} \sim \mathcal{N}(0, \sigma_{i,TOA}^2)$. If it is assumed that the measurements are averaged over some integration time, by the central limit theorem, the bias b_i can be assumed constant, and the time variance of the bias can be reflected in the variance of the zero-mean noise $v_{i,TOA}$ [56].

TDOA: As introduced in Section 2.3.2, the TDOA measurement is a difference of TOA measurements. Assume that a BTS in the NLOS BTS set $\mathcal{B}^{NLOS}$ is chosen as the reference BTS $i = 0$, whose position is (x_0, y_0). For BTS $i = 1, 2, \cdots, m-1$

$$\begin{aligned} z_{i,TDOA}^{NLOS} &= \left(\sqrt{(x-x_i)^2+(y-y_i)^2} + b_i\right) - \left(\sqrt{(x-x_0)^2+(y-y_0)^2} + b_0\right) \\ &\quad + v_{i,TDOA} \qquad (2.23) \\ &= \left(\sqrt{(x-x_i)^2+(y-y_i)^2} - \sqrt{(x-x_0)^2+(y-y_0)^2}\right) + (b_i - b_0) \\ &\quad + v_{i,TDOA} \qquad (2.24) \end{aligned}$$

where b_i indicates the NLOS error of the i^{th} BTS and b_0 denotes the NLOS error of the reference BTS. Defining $\mathbf{z}_{TDOA}^{NLOS}$ as the measurement vector which includes TDOA measurements from $m-1$ BTSs, then the error $\mathbf{v}_{TDOA} = \begin{bmatrix} v_{1,TDOA} & v_{2,TDOA} & \cdots & v_{m-1,TDOA} \end{bmatrix}^T$ is a multivariate Gaussian variable, which conforms to $\mathcal{N}(\mathbf{0}, \boldsymbol{\Upsilon})$ with

$$\boldsymbol{\Upsilon} = \begin{bmatrix} \sigma_1^2+\sigma_0^2 & \sigma_0^2 & \cdots & \sigma_0^2 \\ \sigma_0^2 & \sigma_2^2+\sigma_0^2 & \cdots & \sigma_0^2 \\ \vdots & \vdots & \ddots & \vdots \\ \sigma_0^2 & \sigma_0^2 & \cdots & \sigma_{m-1}^2+\sigma_0^2 \end{bmatrix} \tag{2.25}$$

AOA: The AOA with NLOS error at i^{th} BTS in the NLOS BTS set $\mathcal{B}^{NLOS}$ can be expressed as

$$z_{i,AOA}^{NLOS} = \arctan\frac{y-y_i}{x-x_i} + \varphi_i + v_{i,AOA} \tag{2.26}$$

where φ_i stands for a NLOS induced angle error and $v_{i,AOA}$ indicates a zero-mean white Gaussian noise.

RSS: The signal strength is modeled in dB scale as

$$z_{i,RSS}^{NLOS} = K + 10\beta\log_{10}\sqrt{(\tilde{x}-\tilde{x}_i)^2+(\tilde{y}-\tilde{y}_i)^2} + v_{i,RSS} \tag{2.27}$$

where $v_{i,RSS}$ indicates a zero-mean white Gaussian noise representing log-normal fading. The NLOS effects are implicitly included in the formulation.

To mitigate the NLOS errors, there are two main categories of methods. One is that the NLOS error is modeled as additive bias to the LOS measurement with known or unknown distribution. The NLOS error could be detected, which is a problem of NLOS identification, and then removed, which is called LOS reconstruction [58]. Other methods in this category can be found in [46, 57, 61] and the references therein. Another category is that a multipath delay profile is considered instead of a TOA or RSS measurement, such as signature matching. This approach is especially useful where the propagation environment is complicated. However, it suffers from the requirement of building a big data base and computational complexity.

Reference [46] presents an estimation accuracy analysis in terms of CRLB in a NLOS environment. The discussion is classified into two cases according to whether *a priori* statistics of the NLOS errors are available or not. When there is no prior knowledge of the NLOS error available, the CRLB depends only on the LOS signals. On the contrary, in the case of knowing the prior statistics of the NLOS error, the *Fisher information matrix* (FIM), which is the inverse matrix of the CRLB, consists of two components, which are the information from data and that from the *a priori* as shown in Eq. (2.51). The corresponding CRLB is derived in [46].

2.3.7 Hearability Problem

As introduced, many positioning methods rely on the multilateration of a few measurements from different BTSs, e.g., TOA requires at least three BTSs to get a unique position estimate (see Fig. 2.4). However, the practical problem arises, whether there are more than three BTSs available. The ability of the MS to detect surrounding BTSs in a given time interval is called hearability problem [62], which is usually represented by the number of detectable BTSs. It should be noted that here the hearability refers not only to the near-far effect, but means the detectability of BTSs in general.

The cellular network is consisted of cells, which is an area around a BTS. The size of a cell varies a lot in different areas, which is usually between a few hundreds meters to a few kilometers. The maximum cell size can be 35 km. The density of cells corresponds to the size of cells, i.e., in rural areas the cells have a low density but bigger size, whereas in urban areas there is a high density of cells but with small cell size. As shown in Fig. 2.8, the density of the BTS in the city center of Siegen is relatively high whereas in suburban,

around the university, there is only one base station in the neighbourhood. There are apparently more BTSs in metropolitan cities, e.g., the center area of cologne as shown in Fig. 2.9.

Figure 2.8: Base stations around university of Siegen

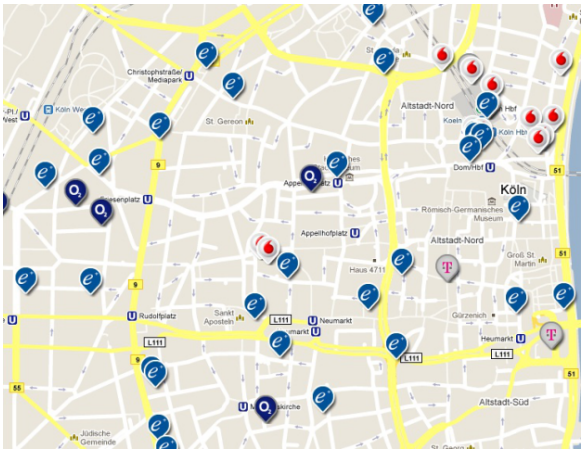

Figure 2.9: Base stations around center of Cologne

The cell has a hexagonal shape (Fig. 2.10) and the MS is usually only connected with the serving BTS and detects signals from up to six neighbouring BTSs. The detectability of a BTS at the MS depends on the received

signal power, which relies on the transition power of the tower and the distance between the BTS and the MS as well. In [18], the hearability of the

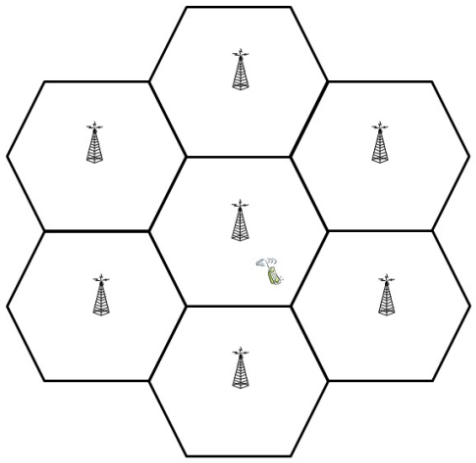

Figure 2.10: Hexagonal cellular networks

neighbouring cell was examined using a car driving through different environments. Over 92% of the time three or more BTSs were received in a metropolitan area. However, in a rural area, only 71% of the time more than three BTSs were received. The percentages of receiving more than five BTSs are below 30% in both environments. In [5], a driving test was implemented in USA. Similar results were obtained that much less BTSs can be observed in rural areas than in urban areas. But the percentage of the detectability is less when compared to the test in [18], e.g., in urban, there is only 40% time to detect more than three stations whereas there is 60% time to observe two base stations. Hence, it can be concluded that the hearablity drops significantly from city to rural areas and it varies a lot in different regions.

Moreover, the TA, a current quantity in GSM networks able for positioning, is only available for the serving BTS and measured on the connected mode. If more TAs want to be obtained, forced handover should be performed. Also, although in big cities more BTSs are available, NLOS propagation is a critical issue due to the block of high buildings, so that the number of LOS base stations will be reduced.

To tackle the hearablity problem for positioning purpose, a good solution is to get as many information as possible and apply data fusion methods. There are more network providers like O2, E-Plus, Telekom and Vodafone in Germany and therefore more possible BTSs if different providers are considered. Moreover, the road network is a promising source to be integrated

with the measurements from GSM networks [63] to improve the estimation accuracy and robustness, which will be explored in Chapter 4.

2.4 Position Estimation

2.4.1 Static Estimation

In the static estimation case, there is no assumption or *a priori* knowledge of the changes of the MS's position with respect to the time. Thus the positions at different times are a sequence of uncorrelated parameters to be estimated in a snap-shot manner.

For this static estimation problem, the measurements of one location can be generally written as

$$\mathbf{z} = \mathbf{h}(\mathbf{x}) + \mathbf{v} \tag{2.28}$$

where $\mathbf{z} = \begin{bmatrix} z_1 & z_2 & \cdots & z_n \end{bmatrix}^T$ stands for the measurement vector including the available n measurements from different BTSs, $\mathbf{x} = \begin{bmatrix} x & y \end{bmatrix}^T$ indicates the two dimensional position of the MS in x and y directions, which stays constant during the measurement process, $\mathbf{h}(\mathbf{x}) = \begin{bmatrix} h_1(\mathbf{x}) & h_2(\mathbf{x}) & \cdots & h_n(\mathbf{x}) \end{bmatrix}^T$ denotes the vector of measurement functions, and $\mathbf{v} = \begin{bmatrix} v_1 & v_2 & \cdots & v_n \end{bmatrix}^T$ is the vector of measurement noises, which can be assumed to be a zero-mean white Gaussian noise with covariance matrix $\mathbf{R}$

$$\mathbf{v} \sim \mathcal{N}(\mathbf{0}, \mathbf{R}) \tag{2.29}$$

$$\mathbf{R} = \mathrm{diag}(\sigma_1^2, \sigma_2^2, \cdots, \sigma_n^2) \tag{2.30}$$

According to different measurement types obtained from GSM networks, the measurement function $h(\cdot)$ has different forms as introduced in Eqs. (2.4), (2.10), (2.13), and (2.15). For TOA, TDOA and RSS measurements, at least three measurements from different BTSs are required, whereas for AOA only two different measurements are necessary. The measurement vector can also consist of different types of measurements, e.g., TOA and AOA. Then some optimization criteria to minimize (or maximize) a given cost function can be applied. The static estimation problem is also called parameter estimation. There are two models for the parameters to be estimated, *nonrandom* or *random*. If the parameters are nonrandom unknown constants, the *least squares* (LS) and the *maximum likelihood* (ML) principle should be utilized. But when the parameters are assumed to be random variables, Bayesian approaches should be considered.

Least Squares

Based on the LS principle, to obtain the estimate from the measurements described by Eq. (2.28) the minimization of the quadratic error

$$\hat{\mathbf{x}}^{WLS} = \arg\min_{\mathbf{x}} \big[\mathbf{z} - \mathbf{h}(\mathbf{x})\big]^T \mathbf{R}^{-1} \big[\mathbf{z} - \mathbf{h}(\mathbf{x})\big] \tag{2.31}$$

is under consideration, where $\mathbf{R}^{-1}$ is a weighting matrix and here is the inverse of the measurement error covariance matrix. It is noted that the problem of Eq. (2.31) is termed as *weighted LS* (WLS), which is an extension of the general LS problem. Using a first order Taylor series expansion, the problem of Eq. (2.31) can be solved iteratively by

$$\hat{\mathbf{x}}_{j+1} = \hat{\mathbf{x}}_j + (\mathbf{H}_j^T \mathbf{R}^{-1} \mathbf{H}_j)^{-1} \mathbf{H}_j^T \mathbf{R}^{-1} \big[\mathbf{z} - \mathbf{h}(\hat{\mathbf{x}}_j)\big] \tag{2.32}$$

where $\mathbf{H}_j$ is the Jacobian matrix of $\mathbf{h}(\mathbf{x})$ at iteration j

$$\mathbf{H}_j = \left.\frac{\partial \mathbf{h}(\mathbf{x})}{\partial \mathbf{x}}\right|_{\hat{\mathbf{x}}_j} \tag{2.33}$$

The above solution, Eq. (2.32), is referred to as the *iterated least squares* (ILS) estimator, which iteratively updates the estimate using the measurements until convergence is achieved. For different types of measurements, the Jacobian matrix defined in Eq. (2.33) (refer to Appendix A.1 for the derivation of the Jacobian matrix) has different forms as the following:

TOA:

$$\mathbf{H}_{j,TOA} = \begin{bmatrix} \frac{x-x_1}{d_1} & \frac{y-y_1}{d_1} \\ \frac{x-x_2}{d_2} & \frac{y-y_2}{d_2} \\ \vdots & \vdots \\ \frac{x-x_n}{d_n} & \frac{y-y_n}{d_n} \end{bmatrix} \tag{2.34}$$

TDOA:

$$\mathbf{H}_{j,TDOA} = \begin{bmatrix} \frac{x-x_1}{d_1} - \frac{x-x_0}{d_0} & \frac{y-y_1}{d_1} - \frac{y-y_0}{d_0} \\ \frac{x-x_2}{d_2} - \frac{x-x_0}{d_0} & \frac{y-y_2}{d_2} - \frac{y-y_0}{d_0} \\ \vdots & \vdots \\ \frac{x-x_{n-1}}{d_{n-1}} - \frac{x-x_0}{d_0} & \frac{y-y_{n-1}}{d_{n-1}} - \frac{y-y_0}{d_0} \end{bmatrix} \tag{2.35}$$

AOA:

$$\mathbf{H}_{j,AOA} = \begin{bmatrix} -\dfrac{y-y_1}{d_1^2} & \dfrac{x-x_1}{d_1^2} \\ -\dfrac{y-y_2}{d_2^2} & \dfrac{x-x_2}{d_2^2} \\ \vdots & \vdots \\ -\dfrac{y-y_n}{d_n^2} & \dfrac{x-x_n}{d_n^2} \end{bmatrix} \tag{2.36}$$

RSS:

$$\mathbf{H}_{j,RSS} = \begin{bmatrix} \dfrac{38(\tilde{x}-\tilde{x}_1)}{\ln 10 \cdot \tilde{d}_1^2} & \dfrac{38(\tilde{y}-\tilde{y}_1)}{\ln 10 \cdot \tilde{d}_1^2} \\ \dfrac{38(\tilde{x}-\tilde{x}_2)}{\ln 10 \cdot \tilde{d}_2^2} & \dfrac{38(\tilde{y}-\tilde{y}_2)}{\ln 10 \cdot \tilde{d}_2^2} \\ \vdots & \vdots \\ \dfrac{38(\tilde{x}-\tilde{x}_n)}{\ln 10 \cdot \tilde{d}_n^2} & \dfrac{38(\tilde{y}-\tilde{y}_n)}{\ln 10 \cdot \tilde{d}_n^2} \end{bmatrix} \tag{2.37}$$

where $d_i = \sqrt{(x-x_i)^2 + (y-y_i)^2}$ stands for the distance from the MS to the i^{th} BTS and $d_0 = \sqrt{(x-x_0)^2 + (y-y_0)^2}$ indicates the distance from the MS to a reference BTS used for TDOA measurements. The 'tilde' notations represent the normalized values. The above Jacobians are evaluated at $\hat{\mathbf{x}}_j$.

Instead of using Taylor series to linearize the nonlinear function, numerical search methods, such as steepest descent and Gauss-Newton, can also be applied to solve the nonlinear optimization problem (Eq. 2.31), and a similar solution can be obtained [7]. In addition, the nonlinear LS problem can also be transfered to a linear LS problem by subtracting and rearranging the measurement equations. In [8], explicit LS formulations for different types of measurements are given.

Maximum Likelihood

The ML method is an alternative way to estimate the position from the measurements modeled as shown in Eq. (2.28), which maximize the likelihood function

$$\hat{\mathbf{x}}^{ML} = \arg\max_{\boldsymbol{\xi}} \Lambda(\boldsymbol{\xi}) = \arg\max_{\boldsymbol{\xi}} f_{\mathbf{z}|\mathbf{x}}(\boldsymbol{\zeta}|\boldsymbol{\xi}) \tag{2.38}$$

Assuming that the measurement noise has zero-mean white Gaussian form as shown in Eq. (2.30), the likelihood function is given by

$$\Lambda(\boldsymbol{\xi}) = \prod_{i=1}^{n} f_{z_i|\mathbf{x}}(\zeta_i|\boldsymbol{\xi}) = \prod_{i=1}^{n} c e^{-\frac{1}{2\sigma_i^2}\left[\zeta_i - h_i(\boldsymbol{\xi})\right]^2} \tag{2.39}$$

where c is a normalizing constant. Since maximizing the likelihood function is to minimize $-\ln\left[\Lambda(\boldsymbol{\xi})\right]$, the above optimization problem is now to solve

$$\hat{\mathbf{x}}^{ML} = \arg\min_{\boldsymbol{\xi}} \left\{ -\ln\left[\Lambda(\boldsymbol{\xi})\right] \right\} \tag{2.40}$$

$$= \arg\min_{\boldsymbol{\xi}} \left\{ \sum_{i=1}^{n} \frac{1}{2\sigma_i^2} \left[\zeta_i - h_i(\boldsymbol{\xi})\right]^2 \right\} \tag{2.41}$$

which is the same as the LS formulation in Eq. (2.31). Therefore, the solution can be obtained in analogy to the nonlinear LS method.

Bayesian Estimator

If the prior *probability density function* (pdf) of the parameter to be estimated, which is the MS's position in our work, is known, we can obtain the *a posteriori* pdf using Bayes' formula

$$f_{x|z}(\xi|\zeta) = \frac{f_{z|x}(\zeta|\xi) f_x(\xi)}{f_z(\zeta)} = \frac{1}{c} f_{z|x}(\zeta|\xi) f_x(\xi) \tag{2.42}$$

where c is the normalization constant. According to different optimization cost functions which can be used for estimating the position, there are different Bayesian estimators. The counterpart of the LS estimator is called the *minimum mean square error* (MMSE) estimator

$$\hat{\mathbf{x}}^{MMSE} = \arg\min_{\hat{\mathbf{x}}} \mathbb{E}\left[(\hat{\mathbf{x}} - \mathbf{x})^T (\hat{\mathbf{x}} - \mathbf{x}) | \mathbf{z} = \mathbf{z}_0\right] \tag{2.43}$$

The solution of the above is the conditional mean of $\mathbf{x}$ given the measurements $\mathbf{z}$

$$\hat{\mathbf{x}}^{MMSE} = \mathbb{E}[\mathbf{x}|\mathbf{z} = \mathbf{z}_0] \triangleq \int_{-\infty}^{\infty} \boldsymbol{\xi} f_{\mathbf{x}|\mathbf{z}}(\boldsymbol{\xi}|\mathbf{z}_0) d\boldsymbol{\xi} \tag{2.44}$$

Moreover, the one that corresponds to the ML estimator is the *maximum a posteriori* (MAP) estimator, which is to maximize the posterior pdf

$$\hat{\mathbf{x}}^{MAP} = \arg\max_{\boldsymbol{\xi}} f_{\mathbf{x}|\mathbf{z}}(\boldsymbol{\xi}|\boldsymbol{\zeta}) = \arg\max_{\boldsymbol{\xi}} \left[f_{\mathbf{z}|\mathbf{x}}(\boldsymbol{\zeta}|\boldsymbol{\xi}) f_{\mathbf{x}}(\boldsymbol{\xi})\right] \tag{2.45}$$

The normalization constant c in Eq. (2.42) is irrelevant to the maximization, therefore it is not considered. Under the Gaussian assumption, the MMSE estimator is equal to the MAP estimator.

Cramér-Rao Lower Bound

As is well known, the *Cramér-Rao lower bound* (CRLB) sets a lower limit on the mean square error of any unbiased estimator

$$\mathbb{E}\left\{\left[\hat{\mathbf{x}}(\mathbf{z})-\mathbf{x}\right]\left[\hat{\mathbf{x}}(\mathbf{z})-\mathbf{x}\right]^T\right\} \geq \mathbf{J}^{-1} \tag{2.46}$$

where $\hat{\mathbf{x}}(\mathbf{z})$ indicates the estimate of $\mathbf{x}$ based on the measurement of $\mathbf{z}$, and $\mathbf{J}$ stands for *Fisher information matrix* (FIM). The inequality $\mathbf{A} \geq \mathbf{B}$ denotes that the matrix $\mathbf{A}-\mathbf{B}$ is non-negative definite. Considering the multidimensional parameters and measurements, Eq. (2.46) is given in vector form and the scalar form can refer to [64,65]. On the base of the parameters to be estimated are *nonrandom* or *random*, there are two different CRLBs, *parametric* CRLB and *posterior* CRLB [66].

For nonrandom vector parameters, the FIM depends on the likelihood function $\Lambda(\boldsymbol{\xi}) = f_{\mathbf{z}|\mathbf{x}}(\boldsymbol{\zeta}|\boldsymbol{\xi})$

$$\mathbf{J} \triangleq -\mathbb{E}\left\{\nabla_{\boldsymbol{\xi}}\nabla_{\boldsymbol{\xi}}^T \ln \Lambda(\boldsymbol{\xi})\right\}\Big|_{\boldsymbol{\xi}=\boldsymbol{\xi}_{true}} \tag{2.47}$$

$$= \mathbb{E}\left\{\left[\nabla_{\boldsymbol{\xi}} \ln \Lambda(\boldsymbol{\xi})\right]\left[\nabla_{\boldsymbol{\xi}} \ln \Lambda(\boldsymbol{\xi})\right]^T\right\}\Big|_{\boldsymbol{\xi}=\boldsymbol{\xi}_{true}} \tag{2.48}$$

where $\nabla_{\boldsymbol{\xi}}$ denotes the gradient operator with respect to $\boldsymbol{\xi}$ (see Appendix A.1). The expectation is taken over the measurements $\mathbf{z}$. $\boldsymbol{\xi}_{true}$ is the true value vector of the parameters.

For random vector parameters, the FIM is calculated by the joint pdf $f_{\mathbf{z},\mathbf{x}}(\boldsymbol{\zeta}, \boldsymbol{\xi})$

$$\mathbf{J} \triangleq -\mathbb{E}\left\{\nabla_{\boldsymbol{\xi}}\nabla_{\boldsymbol{\xi}}^T \ln f_{\mathbf{z},\mathbf{x}}(\boldsymbol{\zeta}, \boldsymbol{\xi})\right\}\Big|_{\boldsymbol{\xi}=\boldsymbol{\xi}_{true}} \tag{2.49}$$

$$= \mathbb{E}\left\{\left[\nabla_{\boldsymbol{\xi}} \ln f_{\mathbf{z},\mathbf{x}}(\boldsymbol{\zeta}, \boldsymbol{\xi})\right]\left[\nabla_{\boldsymbol{\xi}} \ln f_{\mathbf{z},\mathbf{x}}(\boldsymbol{\zeta}, \boldsymbol{\xi})\right]^T\right\}\Big|_{\boldsymbol{\xi}=\boldsymbol{\xi}_{true}} \tag{2.50}$$

where the expectation is taken over the measurements $\mathbf{z}$ and the random parameters $\mathbf{x}$. Since $f_{\mathbf{z},\mathbf{x}}(\boldsymbol{\zeta}, \boldsymbol{\xi}) = f_{\mathbf{z}|\mathbf{x}}(\boldsymbol{\zeta}|\boldsymbol{\xi}) f_{\mathbf{x}}(\boldsymbol{\xi})$, the FIM in Eq. (2.49) can be decomposed into two terms

$$\mathbf{J} = \mathbf{J}_D + \mathbf{J}_P \tag{2.51}$$

where $\mathbf{J}_D$ represents the information from the measurements and $\mathbf{J}_P$ denotes the information of the prior distribution of the parameters.

$$\mathbf{J}_D = \mathbb{E}\left\{\left[\nabla_{\boldsymbol{\xi}} \ln f_{\mathbf{z}|\mathbf{x}}(\boldsymbol{\zeta}|\boldsymbol{\xi})\right]\left[\nabla_{\boldsymbol{\xi}} \ln f_{\mathbf{z}|\mathbf{x}}(\boldsymbol{\zeta}|\boldsymbol{\xi})\right]^T\right\}\Big|_{\boldsymbol{\xi}=\boldsymbol{\xi}_{true}} \tag{2.52}$$

$$\mathbf{J}_P = \mathbb{E}\left\{\left[\nabla_{\boldsymbol{\xi}} \ln f_{\mathbf{x}}(\boldsymbol{\xi})\right]\left[\nabla_{\boldsymbol{\xi}} \ln f_{\mathbf{x}}(\boldsymbol{\xi})\right]^T\right\}\Big|_{\boldsymbol{\xi}=\boldsymbol{\xi}_{true}} \tag{2.53}$$

Reference [45] gives a CRLB accuracy analysis of the multilateration techniques including TOA, TDOA and hybrid solution for the LOS cases. In [46] the CRLBs for different measurements including TOA, TDOA, RSS and AOA in non-line-of-sight environment are explicitly discussed.

2.4.2 Dynamic Estimation

As opposed to the static estimation, by knowing the movement characteristics of the target over a period of time or the temporal correlation of the position, the target's position of the next time can be predicted. This estimation problem is called *state estimation* and formulated as follows

$$\mathbf{x}(k+1) = \mathbf{f}\big[\mathbf{x}(k)\big] + \mathbf{w}(k) \tag{2.54}$$

$$\mathbf{z}(k) = \mathbf{h}\big[\mathbf{x}(k)\big] + \mathbf{v}(k) \tag{2.55}$$

where Eq. (2.54) is the dynamic model and $\mathbf{f}[\cdot]$ is a nonlinear vector-valued mapping function. For the application of target tracking, it is reasonable to include the dynamics of the target into the estimation. Therefore, the work in this thesis is based on the problem formulation of Eqs. (2.54) and (2.55). The general dynamic models for the ground target tracking, an appropriate filter for the estimation, i.e., Kalman filter, and the corresponding posterior CRLB will be introduced in Chapter 3.

2.5 Accuracy Criteria

To evaluate the performance of a mobile positioning system using wireless communication networks, many considerations arise [14, 67]. The most important factor of the performance should be quality of service, which can be characterized by the accuracy of the computed location. Another important factor is grade of service, for which blocking rate can be used as a measure of the instances when there are missing calls or the location determination is above the system requirement for accuracy. The coverage of a positioning system is an area that is provided with an acceptable level of service by the system. Moreover, other performance measures should also be considered like delays of the location calculation and capacity, which represents the expected number calls the location system is designed to handle. Here we summarize some important accuracy criteria using statistical approaches.

2.5.1 Root Mean Square Error

The *root mean square error* (RMSE) in two dimensions is given by

$$RMSE = \sqrt{\frac{\sum_{i=1}^{N}(\hat{x}_i - x)^2 + (\hat{y}_i - y)^2}{N}} = \sqrt{\mathbb{E}\left[(\hat{x} - x)^2 + (\hat{y} - y)^2\right]} \quad (2.56)$$

where (x, y) indicates the real position of the MS, and $(\hat{x}, \hat{y})$ stands for the estimated position of the MS, the subscript i denotes the i^{th} of N realizations. Assuming that the position estimate error in each dimension is a zero-mean Gaussian distribution with equal variance

$$e_x = (\hat{x} - x) \sim \mathcal{N}(0, \sigma^2) \quad (2.57)$$

$$e_y = (\hat{y} - y) \sim \mathcal{N}(0, \sigma^2) \quad (2.58)$$

and they are independent, the joint pdf $f_{e_x,e_y}(\eta_x, \eta_y)$ is the product of the single pdfs

$$f_{e_x,e_y}(\eta_x, \eta_y) = f_{e_x}(\eta_x) \cdot f_{e_y}(\eta_y) = \frac{1}{2\pi\sigma^2} e^{-(\eta_x^2+\eta_y^2)/2\sigma^2} \quad (2.59)$$

Then we have

$$RMSE = \sqrt{\sigma^2 + \sigma^2} \quad (2.60)$$

which is equal to $\sqrt{2}\sigma$.

2.5.2 FCC Requirements for E911

In 1999, the United States FCC revised and tightened the E911 Phase II location accuracy requirements from no more than 125 m for 67 percent of all calls to the following [1]:

- For network-based solutions: 100 m for 67% of calls, 300 m for 95% of calls
- For handset-based solutions: 50 m for 67% of calls, 150 m for 95% of calls

This is often interpreted by the *radial error*

$$e_r = \sqrt{(\hat{x} - x)^2 + (\hat{y} - y)^2} \quad (2.61)$$

which is a random variable. If the *cumulative density function* (CDF) of e_r is determined, then the error at certain percentile, i.e., 67% and 95% will

be compared with the corresponding threshold in the requirement, e.g., for network-based solutions 100 m and 300 m, respectively. In the document [68], some approaches of testing and verifying the accuracy using this standard are given.

In contrast to using the RMSE, where a very small number of relatively large errors will result in a big RMSE since all calls would be used for the error evaluation, the FCC requirement, which is a dual ring method, ignores the 5 percent of calls with the largest errors. Also, the dual ring approach dose not square the errors, a procedure in RMSE that gives greater weight to large errors. Therefore, when there are outliers in the positioning, i.e., the estimate is not Gaussian distributed any more, the dual ring approach is more reasonable than the RMSE criterion.

However, when the Gaussian assumption, Eqs. (2.57) and (2.58), holds, these two approaches are directly connected. Since now the radial error e_r is Rayleigh distributed, the 67% percentile error is about 1.05 RMSE and the 95% percentile error is about 1.73 RMSE.

Considering that the RMSE method is also widely used for other positioning systems, in this thesis we mainly use it to assess the accuracy performance of the position estimation.

2.5.3 Geometric Dilution of Precision

The conception of the *geometric dilution of precision* (GDOP) starts from the use of GPS and it is defined as the geometry factor that relates parameters of the user position and time bias errors to those of the pseudorange errors. Usually the measurement error is assumed to be Gaussian, zero mean, and identically distributed. Then the error covariance matrix of the state to be estimated (for GPS positioning it is normally denoted by $\delta\mathbf{x}$, which is the difference of the state and a nominal state value for linearization [65]) is given by

$$\mathbf{P} = \left[\mathbf{H}^T\mathbf{H}\right]^{-1}\sigma^2 \tag{2.62}$$

where σ^2 is the variance of the measurement errors and the measurement matrix $\mathbf{H}$ depends only on the relative geometry of the satellites and the receiver. The GDOP is then defined as

$$GDOP = \sqrt{tr\left[(\mathbf{H}^T\mathbf{H})^{-1}\right]} \tag{2.63}$$

Based on Eq. (2.63), other DOPs are also defined, such as *position DOP* (PDOP), *horizontal DOP* (HDOP), *vertical DOP* (VDOP), and *time DOP* (TDOP).

Considering the TOA measurement defined in Eq. (2.4), the $\mathbf{H}$ matrix is the Jacobian matrix of the measurement function, see [21] for the derivation,

$$\mathbf{H} = \begin{bmatrix} \frac{x-x_1}{\sqrt{(x-x_1)^2+(y-y_1)^2}} & \frac{y-y_1}{\sqrt{(x-x_1)^2+(y-y_1)^2}} \\ \frac{x-x_2}{\sqrt{(x-x_2)^2+(y-y_2)^2}} & \frac{y-y_2}{\sqrt{(x-x_2)^2+(y-y_2)^2}} \\ \vdots & \vdots \\ \frac{x-x_n}{\sqrt{(x-x_n)^2+(y-y_n)^2}} & \frac{y-y_n}{\sqrt{(x-x_n)^2+(y-y_n)^2}} \end{bmatrix} \tag{2.64}$$

For this TOA measurement, the GDOP is also equal to the PDOP and HDOP. In reference [45] the GDOPs for TOA, TDOA and hybrid approaches are discussed.

It should be noted that a higher value of GDOP means a poor geometry, whereas a lower value indicates a better geometry. In addition, as shown in Eq. (2.62), the relative bigger GDOP will degrade the estimation accuracy. For example, to optimize a communication system the wireless base stations are placed along highways. For comparable measurement errors,such linear geometry will lead to larger errors in positioning. When the Gaussian assumption, Eqs. (2.57) and (2.58), holds, GDOP is the RMSE normalized with the measurement precision. Thus, the concept of GDOP is connected with RMSE and also the FCC requirement.

2.6 Summary

The attributes of the signals transmitted between the MS and multiple BTSs can contribute to the position estimation, mainly including TOA, TDOA, AOA and RSS. The position estimation can be divided into static estimation and dynamic estimation depending on whether the target motion with respect to time is considered. This chapter mainly introduces the static estimation problem, which is also called parameter estimation. Further, non-Bayesian or Bayesian estimators are applied according to modeling the parameters as nonrandom unknown constants or random variables and the corresponding lower bounds are parametric CRLB or posterior CRLB.

The radio propagation environment is complicated and the multipath and NLOS propagation greatly degrades the positioning. Mitigation algorithms should be applied before or with the position estimation. To evaluate the performance of the position estimation, accuracy criteria are introduced.

RMSE is used as the main performance criteria in this thesis since it is widely used for the positioning systems and tracking problems. The FCC requirements for E911 are also important since it is the first standard of positioning using mobile cellular networks. Another term GDOP, mainly used in GPS field, is also introduced. The connection between these criteria is also presented.

Chapter 3

A Data Fusion Solution for Ground Target Tracking

Ground target tracking has different characteristics from other types of target tracking like air targets (detailed comparisons can be found in reference [69]). The motion of ground targets is generally two dimensional, whereas air targets move in the three-dimensional space. Ground targets can be very close to each other, but the air targets should keep distance for safety. The ground target may be obscured by terrain and buildings. For instance, there may be only *non-line-of-sight* (NLOS) propagation from a BTS to a MS, whereas the detection of air targets are less affected by the terrain. Most importantly, the ground target motion is far more variable than the air target motion. Due to the restriction of the terrain, road and traffic, the ground target may frequently start, accelerate, decelerate, stop, or turn on the road, i.e., the state to be estimated may change dramatically. Therefore, the ground target has a distinctive feature of high maneuverability and a proper target dynamic model, which describes the evolution of the target state $\mathbf{x}$ with respect to the time, is very important for tracking the ground target. If the dynamic model matches the motion of the target very well, the estimation will be greatly benefiting from the dynamic information. Otherwise, a wrong dynamic model will degrade the estimation performance.

In this chapter, first the dynamic models are described and the state estimation using *extended Kalman filter* (EKF) is introduced. Then the *posterior Cramér-Rao lower bound* (PCRLB) for the target tracking is derived in Section 3.3. In Section 3.4, a data fusion approach integrating two types of measurements is presented and simulation results are given in Section 3.5. In Section 3.6, the PCRLB for the data fusion approach is derived and the performance of different methods is analyzed in terms of PCRLB.

3.1 Target Dynamic Models

The most well-known representative dynamic models are *nearly constant velocity* (CV), *nearly constant acceleration* (CA), *Singer*, and *coordinated turn* (CT) models [70]. To describe these models, firstly a generic state-space target motion model in discrete time is given by

$$\mathbf{x}(k+1) = \mathbf{F}(k)\mathbf{x}(k) + \mathbf{G}(k)\mathbf{w}(k) \tag{3.1}$$

where k denotes the discrete-time index. $\mathbf{x}(k)$, $\mathbf{F}(k)$, $\mathbf{G}(k)$, and $\mathbf{w}(k)$ stand for the target state vector, state transition matrix, noise Gain matrix and process noise vector, respectively, and they have different forms for different models as follows.

3.1.1 Nearly Constant Velocity Model

The state vector $\mathbf{x} = \begin{bmatrix} x & \dot{x} & y & \dot{y} \end{bmatrix}^T$ includes the position and velocity in two dimensions. The state transition matrix is

$$\mathbf{F}_{CV} = \text{diag}[\mathbf{F}_1, \mathbf{F}_1] \tag{3.2}$$

$$\mathbf{F}_1 = \begin{bmatrix} 1 & T \\ 0 & 1 \end{bmatrix} \tag{3.3}$$

where T indicates the sampling interval. The noise gain matrix $\mathbf{G}_{CV} = \text{diag}[\mathbf{G}_1, \mathbf{G}_1]$, and $\mathbf{G}_1 = \begin{bmatrix} \frac{1}{2}T^2 & T \end{bmatrix}^T$. The process noise $\mathbf{w}(k) = \begin{bmatrix} w_x(k) & w_y(k) \end{bmatrix}^T$ is assumed to be zero-mean white Gaussian noise where the elements correspond to the accelerations in two dimensions. The CV model is usually used for *nonmaneuvering motion* (*uniform motion*), which is a straight and level motion at a constant velocity. It can be also used for a maneuvering motion where the target acceleration is assumed to be white noise and the maneuver is small.

3.1.2 Nearly Constant Acceleration Model

The state vector for CA model $\mathbf{x} = \begin{bmatrix} x & \dot{x} & \ddot{x} & y & \dot{y} & \ddot{y} \end{bmatrix}^T$ contains the position, velocity and acceleration in two dimensions. The state transition matrix is

$$\mathbf{F}_{CA} = \text{diag}[\mathbf{F}_2, \mathbf{F}_2] \tag{3.4}$$

$$\mathbf{F}_2 = \begin{bmatrix} 1 & T & \frac{1}{2}T^2 \\ 0 & 1 & T \\ 0 & 0 & 1 \end{bmatrix} \tag{3.5}$$

The noise gain matrix is $\mathbf{G}_{CA} = \text{diag}[\mathbf{G}_2, \mathbf{G}_2]$, where $\mathbf{G}_2 = \begin{bmatrix}\frac{1}{2}T^2 & T & 1\end{bmatrix}^T$. The process noise $\mathbf{w}(k) = \begin{bmatrix}w_x(k) & w_y(k)\end{bmatrix}^T$ is assumed to be zero-mean white Gaussian noise representing acceleration increments, which means that the acceleration is modeled as a Wiener process.

3.1.3 Singer Model

Not modeling the acceleration as a white noise or a wiener process like the CV and CA model, the Singer model assumes that the target acceleration $a(t)$ is a zero-mean stationary first-order Markov process with autocorrelation

$$\Psi_a(\tau) = \mathbb{E}\left[a(t+\tau)a(t)\right] = \sigma^2 e^{-\alpha|\tau|} \tag{3.6}$$

The time evolution of the acceleration in discrete time is written as

$$\ddot{x}(k+1) = \beta\ddot{x}(k) + w(k) \tag{3.7}$$

where $w(k)$ is a zero-mean white noise sequence with variance $\sigma^2(1-\beta^2)$ and $\beta = e^{-\alpha T}$. The state vector is identical to the CA model, and the state transition matrix is

$$\mathbf{F}_{Singer} = \text{diag}[\mathbf{F}_3, \mathbf{F}_3] \tag{3.8}$$

$$\mathbf{F}_3 = \begin{bmatrix}1 & T & (\alpha T - 1 + e^{-\alpha T})/\alpha^2 \\ 0 & 1 & (1-e^{-\alpha T})/\alpha \\ 0 & 0 & e^{-\alpha T}\end{bmatrix} \tag{3.9}$$

The exact covariance of the process noise is a function of α and T [65]. Therefore, the important part of building a Singer model is designing the parameters α, which depends on the period of the maneuver, and σ^2, which is the instantaneous variance of the acceleration [65, 70]. As the maneuver time constant increases, the Singer model reduces to the CA model, whereas it reduces to the CV model when the maneuver time decreases.

3.1.4 Coordinated Turn Model

The CT model is built for circular motion and assumes that the target speed and turn rate are nearly constant. The state vector $\mathbf{x} = \begin{bmatrix}x & \dot{x} & y & \dot{y} & \omega\end{bmatrix}^T$ consists of the position and velocity in two dimensions, and the turn rate.

The state transition matrix is

$$\mathbf{F}_{CT} = \begin{bmatrix} 1 & \frac{\sin(\omega T)}{\omega} & 0 & -\frac{1-\cos(\omega T)}{\omega} & 0 \\ 0 & \cos(\omega T) & 0 & -\sin(\omega T) & 0 \\ 0 & \frac{1-\cos(\omega T)}{\omega} & 1 & \frac{\sin(\omega T)}{\omega} & 0 \\ 0 & \sin(\omega T) & 0 & \cos(\omega T) & 0 \\ 0 & 0 & 0 & 0 & 1 \end{bmatrix} \tag{3.10}$$

The noise gain matrix is $\mathbf{G}_{CT} = \text{diag}[\mathbf{G}_1, \mathbf{G}_1, T]$. The process noise $\mathbf{w}(k) = \begin{bmatrix} w_x(k) & w_y(k) & w_\omega(k) \end{bmatrix}^T$ includes noise terms for accelerations in x and y directions and for turn rate, and it is assumed to be zero-mean white Gaussian noise.

3.1.5 Curvilinear Model

Besides the standard motion models introduced above, another turn motion model is a first-order Euler discretization of the generic continuous-time curvilinear motion model from kinematics [71, 72], which can be used for describing either a straight or a turn motion.

$$\mathbf{x}(k+1) = \mathbf{f}\big[\mathbf{x}(k)\big] + \mathbf{w}(k) \tag{3.11}$$

$$\mathbf{f}\big[\mathbf{x}(k)\big] = \begin{bmatrix} x(k) + Tv(k)\cos\big(\phi(k)\big) \\ y(k) + Tv(k)\sin\big(\phi(k)\big) \\ v(k) + Ta_t(k) \\ \phi(k) + Ta_n(k)/v(k) \end{bmatrix} \tag{3.12}$$

where the state vector $\mathbf{x} = \begin{bmatrix} x & y & v & \phi \end{bmatrix}^T$ includes the target position in two dimensions, speed v and heading ϕ. a_t and a_n denote tangential (along-track) and normal (cross-track) accelerations, respectively. The process noise $\mathbf{w}(k) = \begin{bmatrix} w_x(k) & w_y(k) & w_v(k) & w_\phi(k) \end{bmatrix}^T$ is assumed to be zero-mean white Gaussian noise. In fact the CV, CA and CT models are special cases of this generic curvilinear model when the tangential and normal accelerations are set to different values [70].

3.2 State Estimation Using EKF

The main task of target tracking is state estimation which consists of prediction and correction. While the prediction depends on the dynamic information of the target, the correction relies on the measurements obtained at

each time step. Usually, the Kalman filter addresses the general problem of estimating the state of a discrete-time controlled process described by a linear model. In some applications, however, the state transition and/or the mapping of the states into the observation space is nonlinear. The state transition with respect to time and the relationship between the state vector $\mathbf{x} \in \Re^n$ and the measurement vector $\mathbf{z} \in \Re^m$ are given by

$$\mathbf{x}(k+1) = \mathbf{f}\big[\mathbf{x}(k)\big] + \mathbf{G}(k)\mathbf{w}(k) \tag{3.13}$$

$$\mathbf{z}(k) = \mathbf{h}\big[\mathbf{x}(k)\big] + \mathbf{v}(k) \tag{3.14}$$

where $\mathbf{w}(k)$ and $\mathbf{v}(k)$ indicate the driving noise and measurement noise, respectively. They are assumed to be zero-mean white Gaussian noises and characterized by their covariance matrices.

$$\mathbb{E}\left\{\mathbf{w}(k)\right\} = 0, \;\; \mathbb{E}\left\{\mathbf{w}(k) \cdot \mathbf{w}(j)^T\right\} = \mathbf{Q}(k) \cdot \delta(k-j) \tag{3.15}$$

$$\mathbb{E}\left\{\mathbf{v}(k)\right\} = 0, \;\; \mathbb{E}\left\{\mathbf{v}(k) \cdot \mathbf{v}(j)^T\right\} = \mathbf{R}(k) \cdot \delta(k-j) \tag{3.16}$$

where $\mathbf{Q}(k)$ denotes the covariance matrix of the driving noise and $\mathbf{R}(k)$ stands for the covariance matrix of the measurement noise. Then the EKF formulated for nonlinear situations is given by the following equations:

Prediction:

$$\hat{\mathbf{x}}^-(k+1) = \mathbf{f}\big[\hat{\mathbf{x}}^+(k)\big] \tag{3.17}$$

$$\mathbf{P}^-(k+1) = \mathbf{F}(k)\mathbf{P}^+(k)\mathbf{F}^T(k) + \mathbf{G}(k)\mathbf{Q}(k)\mathbf{G}(k)^T \tag{3.18}$$

Correction:

$$\begin{aligned}\mathbf{K}(k+1) &= \mathbf{P}^-(k+1)\mathbf{H}^T(k+1) \\ &\quad \cdot \big[\mathbf{H}(k+1)\mathbf{P}^-(k+1)\mathbf{H}^T(k+1) + \mathbf{R}(k+1)\big]^{-1}\end{aligned} \tag{3.19}$$

$$\mathbf{r}(k+1) = \mathbf{z}(k+1) - \mathbf{h}\big[\hat{\mathbf{x}}^-(k+1)\big] \tag{3.20}$$

$$\hat{\mathbf{x}}^+(k+1) = \hat{\mathbf{x}}^-(k+1) + \mathbf{K}(k+1)\mathbf{r}(k+1) \tag{3.21}$$

$$\mathbf{P}^+(k+1) = \mathbf{P}^-(k+1) - \mathbf{K}(k+1)\mathbf{H}(k+1)\mathbf{P}^-(k+1) \tag{3.22}$$

where $\hat{\mathbf{x}}^-(k+1)$ and $\mathbf{P}^-(k+1)$ represent the predicted state estimate and state error covariance, $\hat{\mathbf{x}}^+(k+1)$ and $\mathbf{P}^+(k+1)$ denote the updated state estimate and associated state error covariance, respectively. $\mathbf{K}(k+1)$ indicates the designated Kalman gain and $\mathbf{r}(k+1)$ denotes the measurement residual vector. $\mathbf{F}(k)$ is the Jacobian matrix of $\mathbf{f}[\cdot]$

$$\mathbf{F}(k) = \left.\frac{\partial \mathbf{f}\big[\mathbf{x}(k)\big]}{\partial \mathbf{x}(k)}\right|_{\hat{\mathbf{x}}^+(k)} \tag{3.23}$$

and $\mathbf{H}(k+1)$ indicates the Jacobian matrix of $\mathbf{h}[\cdot]$

$$\mathbf{H}(k+1) = \left.\frac{\partial \mathbf{h}\big[\mathbf{x}(k+1)\big]}{\partial \mathbf{x}(k+1)}\right|_{\hat{\mathbf{x}}^{-}(k+1)} \tag{3.24}$$

The initial value of the estimate is given by

$$\mathbb{E}\left\{\hat{\mathbf{x}}(0)^{+}\right\} = \mathbb{E}\left\{\mathbf{x}(0)\right\} \tag{3.25}$$

$$\mathbb{E}\left\{\mathbf{P}(0)^{+}\right\} = \mathbb{E}\left\{\big(\mathbf{x}(0) - \hat{\mathbf{x}}(0)\big)\big(\mathbf{x}(0) - \hat{\mathbf{x}}(0)\big)^{T}\right\} \tag{3.26}$$

3.3 Posterior CRLB for Target Tracking

The *Cramér-Rao lower bound* (CRLB) is useful to predict the best achievable performance before designing any estimator and to provide a benchmark of assessing different estimation algorithms. As introduced in Section 2.4.1, the *parametric CRLB* is used for nonrandom parameters, whereas the *posterior CRLB* (PCRLB) is a lower bound for random parameters. Obviously in the context of positioning, the parameters to be estimated, mainly position and velocity, should be considered as random, and thus PCRLB should be analyzed.

Similar to the parametric CRLB, PCRLB is the lower bound of the mean square error of any unbiased estimator

$$\mathbb{E}\left\{\big[\hat{\mathbf{x}}(\mathbf{z}) - \mathbf{x}\big]\big[\hat{\mathbf{x}}(\mathbf{z}) - \mathbf{x}\big]^{T}\right\} \geq \mathbf{J}^{-1} \tag{3.27}$$

The bound is the inverse of the *Fisher information matrix* (FIM) $\mathbf{J}^{-1}$. The difference is that the PCRLB depends on the joint probability density of the state and observation vector $f_{\mathbf{z},\mathbf{x}}(\boldsymbol{\zeta}, \boldsymbol{\xi})$, whereas the parametric CRLB depends on the likelihood $f_{\mathbf{z}|\mathbf{x}}(\boldsymbol{\zeta}|\boldsymbol{\xi})$ and the unknown parameter. Using the conditional equation, the FIM $\mathbf{J}$ can be decomposed into the information obtained from the observation data, and the *a priori* information, shown in Eqs. (2.49)-(2.52).

The problem of target tracking is a nonlinear filtering problem modeled as Eqs. (3.13) and (3.14). The FIM can be written as a sequence of the FIM at each time step $\big\{\mathbf{J}(0), \mathbf{J}(1), \cdots, \mathbf{J}(k)\big\}$ for the corresponding target state $\big\{\mathbf{x}(0), \mathbf{x}(1), \cdots, \mathbf{x}(k)\big\}$, respectively. By using submatrix techniques, $\mathbf{J}(k)$ can be calculated recursively from the FIM of the last time step $\mathbf{J}(k-1)$ [73].

After some derivations (see Appendix B), the final PCRLB recursion formula for the nonlinear problem with additive Gaussian noise is

$$\begin{aligned}\mathbf{J}(k+1) = &\left[\mathbf{Q}(k) + \mathbb{E}\left\{\mathbf{F}(k)\mathbf{J}(k)^{-1}\mathbf{F}(k)^T\right\}\right]^{-1} \\ &+ \mathbb{E}\left\{\mathbf{H}(k+1)^T\mathbf{R}(k+1)^{-1}\mathbf{H}(k+1)\right\}\end{aligned} \tag{3.28}$$

where $\mathbf{F}(k)$ indicates the Jacobian matrix of the vector-valued state transition function $\mathbf{f}[\cdot]$ (Eq. 3.13) evaluated at the real value of state $\mathbf{x}(k)$.

$$\mathbf{F}(k) \triangleq \left.\frac{\partial \mathbf{f}\left[\mathbf{x}(k)\right]}{\partial \mathbf{x}(k)}\right|_{\mathbf{x}(k)} \tag{3.29}$$

$\mathbf{H}(k+1)$ denotes the Jacobian matrix of the vector-valued nonlinear measurement function $\mathbf{h}[\cdot]$ (Eq. 3.14) evaluated at the real value of the state $\mathbf{x}(k+1)$.

$$\mathbf{H}(k+1) \triangleq \left.\frac{\partial \mathbf{h}\left[\mathbf{x}(k+1)\right]}{\partial \mathbf{x}(k+1)}\right|_{\mathbf{x}(k+1)} \tag{3.30}$$

$\mathbf{Q}(k)$ stands for the covariance matrix of process noise, and $\mathbf{R}(k+1)$ denotes the covariance matrix of measurement noise. It should be noted that the Jacobians depend on the random realization of $\mathbf{x}$ and are implicitly random variables. Hence the expectation should be taken over Monte Carlo trials. The initial value of the FIM can be given by the inverse of the covariance matrix of the initial state estimate

$$\mathbf{J}(0) = \mathbf{P}(0)^{-1} \tag{3.31}$$

3.4 A Data Fusion Solution

3.4.1 Data Fusion Structure

As introduced in Chapter 2, since the radio propagation environment, such as urban, suburban and rural, is diverse and complicated, and as the communication signals are usually not designed for positioning, it is difficult to achieve an accurate position estimate relying just on a single type of measurements. Therefore, data fusion solutions which integrate two or more types of measurements have been proposed to provide estimation with better accuracy, reliability and coverage.

Reference [35] used TDOA and TOA measurements to obtain the position estimate. The author also analyzed the accuracy of a mixed approach

using both TOA and TDOA measurements compared with only using TOA measurements and only using TDOA measurements in [45]. The results show that the mixed approach provides the best compromise between robustness and accuracy. A hybrid TDOA/AOA approach is proposed in [33] where a two step LS estimator is applied. In [32], power and time measurements are combined and nonparametric MMSE estimation methods are employed to calculate the position estimate. By using these data fusion approaches, the estimation accuracy can be improved compared with using a single type of measurements since the information from independent sources are combined. The advantages of both types of measurements will be utilized. For example, in the two-dimensional scheme of AOA/TDOA [33], the AOA approach requires only two measurements from two BTSs, and the TDOA approach provides higher accuracy than the AOA approach. Moreover, when one type of measurements is degraded, the required estimation accuracy can still be achieved by the other type of measurements.

However, there are few approaches which consider using data fusion for target tracking in a mobile communication environment. In our work, we propose a data fusion solution to integrate two different types of measurements for dynamic position estimation and the EKF is utilized for this purpose. Considering that the RSS and TOA measurements can be obtained in current GSM networks without significant modifications on the handset and the network, they are employed as an example of this fusion approach. The structure of the data fusion solution is illustrated in Fig. 3.1. The EKF

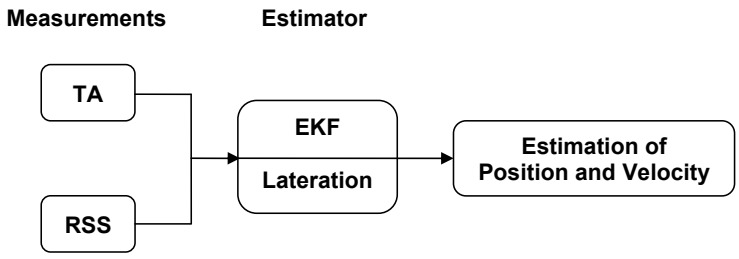

Figure 3.1: The structure of the data fusion solution

provides a convenient structure for integrating different types of measurements by stacking the whole measurements into the vector of measurement functions $\mathbf{h}[\cdot]$ in Eq. (3.14). With the EKF, the lateration techniques are also used. It should be noticed that other measurements, TDOA or AOA, can also be integrated using the proposed data fusion structure.

3.4.2 Dynamic Model and Measurement Model for EKF

The dynamic model should be chosen according to the real trajectory. For the sake of simplicity, a CV model, which is suitable for nonmaneuvering motion or a maneuver motion with small acceleration errors (refer to [70]), can be used. The state vector is $\mathbf{x} = \begin{bmatrix} x & \dot{x} & y & \dot{y} \end{bmatrix}^T$ including the position and velocity in two dimensions.

In general, for two-dimensional positioning, at least three BTSs are required to obtain a unique position estimate. Thus, the TOA and RSS measurements from three BTSs are integrated for the position estimation. Now the measurements, $\mathbf{z} \in \Re^6$, are the distances between the BTSs and the MS according to the TOA measurements and the signal strength losses calculated from the RSS measurements received from three BTSs a, b, and c, whose position coordinates are (x_a, y_a), (x_b, y_b) and (x_c, y_c), respectively. Define the distance between the MS and three BTSs as

$$d_i = \sqrt{(x - x_i)^2 + (y - y_i)^2},\ i = a, b, c \tag{3.32}$$

$$\tilde{d}_i = \frac{d_i}{1 \text{ km}} \tag{3.33}$$

Since NLOS propagation is common in urban area which attracts the most interest for the mobile positioning, the measurement model should consider the tolerance of NLOS propagation. For RSS measurements, a typical propagation loss model, Eq. (2.20), for small cells in urban areas (COST-WI model), which is a NLOS propagation model composed of free space loss, multiple screen diffraction loss, and roof-top-to-street diffraction and scatter loss, is used. For TOA measurements, the NLOS error can be modeled as a bias and it is possible to remove it before the estimation (see Section 2.3.6). Thus, the measurement model for TOA, Eq. (2.4), can be applied. Then the measurement model for EKF (Eq. 3.14) can be written as

$$\mathbf{z}(k) = \mathbf{h}\big[\mathbf{x}(k)\big] + \mathbf{v}(k) \tag{3.34}$$

$$\mathbf{h}\big[\mathbf{x}(k)\big] = \begin{bmatrix} d_a(k) \\ d_b(k) \\ d_c(k) \\ 132.85 + 38 \log_{10}\left(\tilde{d}_a(k)\right) \\ 132.85 + 38 \log_{10}\left(\tilde{d}_b(k)\right) \\ 132.85 + 38 \log_{10}\left(\tilde{d}_c(k)\right) \end{bmatrix} \tag{3.35}$$

where $\mathbf{v}(k)$ stands for a zero-mean white Gaussian noise defined in Eq. (3.16). Since the measurement noises of TOA and RSS measurements are from

different sources, it is reasonable to assume that they are independent from each other. Therefore, the covariance matrix of the measurement noise is $\mathbf{R}(k) = \mathrm{diag}(\sigma_d^2, \sigma_d^2, \sigma_d^2, \sigma_l^2, \sigma_l^2, \sigma_l^2)$. Note that the propagation model is highly dependent on the surrounding environment. So the measurement model for RSS should be updated in real time by specifying several parameters which define the propagation environment (the details are explained in Section 2.3.4).

Once the state transition model and the observation model are established, the EKF of Eqs. (3.17)-(3.22) can be applied, where the Jacobian matrix $\mathbf{H}(k+1)$ is given by

$$\mathbf{H}(k+1) = \begin{bmatrix} \dfrac{\big(x(k+1)-x_a\big)}{d_a(k+1)} & 0 & \dfrac{\big(y(k+1)-y_a\big)}{d_a(k+1)} & 0 \\ \dfrac{\big(x(k+1)-x_b\big)}{d_b(k+1)} & 0 & \dfrac{\big(y(k+1)-y_b\big)}{d_b(k+1)} & 0 \\ \dfrac{\big(x(k+1)-x_c\big)}{d_c(k+1)} & 0 & \dfrac{\big(y(k+1)-y_c\big)}{d_c(k+1)} & 0 \\ \dfrac{38\big(\tilde{x}(k+1)-\tilde{x}_a\big)}{\ln 10 \cdot \big(\tilde{d}_a(k+1)\big)^2} & 0 & \dfrac{38\big(\tilde{y}(k+1)-\tilde{y}_a\big)}{\ln 10 \cdot \big(\tilde{d}_a(k+1)\big)^2} & 0 \\ \dfrac{38\big(\tilde{x}(k+1)-\tilde{x}_b\big)}{\ln 10 \cdot \big(\tilde{d}_b(k+1)\big)^2} & 0 & \dfrac{38\big(\tilde{y}(k+1)-\tilde{y}_b\big)}{\ln 10 \cdot \big(\tilde{d}_b(k+1)\big)^2} & 0 \\ \dfrac{38\big(\tilde{x}(k+1)-\tilde{x}_c\big)}{\ln 10 \cdot \big(\tilde{d}_c(k+1)\big)^2} & 0 & \dfrac{38\big(\tilde{y}(k+1)-\tilde{y}_c\big)}{\ln 10 \cdot \big(\tilde{d}_c(k+1)\big)^2} & 0 \end{bmatrix} \tag{3.36}$$

evaluated at $\hat{\mathbf{x}}^-(k+1)$. The 'tilde' notations denote the normalized values by 1 km.

3.5 Simulation Results

3.5.1 Simulation Scenario

The estimator is tested in a simulated urban square area of 5 km $\times$ 5 km with the environment parameters described in Section 2.3.4. The propagation loss model of Eq. (2.20) typically for a small cell is used for the radio propagation environment simulation. Within this area there are three BTSs, a, b and c , with position coordinates $(x_a, y_a) = (1500\ \mathrm{m}, 2000\ \mathrm{m})$, $(x_b, y_b) = (3500\ \mathrm{m}, 2000\ \mathrm{m})$ and $(x_c, y_c) = (2500\ \mathrm{m}, 4500\ \mathrm{m})$, respectively (see Fig. 3.2). It is supposed that the measurement update is every 480 ms,

$T = 0.48$ s, which is a typical value for the TA parameter in GSM networks. TA is one TOA measurement in GSM networks. The TA measurements and RSS measurements are assumed to be simultaneously obtained by the estimator. It should be noticed that in the current GSM networks only one TA is taken by the serving BTS. To obtain more TA measurements from other BTSs, forced handover must be implemented.

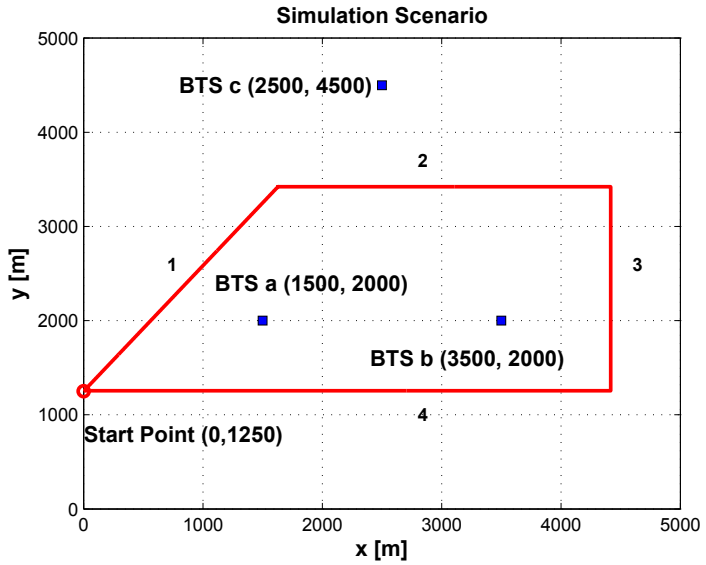

Figure 3.2: Simulation scenario

It is assumed that a vehicle equipped with a MS travels clockwise along a trapezium route starting at the point $(0\text{ m}, 1250\text{ m})$ and made of 4 parts designed for evaluating the performance of the proposed estimator as depicted in Fig. 3.2. The trajectory is generated by the curvilinear motion model, Eqs. (3.11) (3.12), which is called truth model since it represents the real trajectory for the simulation. In the first part, the vehicle first moves under an acceleration of 2 m/s^2 from stationary state, then at a nearly constant speed of about 10 m/s, finally under a deceleration of -2 m/s^2 when it goes to the corner. In part 2, the vehicle moves under an acceleration of 1 m/s^2, then under a deceleration of -1 m/s^2. In part 3, the movement of the vehicle is similar to part 1. In part 4, the vehicle first moves with an acceleration of 2 m/s^2, then at a nearly constant speed of about 20 m/s, and at last decelerates at -2 m/s^2 back to the starting point. The process noise $\mathbf{w}(k) = \begin{bmatrix} w_x(k) & w_y(k) & w_v(k) & w_\phi(k) \end{bmatrix}^T$ is assumed to be zero-mean white Gaussian noise with standard deviations of $\sigma_x = 10^{-4}$ m, $\sigma_y = 10^{-4}$ m, $\sigma_v = 10^{-5}$ m/s, $\sigma_\phi = 10^{-6}$ rad.

3.5.2 EKF Design

Each part of the trajectory in the simulation is a straight motion and during most of the time at nearly constant velocity. As discussed in Section 3.4.2, a CV model is chosen as the state transition model for the EKF. Although the second part of the trajectory is actually a nearly constant acceleration motion, the EKF with CV model can still work by tuning the driving noise to a large value. The measurement model is described by Eqs. (3.34) (3.35), in which three TOA and three RSS measurements are integrated. The driving and measurement noise covariance matrix $\mathbf{Q}(k)$ and $\mathbf{R}(k)$ are set to

$$\mathbf{Q}(k) = \text{diag}(\sigma_x^2, \sigma_y^2) \tag{3.37}$$

$$\mathbf{R}(k) = \text{diag}(\sigma_d^2, \sigma_d^2, \sigma_d^2, \sigma_l^2, \sigma_l^2, \sigma_l^2) \tag{3.38}$$

where σ_d and σ_l stand for the standard deviations of the measurement noises. σ_d is chosen according to the TA error model from the specifications of GSM networks, shown in Eq. (2.6). A typical value is 300 m. The standard deviation of RSS measurement noise σ_l has a typical value of 4-8 dB according to the COST-WI model. The proposed estimator uses one simple CV model to describe the state transition of the MS on the whole route. Unfortunately, in reality the real state of MS has different characteristics, e.g., constant acceleration at the end of each part of the route, thus the standard deviations of the driving noises σ_x and σ_y should be set to different values for different parts of the trajectory as shown in Table 3.1.

Table 3.1: Values of σ_x and σ_y for the different parts of the trajectory

	Part 1	Part 2	Part3	Part 4
σ_x	1 m/s^2	10 m/s^2	10^{-4} m/s^2	1 m/s^2
σ_y	1 m/s^2	10^{-4} m/s^2	1 m/s^2	10^{-4} m/s^2

The initial state values $\hat{x}^+(0)$ and $\hat{y}^+(0)$ of the estimator are calculated by one point measurement [65], which uses a traditional least squares algorithm to achieve an initial position guess from three independent TOA measurements at time step $k = 0$. The initial values of the velocity $\hat{\dot{x}}^+(0)$, $\hat{\dot{y}}^+(0)$ are assumed to be zero-mean Gaussian random variables with an associated standard deviation which is equal to half of the known maximum state values. Then the initial state error covariance matrix is set to be

$$\mathbf{P}^+(0) = \text{diag}\left[\sigma_d^2, (30 \text{ m/s})^2, \sigma_d^2, (30 \text{ m/s})^2\right] \tag{3.39}$$

where the variance elements of the position in two dimensions are set to be the values of the variance of the TOA measurement and the variance elements of the velocity in two dimensions are set to be $(30\ \mathrm{m/s})^2$ as half the value of the possibly biggest velocity.

To prove the advantages of the data fusion approach, two EKF estimators which use only TOA or only RSS measurements are also designed. Each includes three TOA or three RSS measurements from three independent BTSs, respectively. The other parameters of the EKFs are identical to the fusion approach introduced above.

3.5.3 Performance Comparisons

Estimates Compared with True State Values

The estimation results of the proposed estimator, when the standard deviations of the measurement noises are set to be $\sigma_d = 300$ m and $\sigma_l = 4$ dB, are shown in Fig. 3.3. The red lines depict the true state values, $\mathbf{x} = \begin{bmatrix} x & \dot{x} & y & \dot{y} \end{bmatrix}^T$, and the blue curves are the corresponding estimated values by the data fusion approach. The plots show that in all parts of the route the estimator can track the movement of the MS. When the real movement is quite different from the assumption of the proposed state transition model like in part 2, where the real movement is under constant acceleration, whereas the model assumes constant velocity, the estimator can still track the true state value by increasing the driving noise properly. When the real state transition and the model match each other very well, as the state element $\dot{x}$ in part 2 and the state element $\dot{y}$ in part 4, the estimates converge quickly to the real state values. Note that some estimates have relatively big errors although the motion model matches the real movement very well, e.g., the first part. This is because the standard deviation of the driving noise in the EKF is chosen to assume a relatively large values, e.g., 1 $\mathrm{m/s^2}$ for both x and y directions in part 1, in order to cover the maneuvering movement at the beginning and the end of this part of route. Increasing the driving noise makes the estimator more robust to the unpredicted maneuver. However, the CV model can only be used for a maneuver with a short period and a small process noise. When the maneuver takes long time and the maneuver is large, other dynamic models for the maneuver should be chosen or adaptive estimators should be applied. This will be discussed in Chapter 5.

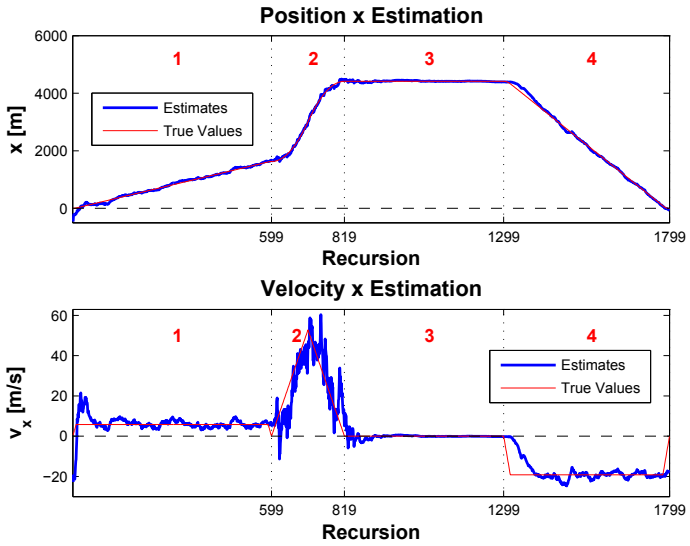

(a) Position and velocity in x dimension

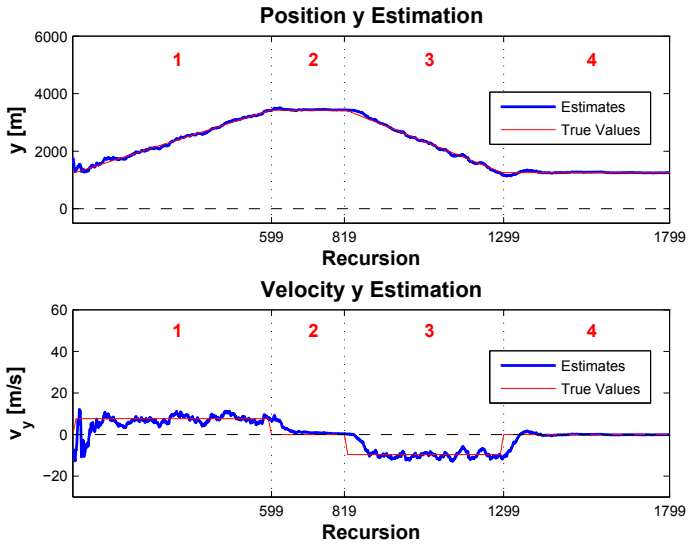

(b) Position and velocity in y dimension

Figure 3.3: The true and estimated state values

RMSE Comparison

One comparative performance of the proposed estimator with the estimators using only one kind of measurements is studied by using the RMSE, Eq. (2.56).

Similarly, the standard deviations of the measurement noises are $\sigma_d = 300$ m and $\sigma_l = 4$ dB. 500 Monte Carlo trials are run and the results are illustrated in Fig. 3.4. In each part of the route, the proposed estimator shows the high-

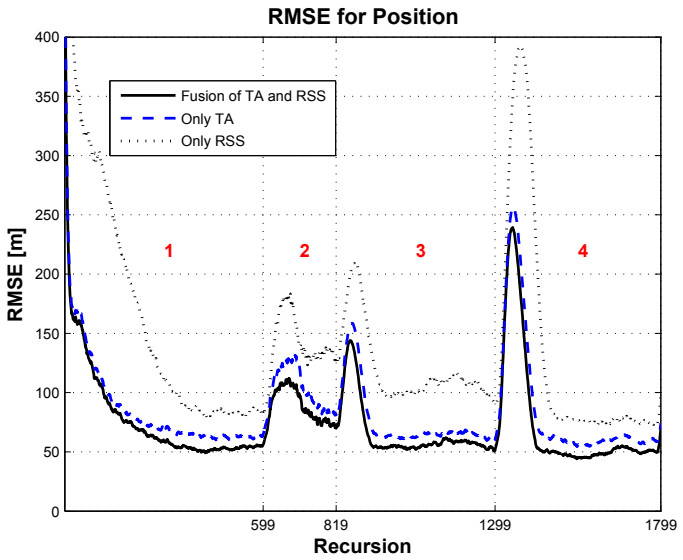

(a) RMSEs of position

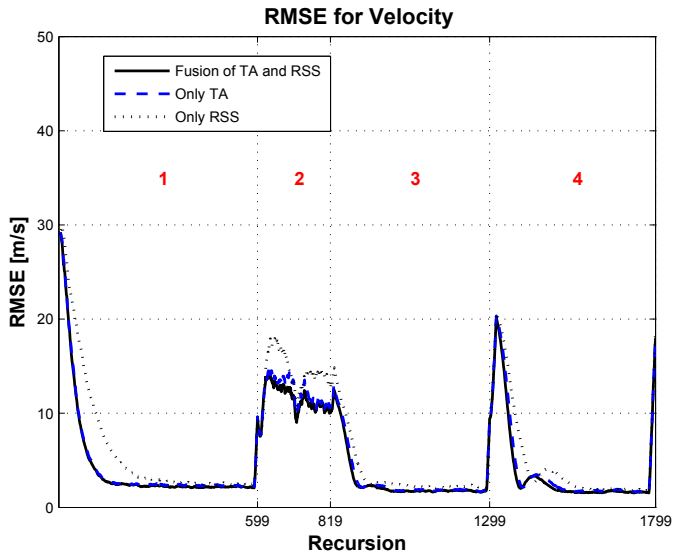

(b) RMSEs of velocity

Figure 3.4: RMSE comparison of three approaches

est accuracy and the RSS only method provides the worst estimate among

three approaches. It is also observed that in part 2 the estimation accuracy is greatly degraded, especially for the velocity estimate, since a wrong dynamic assumption is given. At the beginning of each part of the route, there is a relatively bigger RMSE due to the change of the target movement, which is decreased when the estimates converge to the new state values. It is also observed that the improvement of the velocity estimate is not so big. This is because the velocity is not measured, whereas is derived from the position.

Fusion of RSS Measurements with Only One TA Measurement

As mentioned before, in practice only one TA measurement from the serving BTS is available in current GSM networks. Thus the performance of integrating three RSS measurements with only one TA measurement should be also examined. The simulation is implemented by using three RSS measurements from BTS a, b, c, respectively, and one TA measurement from BTS c. Figure 3.5 shows the position RMSE comparison of fusion of three TA and three RSS measurements, fusion of RSS measurements with only one TA measurement, and using only three RSS measurements. It is shown that among three approaches the fusion of three TA measurements with three RSS measurements has the highest accuracy. However, the integration of three RSS measurements and one TA measurement can also improve the estimation accuracy compared with using only three RSS measurements. This provides a realistic solution which uses only existed position related measurements in GSM networks for the MS tracking.

Fusion under Different Measurement Errors

In this simulation, the data fusion approach is examined under different measurement errors and the performance is compared with that of the RSS only and TOA only approach. The simulations are divided into two groups as shown in Table 3.2. The first group is assumed a fixed RSS measurement error of σ_l =4 dB with varying TA measurement errors of σ_d =100 m, 300 m, 500 m, and 700 m, respectively (see Fig. 3.6). The second group of simulations uses a fixed TOA measurement error of σ_d =300 m with varying RSS measurement errors of σ_l =2 dB, 4 dB, 6 dB and 8 dB, respectively (see Fig. 3.7). The comparisons indicate that when one kind of measurements has degraded accuracy, such as in Fig. 3.6d and Fig. 3.7d, the data fusion approach can still provide relatively accurate estimates. It is observed that if one kind of measurements is much worse than the other type of measurements like in Fig. 3.6a, the RMSE of the fusion approach is close to the approach

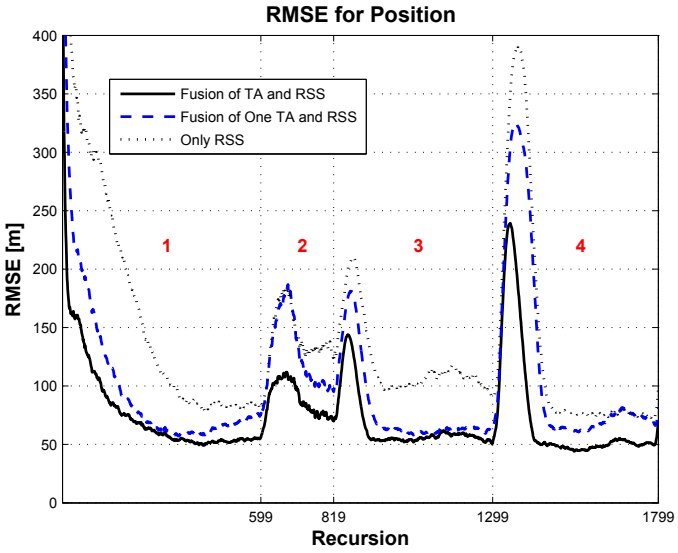

Figure 3.5: Fusion of RSS measurements with only one TA measurement

Table 3.2: Parameters of two groups of simulations

First Group		Second Group	
TA (σ_d)	RSS (σ_l)	TA (σ_d)	RSS (σ_l)
100 m	4 dB	300 m	2 dB
300 m	4 dB	300 m	4 dB
500 m	4 dB	300 m	6 dB
700 m	4 dB	300 m	8 dB

of using single measurements with better accuracy alone. It can also be seen that among all the comparisons the data fusion approach yields the highest accuracy. However, it should be noted that this is because the statistics of the measurement noise is known properly. When the measurement noise is getting worse unpredictably, integrating the measurement data with good accuracy with bad measurement data may cause much worse estimation results.

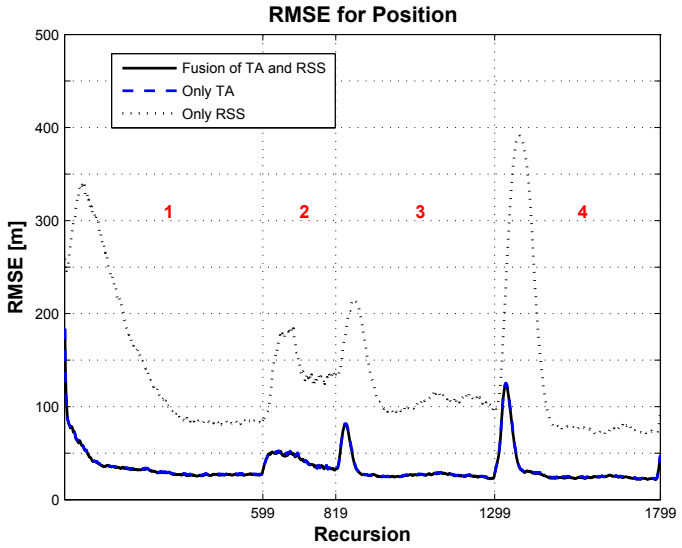

(a) $\sigma_d = 100$ m, $\sigma_l = 4$ dB

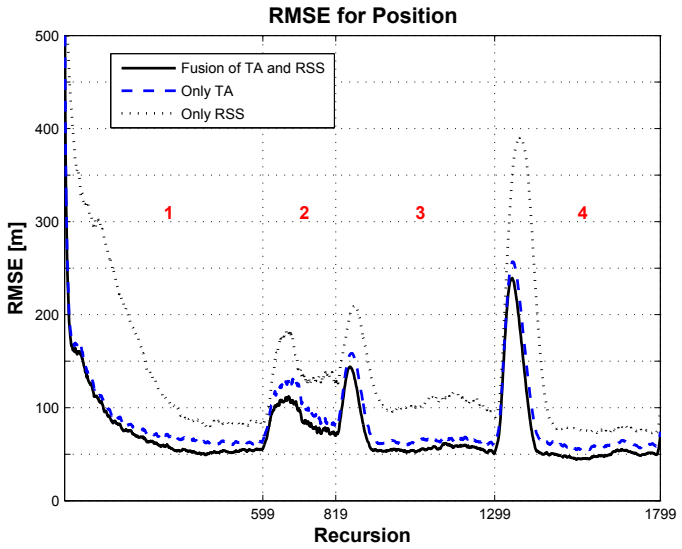

(b) $\sigma_d = 300$ m, $\sigma_l = 4$ dB

Figure 3.6: RMSE comparison of different TA measurement errors

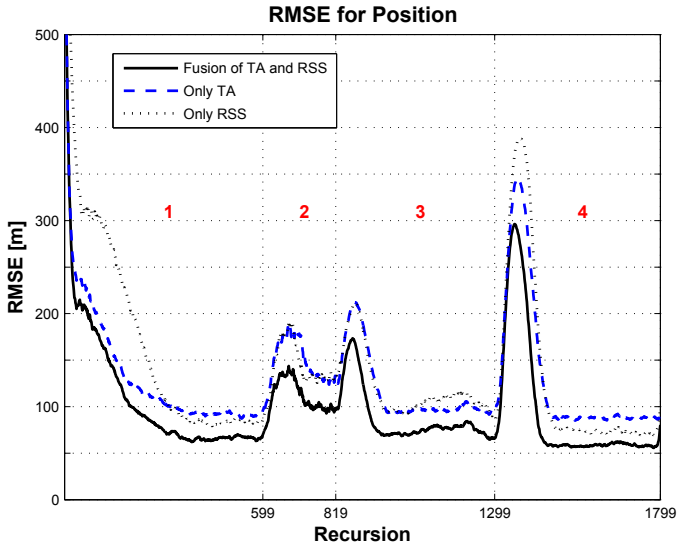

(c) $\sigma_d = 500$ m, $\sigma_l = 4$ dB

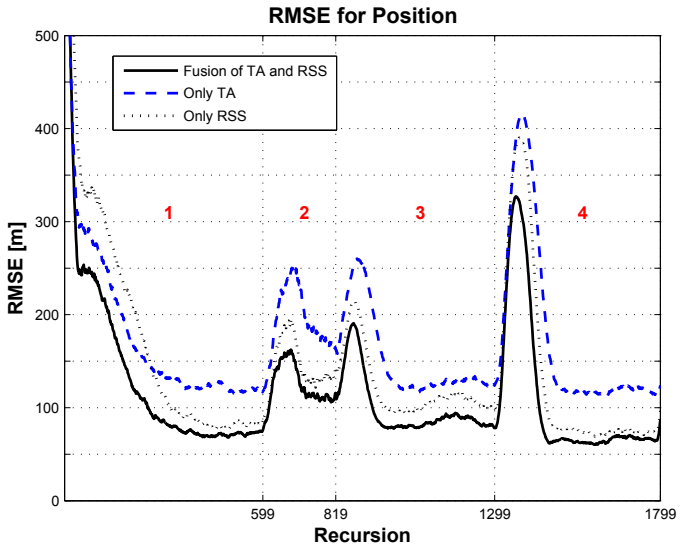

(d) $\sigma_d = 700$ m, $\sigma_l = 4$ dB

Figure 3.6: RMSE comparison of different TA measurement errors (cont'd)

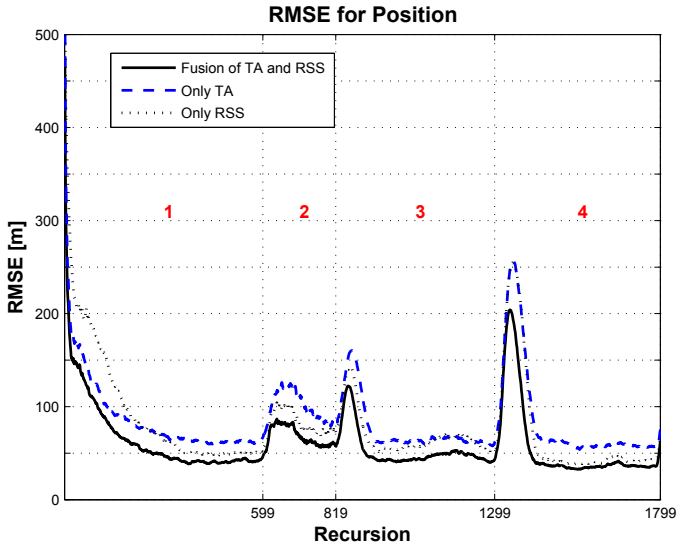

(a) $\sigma_d = 300$ m, $\sigma_l = 2$ dB

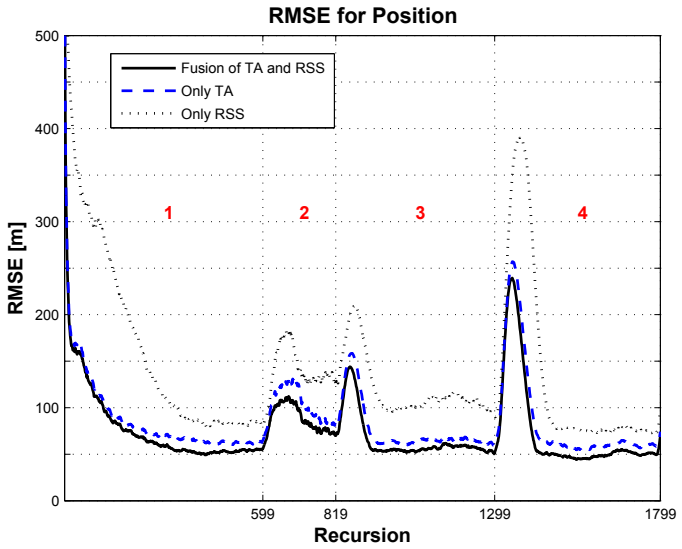

(b) $\sigma_d = 300$ m, $\sigma_l = 4$ dB

Figure 3.7: RMSE comparison of different RSS measurement errors

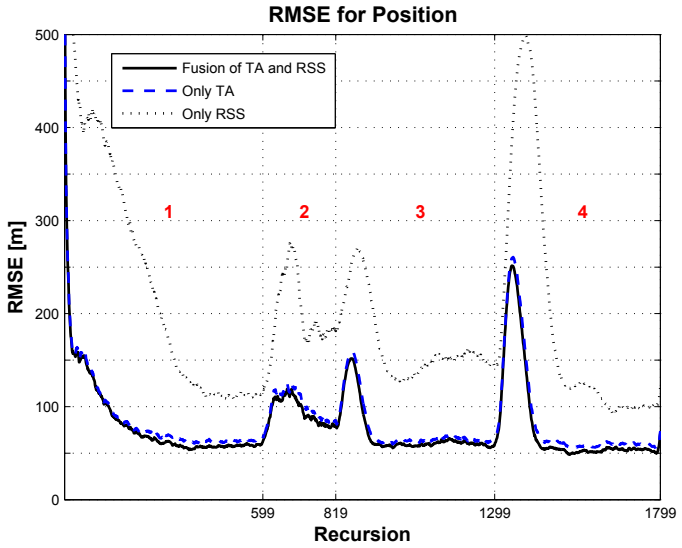

(c) $\sigma_d = 300$ m, $\sigma_l = 6$ dB

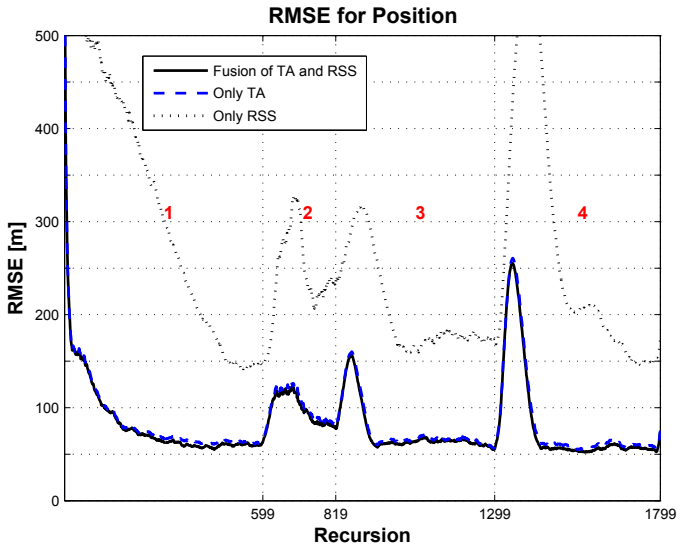

(d) $\sigma_d = 300$ m, $\sigma_l = 8$ dB

Figure 3.7: RMSE comparison of different RSS measurement errors (cont'd)

3.6 PCRLB for the Data Fusion Solution

3.6.1 Derivation

As discussed in Section 3.3, the PCRLB for the target tracking problem has the recursion form of Eq. (3.28). Suppose that a data fusion solution is given as shown in Section 3.4, the measurement function vector can be written as $\mathbf{h} = \begin{bmatrix}\mathbf{h}_1^T & \mathbf{h}_2^T\end{bmatrix}^T$ and thus the corresponding Jacobian matrix can be decomposed into $\mathbf{H} = \begin{bmatrix}\mathbf{H}_1^T & \mathbf{H}_2^T\end{bmatrix}^T$, where $\mathbf{H}_1$ represents one type of measurements and $\mathbf{H}_2$ the other type of measurements. It is assumed that the measurement noises are independent, then the cross covariance terms of measurement noises are zero. Thus, the complete covariance matrix of measurement noises is $\mathbf{R} = \text{diag}(\mathbf{R}_1, \mathbf{R}_2)$. Then the FIM of the data fusion approach at time step of $k+1$ can be written as

$$\begin{aligned}\mathbf{J}(k+1) &= \left[\mathbf{Q}(k) + \mathbb{E}\left\{\mathbf{F}(k)\mathbf{J}(k)^{-1}\mathbf{F}(k)^T\right\}\right]^{-1} \\ &\quad + \mathbb{E}\left\{\mathbf{H}(k+1)^T\mathbf{R}(k+1)^{-1}\mathbf{H}(k+1)\right\} \qquad (3.40)\\ &= \left[\mathbf{Q}(k) + \mathbb{E}\left\{\mathbf{F}(k)\mathbf{J}(k)^{-1}\mathbf{F}(k)^T\right\}\right]^{-1} \\ &\quad + \mathbb{E}\left\{\mathbf{H}_1(k+1)^T\mathbf{R}_1(k+1)^{-1}\mathbf{H}_1(k+1)\right\} \\ &\quad + \mathbb{E}\left\{\mathbf{H}_2(k+1)^T\mathbf{R}_2(k+1)^{-1}\mathbf{H}_2(k+1)\right\} \qquad (3.41)\\ &= \mathbf{J}_P(k+1) + \mathbf{J}_{D_1}(k+1) + \mathbf{J}_{D_2}(k+1) \qquad (3.42)\end{aligned}$$

where $\mathbf{J}_P(k+1)$ denotes the information from *a priori*, $\mathbf{J}_{D_1}(k+1)$ indicates the information from one type of measurements and $\mathbf{J}_{D_2}(k+1)$ stands for the information from another type of measurements. The above equations indicate that the information is additive.

The most important part of deriving the PCRLB is to define the Jacobian matrix of the state transition function $\mathbf{f}[\cdot]$ and measurement function $\mathbf{h}[\cdot]$ (usually nonlinear) with respect to the state vector $\mathbf{x}$. For the data fusion approach proposed in the last section, the measurement model includes two different types of measurements from three BTSs (Eqs. 3.34, 3.35). It should be noticed that to calculate PCRLB the truth model of the real trajectory rather than the dynamic model for the EKF design should be used because PCRLB is the best achievable theoretical performance considering the real data. The truth model might be different with the dynamic model used in EKF. Assuming that the curvilinear model, Eqs. (3.11) and (3.12), is used for generating the trajectory, the state vector is $\mathbf{x} = \begin{bmatrix}x & y & v & \phi\end{bmatrix}^T$, which includes the target position in two dimensions, speed and heading. The

Jacobian matrix of the state transition function is derived as follows

$$\mathbf{F}(k) \triangleq \left.\frac{\partial \mathbf{f}\big[\mathbf{x}(k)\big]}{\partial \mathbf{x}(k)}\right|_{\mathbf{x}(k)} \tag{3.43}$$

$$= \begin{bmatrix} 1 & 0 & T\cos\big(\phi(k)\big) & -Tv(k)\sin\big(\phi(k)\big) \\ 0 & 1 & T\sin\big(\phi(k)\big) & Tv(k)\cos\big(\phi(k)\big) \\ 0 & 0 & 1 & 0 \\ 0 & 0 & -\dfrac{Ta_n(k)}{v(k)^2} & 1 \end{bmatrix} \tag{3.44}$$

where $\mathbf{F}(k)$ is evaluated at the real value of state $\mathbf{x}(k)$. The Jacobian matrix of the measurement function is

$$\mathbf{H}(k+1) \triangleq \left.\frac{\partial \mathbf{h}\big[\mathbf{x}(k+1)\big]}{\partial \mathbf{x}(k+1)}\right|_{\mathbf{x}(k+1)} \tag{3.45}$$

$$= \begin{bmatrix} \dfrac{x(k+1)-x_a}{d_a(k+1)} & \dfrac{y(k+1)-y_a}{d_a(k+1)} & 0 & 0 \\ \dfrac{x(k+1)-x_b}{d_b(k+1)} & \dfrac{y(k+1)-y_b}{d_b(k+1)} & 0 & 0 \\ \dfrac{x(k+1)-x_c}{d_c(k+1)} & \dfrac{y(k+1)-y_c}{d_c(k+1)} & 0 & 0 \\ \dfrac{38\big(\tilde{x}(k+1)-\tilde{x}_a\big)}{\ln 10\cdot(\tilde{d}_a(k+1))^2} & \dfrac{38\big(\tilde{y}(k+1)-\tilde{y}_a\big)}{\ln 10\cdot(\tilde{d}_a(k+1))^2} & 0 & 0 \\ \dfrac{38\big(\tilde{x}(k+1)-\tilde{x}_b\big)}{\ln 10\cdot(\tilde{d}_b(k+1))^2} & \dfrac{38\big(\tilde{y}(k+1)-\tilde{y}_b\big)}{\ln 10\cdot(\tilde{d}_b(k+1))^2} & 0 & 0 \\ \dfrac{38\big(\tilde{x}(k+1)-\tilde{x}_c\big)}{\ln 10\cdot(\tilde{d}_c(k+1))^2} & \dfrac{38\big(\tilde{y}(k+1)-\tilde{y}_c\big)}{\ln 10\cdot(\tilde{d}_c(k+1))^2} & 0 & 0 \end{bmatrix} \tag{3.46}$$

where $\mathbf{H}(k+1)$ is evaluated at the real value of state $\mathbf{x}(k+1)$. The expectation should be taken over Monte Carlo trials.

3.6.2 Simulation Results

Simulation Scenario

The simulations are carried out in a simulated urban square area as described in Section 3.5.1. It is assumed that a vehicle equipped with a MS travels at nearly constant velocity from location $(0\text{ m}, 3000\text{ m})$ as shown in Fig. 3.8. The initial state comprises the position and velocity of the MS in two dimensions as $\mathbf{x}(0) = \big[0\text{ m} \quad 15\text{ m/s} \quad 3000\text{ m} \quad 0\text{ m/s}\big]^T$. The measurement update

is $T = 0.48$ s. The trajectory is generated by the curvilinear model, where the accelerations are set to be $a_t = 0$ m/s^2 and $a_n = 0$ m/s^2. The process noise is assumed to be zero-mean white Gaussian noise with standard deviations of $\sigma_x = 10^{-4}$ m, $\sigma_y = 10^{-4}$ m, $\sigma_v = 10^{-5}$ m/s, $\sigma_\phi = 10^{-6}$ rad.

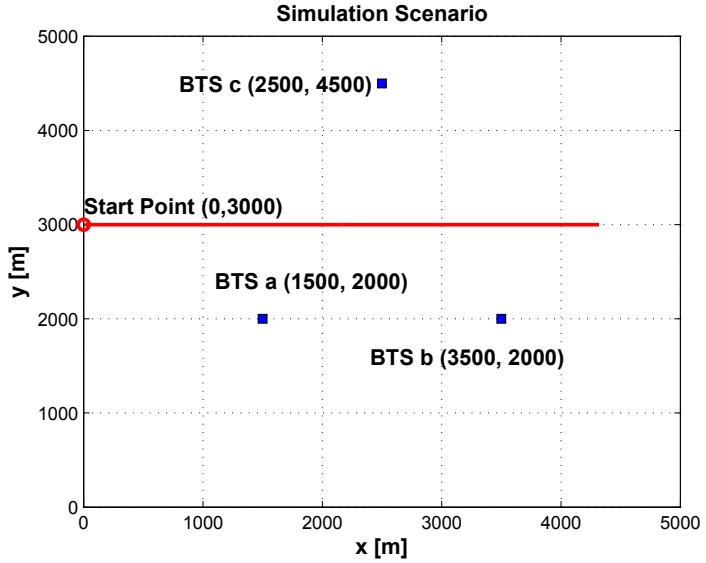

Figure 3.8: Simulation Scenario

To compare the estimation results with the corresponding PCRLBs, an EKF is applied. The state transition and measurement models are the same with the EKF in the last section. Only the standard deviations of the process noise in the CV model are set to be $\sigma_x = 10^{-4}$ m/s^2 and $\sigma_y = 10^{-4}$ m/s^2 because the real motion is nearly constant velocity. The calculation of the PCRLBs uses the truth model, i.e., curvilinear model. The initial FIM is given by the inverse of $\mathbf{P}^+(0)$ (see Eq. 3.39), which is the covariance matrix of the initial state assumed to be Gaussian.

Performance Comparisons of Fusion Approach and Single Type of Measurements Approach

For comparing the PCRLB with the RMSE, we take the root of the PCRLB of the state element x plus the PCRLB of y, which is called PCRLB of position. 500 Monte Carlo trials are run. Figure 3.9 shows the RMSEs of the data fusion approach, using only TA measurements, and using only RSS measurements comparing with the corresponding PCRLBs. The measurement noises

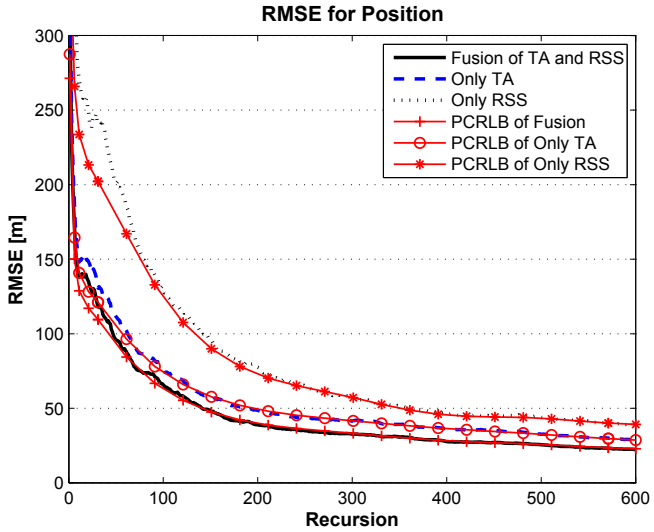

Figure 3.9: RMSEs and PCRLBs of position

have the standard deviations of $\sigma_d = 300$ m, $\sigma_l = 4$ dB. It is observed that the estimation results of the designed EKF are close to the corresponding PCRLB in this simple scenario, and among these three methods, the data fusion method yields the highest accuracy.

Figure 3.10 shows the PCRLBs of position and velocity of the data fusion

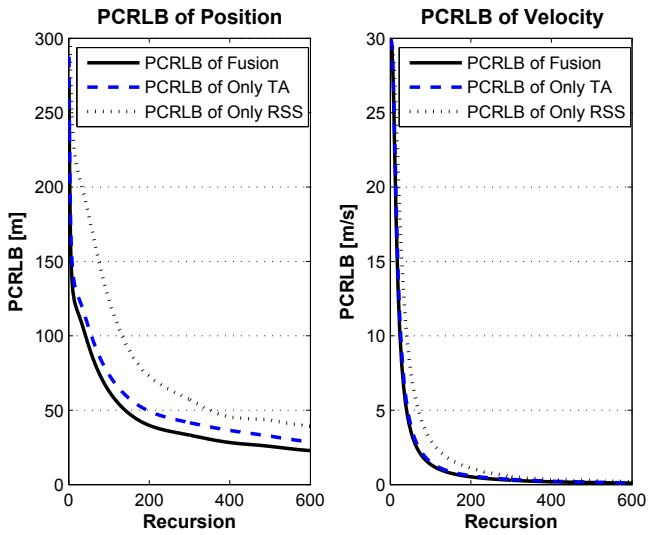

Figure 3.10: PCRLBs comparsion

approach, TA only approach and RSS only approach, respectively. Similarly, the measurement noises have the standard deviations $\sigma_d = 300$ m, $\sigma_l = 4$ dB. As expected, the comparison of the PCRLBs reveals that theoretically the integration of these two kinds of measurements yields better accuracy than using only one type of measurements. This comparison is analogous to the RMSE comparison using EKF shown in Fig. 3.4 and it demonstrates the solution of the estimation results comparison from a theoretical point of view.

PCRLB Analysis

Since the PCRLB represents the best achievable estimation accuracy, it can be used to evaluate the tracking performance before designing any estimator. Recalling the recursive equation of calculating the PCRLB (Eqs. 3.40-3.42), the PCRLB is influenced by the following factors: the initial information, $\mathbf{J}_0$; the process noise, $\mathbf{Q}(k)$; the dynamics of the trajectory, $\mathbf{F}(k)$ (see Eq. 3.44); the measurement noise, $\mathbf{R}(k)$; the geometric relationship of the BTSs and the MS, i.e., *geometric dilution of precision* (GDOP). It is observed that the value of $\mathbf{J}_0$ influences the initial stage of the estimation and has little effect on the estimation accuracy when the estimator converges. The analysis of GDOP has been discussed in [45]. The relatively higher GDOP, in other words, worse geometry, will degrade the estimation accuracy. Therefore, in this section, we mainly discuss the influences of the process noise, the measurement noise and the dynamics on the PCRLB.

Firstly, the parameters of the simulation are set similarly as introduced above except that the process noise of the curvilinear model is set to be different levels as:

- $\mathbf{Q}_1$: $\sigma_x = 10^{-4}$ m, $\sigma_y = 10^{-4}$ m, $\sigma_v = 10^{-5}$ m/s, $\sigma_\phi = 10^{-6}$ rad;
- $\mathbf{Q}_2$: $\sigma_x = 10^{-2}$ m, $\sigma_y = 10^{-2}$ m, $\sigma_v = 10^{-3}$ m/s, $\sigma_\phi = 10^{-4}$ rad;
- $\mathbf{Q}_3$: $\sigma_x = 5 \times 10^{-1}$ m, $\sigma_y = 5 \times 10^{-1}$ m, $\sigma_v = 5 \times 10^{-2}$ m/s, $\sigma_\phi = 5 \times 10^{-3}$ rad;
- $\mathbf{Q}_4$: $\sigma_x = 1$ m, $\sigma_y = 1$ m, $\sigma_v = 10^{-1}$ m/s, $\sigma_\phi = 10^{-2}$ rad.

Figure 3.11 shows the PCRLBs of the fusion approach, TOA only approach and RSS only approach under different process noises. The fusion approach has the highest accuracy for all simulations of different process noises. It is also observed that the PCRLBs are degraded when the process noises are high. When the process noise is as low as to be neglected, the PCRLBs have

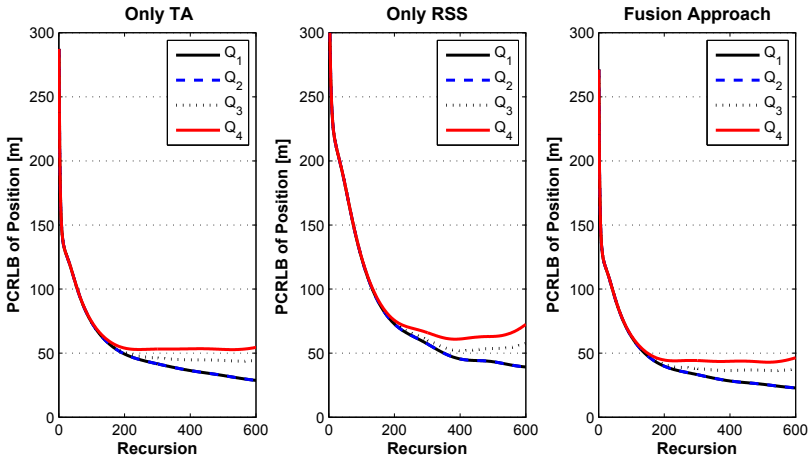

Figure 3.11: PCRLBs of different process noises

not too much difference with the change of the process noise. For example, for $\mathbf{Q}_1$ and $\mathbf{Q}_2$ the PCRLBs are very close.

Another comparison is done to analyze how the measurement noise influences the data fusion and the single type measurement method, which is a theoretical analysis analogous to the estimate comparison shown in Fig. 3.6 and Fig. 3.7. Firstly the standard deviation of the TA measurement noise is fixed as $\sigma_d = 300$ m, but various standard deviations of the RSS measurement noise are applied, σ_l=2 dB, 4 dB, 6 dB and 8 dB, respectively. The PCRLBs of position using data fusion approach and using only RSS measurements are given in Fig. 3.12. The plots indicate that for more noisy measurements, the data fusion approach will yield results with remarkably improved accuracy. Then a similar simulation is implemented fixing the standard deviation of the RSS measurement noise at $\sigma_l = 4$ dB, but the standard deviation of the TA measurement noise is varied as σ_d=100 m, 300 m, 500 m and 700 m. The results, as shown in Fig. 3.13, demonstrate the above conclusion that the fusion approach provides more stable and better results when one kind of measurements has higher error.

Finally, a simulation of different dynamics, a nearly constant acceleration motion, is implemented. The initial velocity is set to be $(0 \text{ m/s}, 0 \text{ m/s})$, and the tangential acceleration is set to be $a_t = 1 \text{ m/s}^2, 3 \text{ m/s}^2, 6 \text{ m/s}^2, 10 \text{ m/s}^2$, respectively. The process noise is assumed to be very small as $\mathbf{Q}_1$. Figure 3.14 shows the PCRLBs of the data fusion approach, TA only, and RSS only approach under different accelerations. Similarly, the fusion approach provides the highest accuracy among the three approaches. It is observed

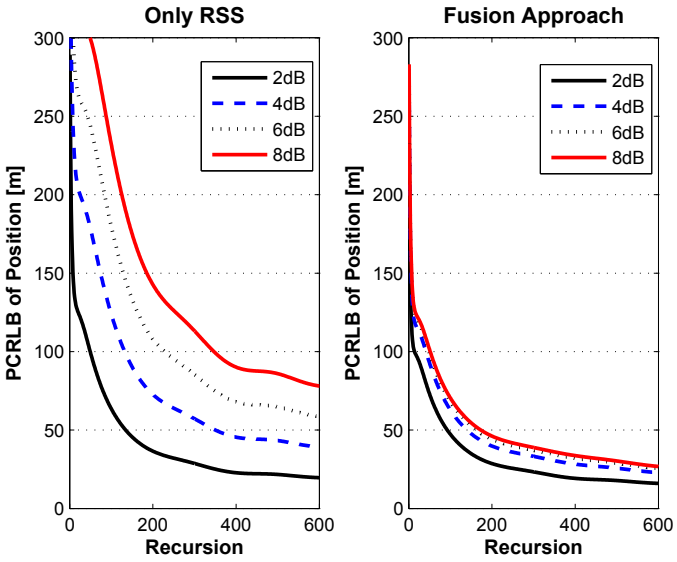

Figure 3.12: PCRLBs of position for σ_d=300 m and σ_l=2 dB, 4 dB, 6 dB, 8 dB

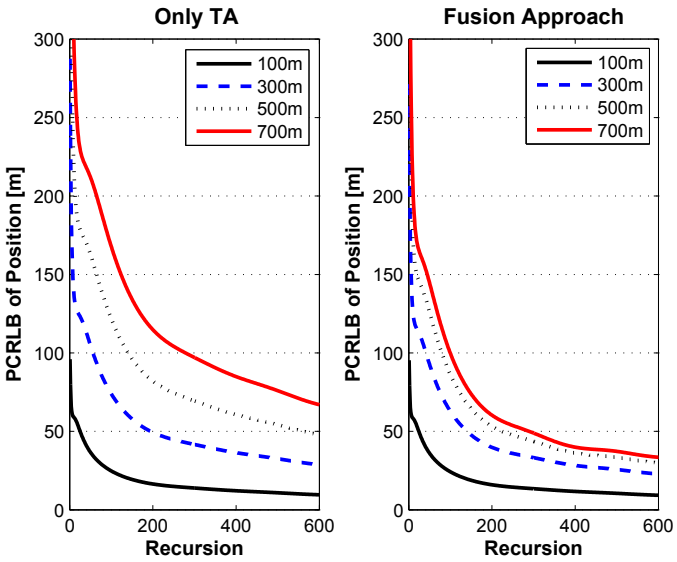

Figure 3.13: PCRLBs of position for σ_d=100 m, 300 m, 500 m, 700 m and σ_l=4 dB

that for the CA motion the PCRLBs have a peak at the beginning, then are decreasing. For the acceleration of $a_t = 10$ m/s^2 the PCRLBs increase

greatly at the end of the trajectory. This is because the influence of the relative geometry of the MS and the BTSs.

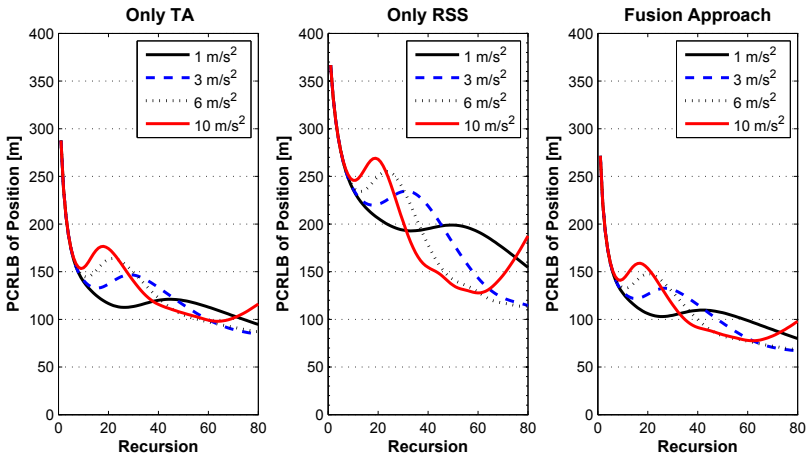

Figure 3.14: PCRLBs of different tangential accelerations

3.7 Summary

In this chapter, the state estimation problem of ground target tracking is considered and the PCRLB, which is a variant of CRLB for random parameters, for the target tracking problem is presented. On the base of this understanding, a data fusion approach using an EKF is proposed to integrate two different types of measurements, TOA and RSS measurements from GSM networks. The simulation results show that the fusion approach yields highest accuracy as compared with single type measurement approaches, TOA only and RSS only. And the fusion of three RSS measurements with one TOA measurement provides a realistic solution for the MS tracking. Another comparison of different measurement errors shows that the data fusion approach is more tolerant than the single type measurement approaches.

The PCRLB for the fusion approach is also derived and analyzed. PCRLB clearly depicts the underlying principle of data fusion, i.e., information is additive. It is shown that the position RMSE of EKF can be very close to the corresponding PCRLB. Comparisons of PCRLBs, which are analogous to the comparisons of the estimation results using EKF, demonstrate the conclusion that the data fusion approach provides better accuracy and is more robust to the noisy measurement from a theoretical point of view.

Chapter 4

Road-Constrained Target Tracking

A GSM positioning system based on current specifications faces many difficulties when trying to obtain accurate position estimates. From the measurement point of view, the resolution of the measurements in GSM networks related to positioning is coarse, e.g., *Timing Advance* (TA) is only reported in units of a bit period. Moreover, ambiguities of the position estimate arise when there are not a sufficient number of measurements available since usually measurements from three BTSs are required for two-dimensional positioning. All of these factors will degrade the position estimation accuracy. In order to achieve better performance, additional information about the targets should be incorporated into the estimation process. The road constraint is such a promising *a priori* information.

In this chapter, the road constraint is incorporated into an EKF as a pseudomeasurement for target tracking in GSM networks to improve the estimation accuracy. In Section 4.1, the road information is described. The approaches of constrained state estimation are introduced in Section 4.2. The proposed approach is presented in Section 4.3 for a linear road constraint and in Section 4.4 for a nonlinear road constraint.

4.1 Road Information

Assume that the targets considered here are mostly ground vehicles, such as civil cars, trucks, and so on, and they are strictly linked to the road network.

The road information can be obtained from a digital map database, which typically represents the road data using line segments [74]. There are three

types of road data: *node*, *segment*, and *shape point*, as shown in Fig. 4.1. A *node* is a cross point or an endpoint of a road, and is used to represent an intersection or a dead-end of a road. It is commonly represented in the map database by a latitude and a longitude. A *segment* is a piece of road ways between two nodes and is used to represent fragments of roadways and other features. *Shape points* are ordered collections of points which map the curved portion of a given segment to a series of consecutive straight-line pieces in such a way as to make the calculated segment distance close to the actual length.

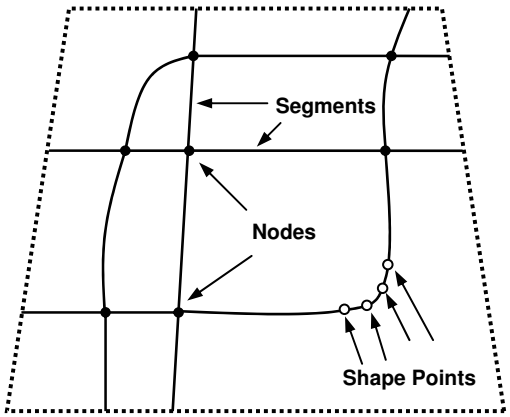

Figure 4.1: Segments, nodes, and shape points

Therefore, a road can typically be represented by a sequence of straight lines selected to approximate the real curvature of the road, and the road network is defined using waypoints and associated properties [75], such as road names, types of roads, road segment lengths, expected driving speeds, turn restrictions, etc. The digital map database compiles these data into files that can be readily accessed by other modules in a location and navigation system. It provides all location-related features once the position of a vehicle has been determined. It can be used as a reference to visualize and locate vehicles. Moreover, it can also help to determine vehicle location using the geometry and topology of road networks. In this work, the road network information is considered as constraints of the target motion, i.e., the target must lie on the road, and the velocity of the target is in the direction of the road.

There are many approaches to incorporate the road information into the

tracking process, including tuning the covariance of the process noise adaptively according to road maps [76], building the tracking filters upon the 1D representation of road segments [77], and so on. Here the constrained state estimation approaches are considered.

4.2 Constrained State Estimation

For a state estimation problem, the system is usually described by dynamic model and measurement model

$$\mathbf{x}(k+1) = \mathbf{f}\big[\mathbf{x}(k)\big] + \mathbf{w}(k) \tag{4.1}$$

$$\mathbf{z}(k) = \mathbf{h}\big[\mathbf{x}(k)\big] + \mathbf{v}(k) \tag{4.2}$$

Besides, in some physical systems there exists some information or constraints between the state variables, which can not be described by Eqs. (4.1) and (4.2). That is, it is supposed that the states satisfy some constraints

$$\mathbf{D}\mathbf{x} = \mathbf{d} \tag{4.3}$$

where $\mathbf{x}$ is the state vector, $\mathbf{D}$ is a known matrix and $\mathbf{d}$ is a known vector. They might be given by the basic laws of physics, from the mathematical description of a state vector, and also from kinematic or geometric considerations of the system [78], such as the road information.

The main approach categories of incorporating such constraints into the state estimation process are model reduction, pseudomeasurement, projection and pdf truncation. The model reduction approach reduces the system model parameterization by replacing some states using the constraints [79]. It is conceptually straightforward and can be easily implemented, but it loses the physical meaning of the system model. The pseudomeasurement [80–82] approach treats the state constraints as fictitious measurements. Accordingly, the original measurement model is augmented and the classic Kalman filter is ready to be applied. The projection [83–85] approaches project the unconstrained state estimate at each time step onto the state constraint surface. Another approach is the pdf truncation approach, in which the probability density function of the unconstrained state estimate is truncated at the constraint edges and the constrained state estimate is the mean of the truncated pdf. This approach is specially suitable for inequality constraints. Exhaustive investigations can be found in [78, 86, 87]. In the following we mainly introduce and compare the pseudomeasurement and projection approach.

4.2.1 Pseudomeasurement Approach

The idea of introducing a kinematic constraint into the tracking process through a pseudomeasurement was firstly proposed in [80]. Suppose that various constraints (Eq. 4.3) are considered, the constraints on the state vector $\mathbf{x}$ can be formulated as pseudomeasurements

$$\mathbf{z}_c(k) = \mathbf{H}_c\mathbf{x}(k) + \mathbf{v}_c(k) \tag{4.4}$$

where $\mathbf{z}_c(k) = \mathbf{0}$ is a zero-valued pseudomeasurement vector, $\mathbf{H}_c\mathbf{x}(k) = \mathbf{D}\mathbf{x} - \mathbf{d}$ and $\mathbf{v}_c(k)$ is a zero-mean white Gaussian noise vector introduced to relax the constraints. The subscript 'c' denotes the terms for constraints.

$$\mathbf{v}_c(k) \sim \mathcal{N}\big(\mathbf{0}, \mathbf{R}_c(k)\big) \tag{4.5}$$

Then the original measurement model can be augmented by the pseudomeasurement model (Eq. 4.4)

$$\mathbf{z}_a(k) = \mathbf{h}_a\big[\mathbf{x}(k)\big] + \mathbf{v}_a(k) \tag{4.6}$$

where $\mathbf{z}_a(k) = \begin{bmatrix}\mathbf{z}(k)^T & \mathbf{z}_c(k)^T\end{bmatrix}^T$, $\mathbf{h}_a\big[\mathbf{x}(k)\big] = \begin{bmatrix}\mathbf{h}\big[\mathbf{x}(k)\big]^T & \mathbf{H}_c\mathbf{x}(k)^T\end{bmatrix}^T$, and $\mathbf{v}_a(k) = \begin{bmatrix}\mathbf{v}(k)^T & \mathbf{v}_c(k)^T\end{bmatrix}^T$. The subscript '$a$' denotes the augmented terms. Because of the nonlinear mapping of the states into the observation space, an EKF can be applied to obtain the constrained state estimates:
Prediction:

$$\hat{\mathbf{x}}^-(k+1) = \mathbf{f}[\hat{\mathbf{x}}^+(k)] \tag{4.7}$$
$$\mathbf{P}^-(k+1) = \mathbf{F}(k)\mathbf{P}^+(k)\mathbf{F}^T(k) + \mathbf{Q}(k) \tag{4.8}$$

Correction:

$$\begin{aligned}\mathbf{K}_a(k+1) &= \mathbf{P}^-(k+1)\mathbf{H}_a^T(k+1) \\ &\quad \cdot\big[\mathbf{H}_a(k+1)\mathbf{P}^-(k+1)\mathbf{H}_a^T(k+1) + \mathbf{R}_a(k+1)\big]^{-1}\end{aligned} \tag{4.9}$$
$$\mathbf{r}_a(k+1) = \mathbf{z}_a(k+1) - \mathbf{h}_a\big[\hat{\mathbf{x}}^-(k+1)\big] \tag{4.10}$$
$$\hat{\mathbf{x}}_a^+(k+1) = \hat{\mathbf{x}}^-(k+1) + \mathbf{K}_a(k+1)\mathbf{r}_a(k+1) \tag{4.11}$$
$$\mathbf{P}_a^+(k+1) = \mathbf{P}^-(k+1) - \mathbf{K}_a(k+1)\mathbf{H}_a(k+1)\mathbf{P}^-(k+1) \tag{4.12}$$

where $\hat{\mathbf{x}}^-(k+1)$ and $\mathbf{P}^-(k+1)$ represent the predicted state estimate and state error covariance, $\hat{\mathbf{x}}_a^+(k+1)$ and $\mathbf{P}_a^+(k+1)$ denote the constrained state estimate and associated state error covariance, respectively. The prediction is exactly the same as the normal EKF. Only in the update stage, the Jacobian

matrix of the measurement function $\mathbf{H}(k+1)$ is replaced by the Jacobian matrix of the augmented measurement function $\mathbf{H}_a(k+1)$. The measurement residual vector $\mathbf{r}_a(k+1)$ is calculated by augmented measurement model. The measurement noise covariance matrix is also augmented as $\mathbf{R}_a(k) = \text{diag}\left[\mathbf{R}(k), \mathbf{R}_c(k)\right]$.

The pseudomeasurement approach provides a convenient framework for incorporating such constraints without greatly increasing the computational cost. Since using the constraints removes some of the target dynamic uncertainty, the estimation performance will be improved. In addition, it has less computation complexity to incorporate the constraints into the measurement model rather than into the state transition model, especially in the case of nonlinear constraints [80].

4.2.2 Projection Approach

The constrained state estimate can be also derived through projecting the unconstrained state estimate $\hat{\mathbf{x}}(k)$ onto the constrained surface. For the simplicity of notation, the time subscript 'k' is eliminated in the following of this section since the projection is implemented only related with time step k. The problem can be formulated as a constrained optimization problem

$$\tilde{\mathbf{x}} = \arg\min_{\tilde{\mathbf{x}}}(\tilde{\mathbf{x}} - \hat{\mathbf{x}})^T\mathbf{W}(\tilde{\mathbf{x}} - \hat{\mathbf{x}}) \text{ such that } \mathbf{D}\tilde{\mathbf{x}} = \mathbf{d} \tag{4.13}$$

where $\mathbf{W}$ is any positive definite weighting matrix, $\hat{\mathbf{x}}$ represents the unconstrained state estimate and $\tilde{\mathbf{x}}$ denotes the constrained state estimate. Applying the method of Lagrange multipliers to solve this problem, a Lagrangian L can be formed

$$L = (\tilde{\mathbf{x}} - \hat{\mathbf{x}})^T\mathbf{W}(\tilde{\mathbf{x}} - \hat{\mathbf{x}}) + 2\boldsymbol{\lambda}^T(\mathbf{D}\tilde{\mathbf{x}} - \mathbf{d}) \tag{4.14}$$

where $\boldsymbol{\lambda}$ is the multiplier vector. To obtain the optimization, let the partial derivatives of the Lagrangian with respect to $\tilde{\mathbf{x}}$ and $\boldsymbol{\lambda}$ equal to zero and solve them simultaneously

$$\frac{\partial L}{\partial \tilde{\mathbf{x}}} = \mathbf{W}(\tilde{\mathbf{x}} - \hat{\mathbf{x}}) + \mathbf{D}^T\boldsymbol{\lambda} = \mathbf{0} \tag{4.15}$$

$$\frac{\partial L}{\partial \boldsymbol{\lambda}} = \mathbf{D}\tilde{\mathbf{x}} - \mathbf{d} = \mathbf{0} \tag{4.16}$$

The solutions are

$$\boldsymbol{\lambda} = (\mathbf{D}\mathbf{W}^{-1}\mathbf{D}^T)^{-1}(\mathbf{D}\hat{\mathbf{x}} - \mathbf{d}) \tag{4.17}$$

$$\tilde{\mathbf{x}} = \hat{\mathbf{x}} - \mathbf{W}^{-1}\mathbf{D}^T(\mathbf{D}\mathbf{W}^{-1}\mathbf{D}^T)^{-1}(\mathbf{D}\hat{\mathbf{x}} - \mathbf{d}) \tag{4.18}$$

The constrained state estimate $\tilde{\mathbf{x}}$ is equal to the unconstrained state estimate $\hat{\mathbf{x}}$ minus a correction term. Note that this derivation does not depend on the conditional Gaussian nature of $\hat{\mathbf{x}}$. As shown in [83], the constrained state estimate obtained by Eq. (4.18) is unbiased, the constrained state estimate when $\mathbf{W} = \mathbf{P}^{-1}$, i.e., the inverse of the unconstrained state estimation error covariance, has a smaller estimation error covariance than that of the unconstrained state estimate. The covariance of the constrained state estimate error is given by

$$\tilde{\mathbf{P}} = \mathbf{P} - \mathbf{P}\mathbf{D}^T(\mathbf{D}\mathbf{P}\mathbf{D}^T)^{-1}\mathbf{D}\mathbf{P} \tag{4.19}$$

where $\mathbf{P}$ is the covariance matrix of the unconstrained state estimate error and $\tilde{\mathbf{P}}$ denotes the covariance matrix of the constrained state estimate error. Among all the constrained Kalman filters of Eq. (4.18), the filter which uses $\mathbf{W} = \mathbf{P}^{-1}$ has the smallest estimation error covariance. This solution can be given by solving the maximization of the posterior conditional probability.

The above derivation is a general solution. In the following, the projection approach of the constrained state estimation is derived from maximum conditional probability point of view and mean square point of view, respectively.

Maximum Conditional Probability Method

From maximum conditional probability point of view, Kalman filter solves the problem

$$\hat{\mathbf{x}} = \arg\max_{\boldsymbol{\xi}} f_{\mathbf{z}|\mathbf{x}}(\boldsymbol{\zeta}|\boldsymbol{\xi}) \tag{4.20}$$

To maximize $f_{\mathbf{z}|\mathbf{x}}(\boldsymbol{\zeta}|\boldsymbol{\xi})$, we can maximize $\ln f_{\mathbf{z}|\mathbf{x}}(\boldsymbol{\zeta}|\boldsymbol{\xi})$, which means minimizing $(\mathbf{x}-\bar{\bar{\mathbf{x}}})^T\mathbf{P}^{-1}(\mathbf{x}-\bar{\bar{\mathbf{x}}})$ when the Gaussian assumptions hold. In the above, $\bar{\bar{\mathbf{x}}}$ denotes the conditional mean of $\mathbf{x}$ given the measurement $\mathbf{z}$, $\bar{\bar{\mathbf{x}}} = \mathbb{E}\{\mathbf{x}|\mathbf{z}\}$, and $\mathbf{P}$ is the covariance matrix of the state estimate error. Now the constrained minimization problem is formulated as

$$\tilde{\mathbf{x}} = \arg\min_{\tilde{\mathbf{x}}}(\tilde{\mathbf{x}} - \bar{\bar{\mathbf{x}}})^T\mathbf{P}^{-1}(\tilde{\mathbf{x}} - \bar{\bar{\mathbf{x}}}) \text{ such that } \mathbf{D}\tilde{\mathbf{x}} = \mathbf{d} \tag{4.21}$$

Similar to the derivation of the general projection approach, a Lagrangian can be formed and solved.

$$\tilde{\mathbf{x}} = \hat{\mathbf{x}} - \mathbf{P}\mathbf{D}^T(\mathbf{D}\mathbf{P}\mathbf{D}^T)^{-1}(\mathbf{D}\hat{\mathbf{x}} - \mathbf{d}) \tag{4.22}$$

Refer to Appendix C.1 for the derivation.

Mean Square Method

The problem can also be solved from a mean square point of view. The constrained state estimate is to solve

$$\tilde{\mathbf{x}} = \arg\min_{\tilde{\mathbf{x}}} \mathbb{E}\left\{\|\mathbf{x}-\tilde{\mathbf{x}}\|^2 | \mathbf{z}=\mathbf{z}_0\right\} \text{ such that } \mathbf{D}\tilde{\mathbf{x}} = \mathbf{d} \tag{4.23}$$

Again, a Lagrangian can be formed and the solution of this minimization could be obtained, as shown in Appendix C.2.

$$\tilde{\mathbf{x}} = \hat{\mathbf{x}} - \mathbf{D}^T(\mathbf{D}\mathbf{D}^T)^{-1}\big(\mathbf{D}\hat{\mathbf{x}}(k) - \mathbf{d}\big) \tag{4.24}$$

Comparing to Eq. (4.18), the solution by the mean square method is equivalent to setting $\mathbf{W} = \mathbf{I}$.

4.2.3 Comparison of Pseudomeasurement and Projection Approach

As discussed above, the principle and derivation of the psudomeasurement and projection approaches are different. However, when we compare the pseudomeasurement approach (Eq. 4.11), which uses Kalman filter measurement update equation, and the projection approach (Eq. 4.18), they are both equal to a preliminary estimate plus one correction term, which is proportional to the measurement residual. Therefore, it is necessary to look at the detail of the formulae and to find out the similarity and difference of these two approaches.

Comparison of the Formulation

The constrained estimation obtained by the pseudomeasurement approach in Eq. (4.11) consists of two terms, the predicted estimation and the correction part. In order to compare it with that of the projection approach Eq. (4.18), which consists of the unconstrained state estimate and a correction term, the constrained state estimate of the pseudomeasurement approach (Eq. 4.11) in terms of the unconstrained estimate should be derived.

The augmented system by constraints $\mathbf{D}\mathbf{x} = \mathbf{d}$ is written as

$$\mathbf{x}(k+1) = \mathbf{f}\big[\mathbf{x}(k)\big] + \mathbf{w}(k) \tag{4.25}$$

$$\mathbf{z}_a(k) = \mathbf{h}_a\big[\mathbf{x}(k)\big] + \mathbf{v}_a(k) \tag{4.26}$$

where $\mathbf{z}_a(k) = \begin{bmatrix}\mathbf{z}(k)^T & \mathbf{z}_c(k)^T\end{bmatrix}^T$, $\mathbf{h}_a\big[\mathbf{x}(k)\big] = \begin{bmatrix}\mathbf{h}[\mathbf{x}(k)]^T & \mathbf{H}_c\mathbf{x}(k)^T\end{bmatrix}^T$, and $\mathbf{v}_a(k) = \begin{bmatrix}\mathbf{v}(k)^T & \mathbf{v}_c(k)^T\end{bmatrix}$. Note that $\mathbf{H}_c = \mathbf{D}$ and $\mathbf{z}_c = \mathbf{d}$. Keeping the above

augmented form and after some derivations, the constrained state estimation using pseudomeasurement approach can be written as

$$\hat{\mathbf{x}}_a^+ = \hat{\mathbf{x}}^+ - \mathbf{P}^+\mathbf{H}_c^T(\mathbf{H}_c\mathbf{P}^+\mathbf{H}_c^T + \mathbf{R}_c)^{-1}(\mathbf{H}_c\hat{\mathbf{x}}^+ - \mathbf{z}_c) \tag{4.27}$$

$$\mathbf{P}_a^+ = \mathbf{P}^+ - \mathbf{P}^+\mathbf{H}_c^T(\mathbf{H}_c\mathbf{P}^+\mathbf{H}_c^T + \mathbf{R}_c)^{-1}\mathbf{H}_c\mathbf{P}^+ \tag{4.28}$$

where $\hat{\mathbf{x}}_a^+$ denotes the constrained state estimate and $\mathbf{P}_a^+$ is the covariance matrix of the constraint state estimate. $\hat{\mathbf{x}}^+$ represents the unconstrained state estimate and $\mathbf{P}^+$ is the covariance matrix of the unconstrained state estimate.

Comparing Eqs. (4.27) and (4.28) with the constrained state estimate $\tilde{\mathbf{x}}$ obtained by projection approach (Eq. 4.18) and the corresponding covariance (Eq. 4.19), two differences are observed. One is that the pseudomeasurement has a term of constraint error covariance which is to account for the uncertainty of the constraint, i.e., soft constraint. Another is that the pseudomeasurement approach uses the covariance matrix of the unconstrained state estimate $\mathbf{P}$ in contrast with any positive definite weighting matrix $\mathbf{W}$ in projection approach. Therefore, if only hard constraint, i.e., there is no constraint uncertainty, is considered and $\mathbf{W} = \mathbf{P}^{-1}$, the two approaches have an identical solution. In practice, the road information obtained from digital maps always has errors, such as the modeling error, the road width, and so on. Therefore, using a pseudomeasurement approach can better incorporate the soft road constraint into the tracking process as compared to the projection approach. Moreover, the pseudomeasurement approach can be easily extended to the nonlinear road constraint by simply using the EKF equation.

The derivation of the constrained state estimate in terms of the unconstrained estimate obtained by the pseudomeasurement approach applying soft constraint, Eqs. (4.27) and (4.28), is given in Appendix C.3. The corresponding derivation for hard constraints can be found in [88].

Comparison of the Estimation Process

From the estimation process point of view, these two approaches are different as shown in Fig. 4.2. For the pseudomeasurement approach, the constraint is dealt with simultaneously with the measurement update. For the projection approach, however, the constraint is applied after the measurement update. In the linear case and for independent assumptions of the measurement noises, these two ways are equivalent. But in nonlinear case, the projection approach may diverge since the ambiguity arises when there are less than three measurements available. Therefore, an advantage of pseudomeasurement approach can be naturally obtained that the constraint is re-

garded as an extra measurement and hence it will improve the observability when there are not a sufficient number of measurements available for obtain a unique position estimate.

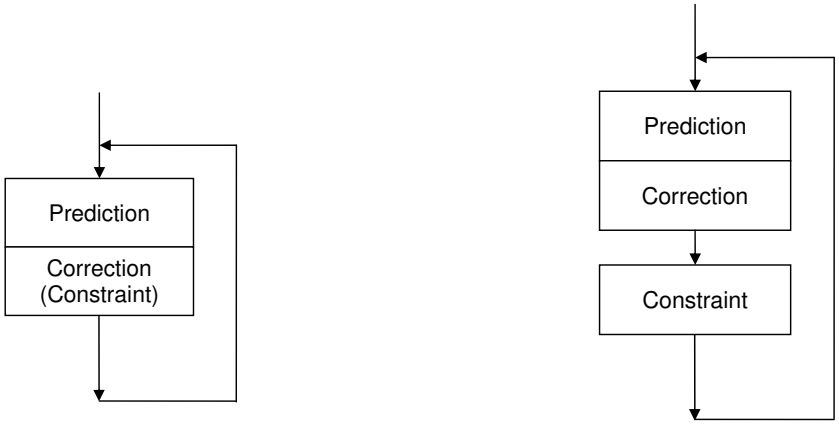

(a) Pseudomeasurement approach (b) Projection approach

Figure 4.2: Estimation process

4.3 Road Constraint as Pseudomeasurement: Linear Case

Since the road constraint is a soft constraint considering the uncertainty of the digital map and the ignorance of road width, we will apply the pseudomeasurement approach to incorporate the road constraint into the estimation process. This section will focus on a linear formulation of the straight road constraint, and next section will deal with a curve road, which is a nonlinear constraint. On one hand, a theoretical performance comparison using the *posterior Cramér-Rao lower bound* (PCRLB) and a numerical performance comparison of an EKF with the proposed road constraints and without constraints is given. We will show that the road-constrained approach can significantly improve the tracking accuracy. On the other hand, the benefits of the proposed road-constrained approach are demonstrated by different simulation scenarios, including uniform motion, maneuver motion, and also the scenario when there are fewer than three independent measurements available.

4.3.1 Position Estimation without Constraints

As discussed in Chapter 3, for the problem of target tracking, the target motion and its observations are usually described by state space model

$$\mathbf{x}(k+1) = \mathbf{f}\big[\mathbf{x}(k)\big] + \mathbf{G}(k)\mathbf{w}(k) \tag{4.29}$$

$$\mathbf{z}(k) = \mathbf{h}\big[\mathbf{x}(k)\big] + \mathbf{v}(k) \tag{4.30}$$

It is assumed that the states to be estimated are position and velocity of a MS in two dimensions, i.e., $\mathbf{x} = \begin{bmatrix} x & \dot{x} & y & \dot{y} \end{bmatrix}^T$. The state transition model (Eq. 4.29) can be described by a CV model (see Section 3.1.1).

The measurements can be *time of arrival* (TOA), *time difference of arrival* (TDOA), *received signal strength* (RSS), *angle of arrival* (AOA), and so on. Here we will use the TOA measurement as an example and this method can be also utilized for other types of measurements. Let the position of the MS be (x, y) and the position of the BTS be (x_i, y_i), where i represents a certain BTS. For finding a position in two dimensions, at least three base stations are required, whose position coordinates are (x_a, y_a), (x_b, y_b) and (x_c, y_c), respectively. We define

$$d_i = \sqrt{(x - x_i)^2 + (y - y_i)^2}, \quad i = a, b, c \tag{4.31}$$

Then the measurement model (Eq. 4.30) can be written as

$$\mathbf{z}(k) = \begin{bmatrix} d_a(k) \\ d_b(k) \\ d_c(k) \end{bmatrix} + \mathbf{v}(k) \tag{4.32}$$

where $\mathbf{v}(k)$ is the measurement noise vector which is assumed to be a zero-mean white Gaussian noise.

$$\mathbf{v}(k) \sim \mathcal{N}\big(\mathbf{0}, \mathbf{R}(k)\big) \tag{4.33}$$

$$\mathbf{R}(k) = \mathrm{diag}(\sigma_d^2, \sigma_d^2, \sigma_d^2) \tag{4.34}$$

4.3.2 Road Constraints as Pseudomeasurements

Assuming that the target is traveling on a given road segment, the following constraints exist: the position of the target lies on the road and the associated velocity is along with the direction of the road. There is an important step before incorporating the road constraint into the estimation process, i.e.,

creating an analytical representation for a given road segment [89]. As introduced in section 4.1, the road network is usually represented by waypoints in the digital map database. Thus a straight road segment can be built by connecting the waypoints. On the other hand, if the road is a curve, it is represented by shapepoints in database. A polynomial function can be used to define the road, which is a nonlinear function (to be discussed in the next section).

Let $s\big(x(t), y(t)\big) = 0$ denote the road segment function, which can be linear or curved, and $\mathbf{n}_s(t)$ represents the normal vector of the road segment, the constraints can be described by

$$s\big(x(t), y(t)\big) = 0 \tag{4.35}$$

$$\mathbf{v}(t) \cdot \mathbf{n}_s(t) = 0 \tag{4.36}$$

where Eq. (4.36) denotes that the velocity vector $\mathbf{v}(t) = \begin{bmatrix}\dot{x}(t) & \dot{y}(t)\end{bmatrix}^T$ and $\mathbf{n}_s(t)$ are orthogonal.

Supposing that the road is straight, the general road constraint (Eq. 4.35) and (Eq. 4.36) can be put in the following discrete time form

$$\tan\theta \cdot x(k) - y(k) + c = 0 \tag{4.37}$$

$$\tan\theta \cdot \dot{x}(k) - \dot{y}(k) = 0 \tag{4.38}$$

where θ is the road direction, c is the parameter of the linear function for the road segment, which are both *a priori* information. The above equations can be written as the pseudomeasurement model (Eq. 4.4)

$$\mathbf{z}_c(k) = \mathbf{H}_c\mathbf{x}(k) + \mathbf{v}_c(k) \tag{4.39}$$

$$\mathbf{z}_c(k) = \begin{bmatrix}-c \\ 0\end{bmatrix}, \mathbf{H}_c = \begin{bmatrix}\tan\theta & 0 & -1 & 0 \\ 0 & \tan\theta & 0 & -1\end{bmatrix} \tag{4.40}$$

where $\mathbf{v}_c(k)$ is assumed to be a zero-mean white Gaussian noise (Eq. 4.5), which accounts for the uncertainty of the constraints, such as road width, error of the road function, and so on.

4.3.3 EKF for Road-Constrained Tracking

After defining the road constraints as pseudomeasurements, the original measurement model of TOA (Eq. 4.32) will be augmented by the pseudomeasurement model of Eq. (4.39). The measurement covariance matrix is also augmented as $\mathbf{R}_a(k) = \text{diag}\big[\mathbf{R}(k), \mathbf{R}_c(k)\big]$, where $\mathbf{R}_c(k)$ is the covariance matrix of the pseudomeasurement noise $\mathbf{v}_c(k)$.

Because of the nonlinear mapping of the states into the observation space (Eq. 4.32), an EKF can be applied to obtain a suboptimal estimate of the states[4]. $\mathbf{H}_a(k+1)$ is the Jacobian matrix of the augmented measurement function $\mathbf{h}_a$

$$\mathbf{H}_a(k+1) \triangleq \left.\frac{\partial \mathbf{h}_a\big[\mathbf{x}(k+1)\big]}{\partial \mathbf{x}(k+1)}\right|_{\hat{\mathbf{x}}^-(k+1)} \tag{4.41}$$

$$= \begin{bmatrix} \dfrac{x(k+1)-x_a}{d_a(k+1)} & 0 & \dfrac{y(k+1)-y_a}{d_a(k+1)} & 0 \\ \dfrac{x(k+1)-x_b}{d_b(k+1)} & 0 & \dfrac{y(k+1)-y_b}{d_b(k+1)} & 0 \\ \dfrac{x(k+1)-x_c}{d_c(k+1)} & 0 & \dfrac{y(k+1)-y_c}{d_c(k+1)} & 0 \\ \tan\theta & 0 & -1 & 0 \\ 0 & \tan\theta & 0 & -1 \end{bmatrix} \tag{4.42}$$

evaluated at the predicted value of the state $\hat{\mathbf{x}}^-(k+1)$, where $p_a = (x_a, y_a)$, $p_b = (x_b, y_b)$, and $p_c = (x_c, y_c)$ are the two dimensional position coordinates of the three BTSs a, b, c, respectively.

4.3.4 Simulation Results

Simulation Scenario

The simulations are carried out in a simulated urban square area of 5 km by 5 km as shown in Fig. 4.3. Within this area there are three BTSs, a, b and c. We assume that a vehicle equipped with a MS travels along a linear route, the direction of which is 0° and the y coordinate is always 3000 m. Therefore, the pseudomeasurement model for road constraints (Eq. 4.39) is specified by $\mathbf{z}_c(k) = \begin{bmatrix} -3000 \\ 0 \end{bmatrix}$ and $\mathbf{H}_c = \begin{bmatrix} 0 & 0 & -1 & 0 \\ 0 & 0 & 0 & -1 \end{bmatrix}$.

The target movements are generated by the curvilinear motion model (Eq. 3.11), which is called truth model since it represents the real trajectory for our simulations. The state vector $\mathbf{x}_t(k) = \begin{bmatrix} x(k) & y(k) & v(k) & \phi(k) \end{bmatrix}^T$ includes the target position in two dimensions, speed and heading. a_t and a_n denote tangential and normal accelerations, respectively. Through setting

[4]It is assumed in optimal filters that exact descriptions of system dynamics, error statistics and the measurement process are known. However, for nonlinear systems, this can bot be available and approximations of these factors in the filters should be applied, which results in suboptimal filters.

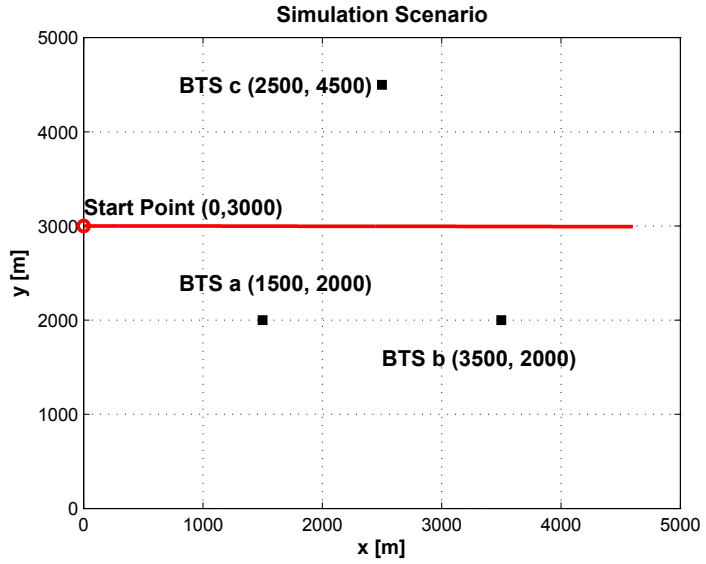

Figure 4.3: Simulation scenario

different values of them, we can generate not only uniform motion but also maneuver motion. The process noise $\mathbf{w}_t(k) = \begin{bmatrix} w_x(k) & w_y(k) & w_v(k) & w_\phi(k) \end{bmatrix}^T$ is assumed to be zero-mean white Gaussian noise

$$\mathbf{w}_t(k) \sim \mathcal{N}\big(\mathbf{0}, \mathbf{Q}_t(k)\big) \tag{4.43}$$

$$\mathbf{Q}_t(k) = \mathrm{diag}(\sigma_x^2, \sigma_y^2, \sigma_v^2, \sigma_\phi^2) \tag{4.44}$$

where σ_x, σ_y, σ_v, σ_ϕ are the standard deviations of the process noise set to be the values of 10^{-2} m, 10^{-2} m, 10^{-3} m/s and 10^{-4} rad, respectively. The measurement update rate is $T = 0.48$ s. The standard deviation of the measurement noise (Eq. 4.34) is assumed to be $\sigma_d = 300$ m.

In the following, we will analyze the performance of an EKF using the proposed road-constrained approach in comparison to a normal EKF without constraints in different simulated movements including uniform motion and maneuver motion. In order to show the performance of the EKF, for each comparison the corresponding PCRLB, which represents the theoretically best achievable estimation performance for the given simulation scenario, will also be plotted. Moreover, the performance comparison under the situation, when less than three measurements are available, will also be shown. All of the results are obtained by Monte Carlo simulations with 500 runs.

PCRLB for the Road-Constrained Approach

The calculation of the PCRLB has already been introduced in Section 3.3. The two important issues for the PCRLB are the Jacobian matrix of the state transition function and the measurement function. It should be noticed that in order to calculate PCRLB the truth model of the real trajectory, i.e., the curvilinear model, as opposed to the simplified dynamic model for the EKF design should be used. Let $\mathbf{F}_t(k)$ be the Jacobian matrix of the state transition function in the truth model $\mathbf{f}_t[\cdot]$

$$\mathbf{F}_t(k) \triangleq \left.\frac{\partial \mathbf{f}_t\big[\mathbf{x}_t(k)\big]}{\partial \mathbf{x}_t(k)}\right|_{\mathbf{x}_t(k)} \tag{4.45}$$

$$= \begin{bmatrix} 1 & 0 & T\cos\big(\phi(k)\big) & -Tv(k)\sin\big(\phi(k)\big) \\ 0 & 1 & T\sin\big(\phi(k)\big) & Tv(k)\cos\big(\phi(k)\big) \\ 0 & 0 & 1 & 0 \\ 0 & 0 & -\dfrac{Ta_n(k)}{v(k)^2} & 1 \end{bmatrix} \tag{4.46}$$

evaluated at the real value of state $\mathbf{x}_t(k) = \begin{bmatrix} x(k) & y(k) & v(k) & \phi(k) \end{bmatrix}^T$. Let $\mathbf{H}_t(k+1)$ be the Jacobian matrix of the nonlinear augmented measurement function $\mathbf{h}_t[\cdot]$ evaluated at the real value of the state $\mathbf{x}_t(k+1)$. $\mathbf{h}_t$ consists of the measurement (Eq. 4.32) and the pseudomeasurement functions (Eq. 4.39), except that the second pseudomeasurement equation is replaced by

$$\theta = \phi(k) + v_\phi(k) \tag{4.47}$$

because of the different state $\phi(k)$ in the truth model $\mathbf{x}_t$, where $v_\phi(k)$ is the corresponding pseudomeasurement noise and θ is the known road direction. Thus,

$$\mathbf{H}_t(k+1) \triangleq \left.\frac{\partial \mathbf{h}_t\big[\mathbf{x}_t(k+1)\big]}{\partial \mathbf{x}_t(k+1)}\right|_{\mathbf{x}_t(k+1)} \tag{4.48}$$

$$= \begin{bmatrix} \dfrac{x(k+1)-x_a}{d_a(k+1)} & \dfrac{y(k+1)-y_a}{d_a(k+1)} & 0 & 0 \\ \dfrac{x(k+1)-x_b}{d_b(k+1)} & \dfrac{y(k+1)-y_b}{d_b(k+1)} & 0 & 0 \\ \dfrac{x(k+1)-x_c}{d_c(k+1)} & \dfrac{y(k+1)-y_c}{d_c(k+1)} & 0 & 0 \\ \tan\theta & -1 & 0 & 0 \\ 0 & 0 & 0 & 1 \end{bmatrix} \tag{4.49}$$

evaluated at $\mathbf{x}_t(k+1)$, where $p_a = (x_a, y_a)$, $p_b = (x_b, y_b)$, and $p_c = (x_c, y_c)$ are the two dimensional position coordinates of the three BTSs a, b, c, respectively. In this simulation $\theta = 0$ rad. $\mathbf{Q}_t$ is the covariance matrix of process noise in the truth model as shown in Eq. (4.43), and $\mathbf{R}_t$ is the covariance matrix of measurement noise. The expectation should be taken over the whole 500 Monte Carlo trials.

Uniform Motion

Uniform motion refers to the straight and level motion at constant velocity, which is the simplest target motion. We generate the uniform motion by setting the parameters of the truth model: the tangential acceleration is $a_t = 0$ m/s^2, the normal acceleration is $a_n = 0$ m/s^2, the initial position is $(0 \text{ m}, 3000 \text{ m})$ and the initial velocity is $(15 \text{ m/s}, 0 \text{ m/s})$. The parameters for the EKF are chosen as follows: a *nearly constant velocity* (CV) model is chosen as the dynamic model, the standard deviations of the process noise $\sigma_x = \sigma_y = 10^{-4}$ m/s^2; the covariance matrix of the pseudomeasurement noise $\mathbf{R}_c = \text{diag}\left[(10 \text{ m})^2, (1 \text{ m/s})^2\right]$. The initial state values of the EKF are calculated by one point TOA measurement, and the initial $\mathbf{P}$ matrix is set to be $\mathbf{P}^+(0) = \text{diag}\left[(300 \text{ m})^2, (30 \text{ m/s})^2, (300 \text{ m})^2, (30 \text{ m/s})^2\right]$.

The *root mean square error* (RMSE) is shown in Fig. 4.4. It is observed that the EKF with road constraints outperforms the normal EKF without constraints. Especially at the initial phase the accuracy improvement is significant, which means that the estimates converge to the real values very quickly. By comparing the RMSE to the corresponding PCRLB, not only the EKF without constraints but also the EKF with constraints are very close to the best theoretical performance under uniform motion.

Maneuver Motion

However, in the real world maneuver motion occurs more often. In this section we only discuss the performance of the maneuver motion under tangential accelerations. The trajectory consists of uniform motion parts and two maneuvers of only tangential accelerations, both of which are about 10 seconds. In the first maneuver, the vehicle accelerates under $a_t = 3$ m/s^2 and the second maneuver is a deceleration of $a_t = -3$ m/s^2. During the whole time the normal acceleration is $a_n = 0$ m/s^2. The initial position is $(0 \text{ m}, 3000 \text{ m})$ and the initial velocity is $(5 \text{ m/s}, 0 \text{ m/s})$. The dynamic model of the EKF is still a CV model. But the parameters of the EKF are modified as: the standard deviations of the process noises $\sigma_x = \sigma_y = 3$ m/s^2

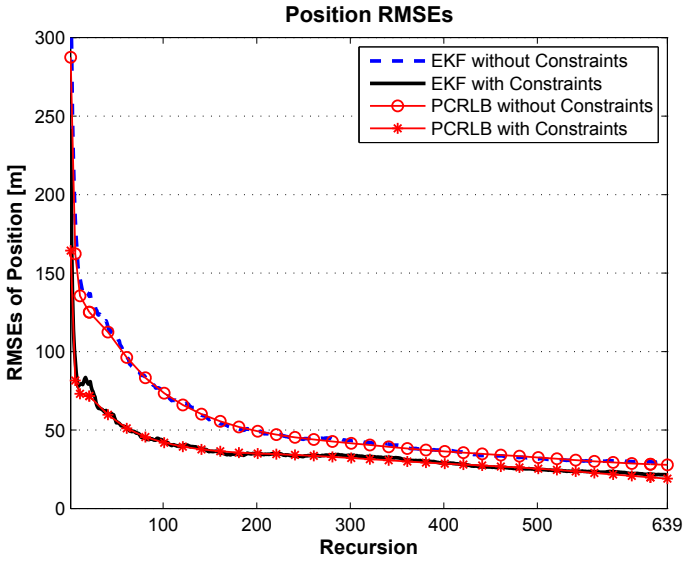

Figure 4.4: Comparison of position RMSEs for uniform motion

considering the maneuver. The covariance matrix of the measurement and pseudomeasurement noise are the same as in the uniform motion case.

The RMSE performance comparisons are given in Fig. 4.5. It is obviously that the EKF with road constraints has better accuracy than the EKF

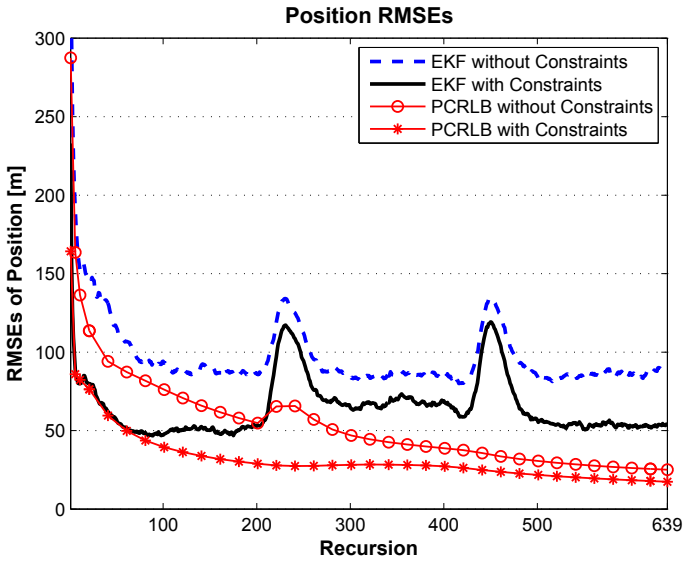

Figure 4.5: Comparison of position RMSEs for maneuver motion

without constraints not only during uniform motions but also during the maneuvers. It is observed that the RMSEs do not achieve the corresponding PCRLBs, even in case of uniform motion, because we have chosen a bigger value for the standard deviation of the process noise in order to get a satisfying performance during the maneuver period. Choosing a smaller process noise can decrease the RMSE during uniform motion but obtain bigger peak errors during the maneuvers. However, on the other hand, it should also be noticed that the PCRLB for the maneuver motion is too conservative since it assumes that the maneuver is completely known, which should be actually estimated by the estimator [90].

Performance of Different Numbers of BTSs

As is well known, to uniquely determine a position in two dimensions using trilateration technique, at least three BTSs are required to solve the ambiguities. However, sometimes this condition can not be satisfied. In many rural and suburban areas the cell size is large and the cell density is low. In urban areas the blockage of high-rise buildings will introduce NLOS errors and even there is no LOS propagation available. Moreover, under current GSM specifications a TA measurement is only taken in the current serving BTS. To obtain more TAs, artificially forced handovers should be carried out, but this will degrade the call quality and reduce the system capacity. Therefore, in such situations the available number of BTSs might be less than three, or in order to obtain more measurements from other BTSs may cause more efforts and introduce errors. Although the EKF can always run and provide a position estimate since the EKF can predict the state, the estimation will be unreliable when less than three BTSs are available. In this part of the study, we examine the performance of a standard EKF and an EKF with road constraints when less than three measurements are available.

The trajectory of a uniform motion is generated similar to the first simulation. The performance of different approaches, when measurements from four BTSs of a, b, c and d, three BTSs of a, b and c, only two BTSs of a and b, or only one BTS of b are available, are compared. The coordinate of BTS d is $(2500\text{ m}, 0\text{ m})$, and the coordinates of other BTSs are the same as before. The parameters of the EKF are similar to the first simulation. But the initial values of the states are set to the true initial values $\mathbf{x}^+(0) = \begin{bmatrix}0\text{ m} & 15\text{ m/s} & 3000\text{ m} & 0\text{ m/s}\end{bmatrix}^T$, since there are not enough measurements available to calculate the initial position.

Figure 4.6a shows that using the standard EKF it is possible to obtain an estimate when only two observations are available and the estimate di-

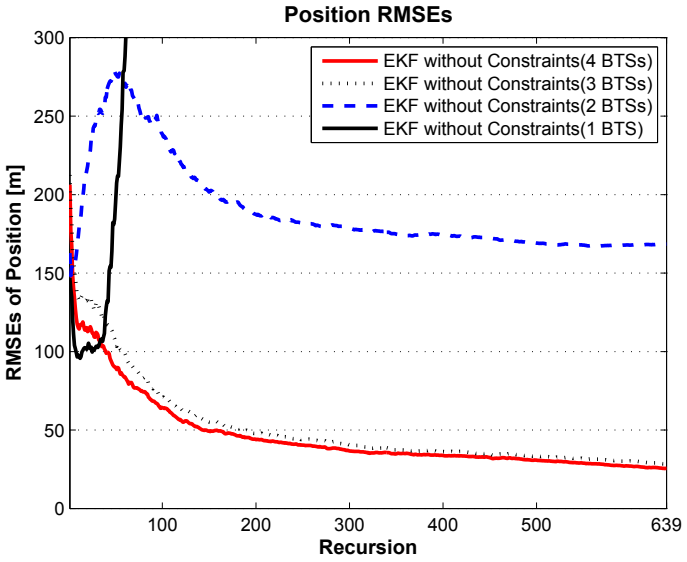

(a) Position RMSEs for EKF without constraint

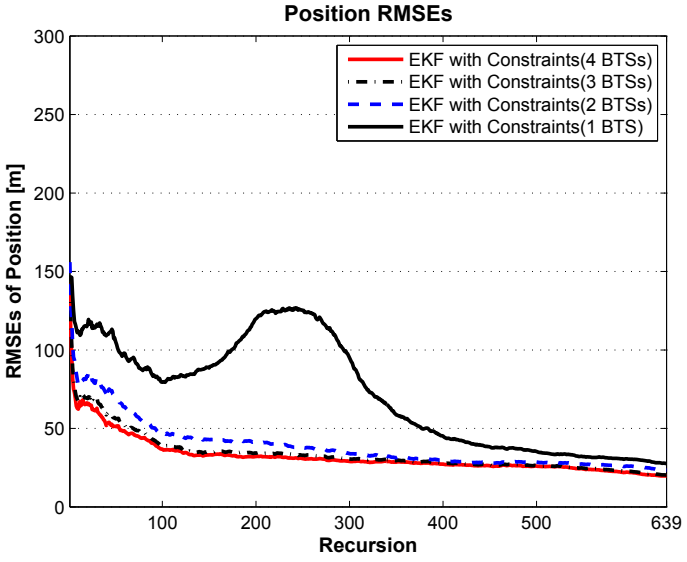

(b) Position RMSEs for EKF with constraint

Figure 4.6: Position RMSEs for different numbers of BTSs

verges in case of only one observation, which corresponds to the observability analysis in [40] that in principle two independent measurements can be sufficient for tracking, and in case of only one measurement the estimate cannot be found. It should be noticed, however, that the results of the standard

EKF with two measurements may not be accurate enough and it depends on the configuration of the base stations. In contrast, Fig. 4.6b shows the results of the EKF with constraints. The estimator can still provide stable and accurate estimates when two measurements are available, because the road constraints strengthen the observability condition. Even in the case of only one measurement, the estimates can converge. Moreover, for both unconstrained and constrained approaches, the EKF using four measurements provides the best accuracy, but it doesn't improve much compared with using three measurements.

4.4 Road Constraint as Pseudomeasurement: Nonlinear Case

In the last section, we expand the approach of treating straight road constraints as pseudomeasurements for target tracking in GSM networks. However, as Geeter [82] and Julier [78] argued that nonlinear equality constraints are fundamentally different from linear equality constraints since two errors arise, i.e., truncation error and base point error, the performance of tracking ground targets in GSM networks in the presence of nonlinear road constraints deserves to be examined. The objective of this work is to demonstrate the benefits of applying nonlinear road constraints in ground target tracking in GSM networks. Comparative studies of utilizing an EKF without constraint and with constraint verify that the road-constrained approach significantly improves the tracking accuracy. Another performance study on different numbers of available measurements demonstrates the efficiency and robustness of this approach. Moreover, by comparing the performance of the pseudomeasurement and the projection approach in the presence of nonlinear road constraints, the former has a better performance. The results of the comparison will be analyzed and discussed.

4.4.1 Formulation

Assuming that the target is traveling on a given road segment, the two-dimensional position of the target $\big(x(t), y(t)\big)$ must lie on the road. Then the constraint $s\big(x(t), y(t)\big) = 0$ exists, where $s(\cdot)$ denotes the road segment and normally the road can be modeled by straight lines, arcs, or low-order polynomials. Without losing generality, we assume a polynomial function of

second degree to represent a road segment as

$$s\big(x(t), y(t)\big) = a \cdot x(t)^2 + b \cdot y(t)^2 + c \cdot x(t)y(t) + d \cdot x(t) + e \cdot y(t) + f \quad (4.50)$$

where the parameters a, b, c, d, e, f are all *a priori* information given for a specific road segment. Compared to the real measurement model, the road constraint (Eq. 4.50) can be rewritten as a pseudomeasurement model in discrete time

$$z_c(k) = h_c\big[\mathbf{x}(k)\big] + v_r(k) \quad (4.51)$$

where $z_c(k) = 0$, $h_c\big[\mathbf{x}(k)\big] = s\big(x(k), y(k)\big)$, and $v_r(k)$ is assumed to be zero-mean white Gaussian noise, which accounts for the uncertainty of the road constraint, such as road width, error of the road function, and so on.

$$v_r(k) \sim \mathcal{N}\big(0, R_r(k)\big) \quad (4.52)$$

$$R_r(k) = \sigma_r^2 \quad (4.53)$$

With the formulation of Eq. (4.51), an EKF is readily applied.

4.4.2 EKF for Road-Constrained Tracking

After defining the road constraint as a pseudomeasurement, the original measurement model of TOA can be augmented by the pseudomeasurement model (Eq. 4.51) as

$$\mathbf{z}_a(k) = \mathbf{h}_a\big[\mathbf{x}(k)\big] + \mathbf{v}_a(k) \quad (4.54)$$

where $\mathbf{z}_a(k) = \begin{bmatrix}\mathbf{z}(k)^T & z_c(k)\end{bmatrix}^T$, $\mathbf{h}_a\big[\mathbf{x}(k)\big] = \begin{bmatrix}\mathbf{h}\big[\mathbf{x}(k)\big]^T & h_c\big[\mathbf{x}(k)\big]\end{bmatrix}^T$, and $\mathbf{v}_a(k) = \begin{bmatrix}\mathbf{v}(k)^T & v_r(k)\end{bmatrix}^T$. Because of the nonlinear mapping of the states into the observation space, an EKF can be applied to obtain a suboptimal estimate of the states (Eqs. 4.7-4.12) as introduced in Section 4.2.1.

To deal with the nonlinear constraint, the measurement noise covariance matrix in EKF is augmented as $\mathbf{R}_a(k) = \text{diag}\begin{bmatrix}\mathbf{R}(k), R_c(k)\end{bmatrix}$. The variance of the pseudomeasurement error $R_c(k)$ should consist of two components

$$R_c(k) = R_r + R_0 \cdot \beta^{k-1} \quad (4.55)$$

where R_r (Eq. 4.52) represents the road modeling error, and a weakening component $R_0 \cdot \beta^{k-1}$ is to account for the linearization error, which includes truncation error resulting from neglecting the higher order terms of the Taylor series expansion in EKF and base point error due to linearizing around the predicted state estimate [82]. Considering the large initial estimation error,

this linearization error should be large at the beginning of the estimation and decrease as the estimation process proceeds. Therefore, the weakening component can be chosen as an initial value $R_0 = \alpha \cdot \mathbf{H}_c(1)\mathbf{P}^-(1)\mathbf{H}_c^T(1)$ at $k = 1$, which is a fraction α of the predicted state error covariance transformed to constraint space via the constraint Jacobian $\mathbf{H}_c(1)$, multiplying a decreasing term β^{k-1}, $0 < \beta < 1$. The choice of α and β needs to be verified in Monte Carlo simulations. This manipulation is the difference of applying a nonlinear road constraint compared with incorporating linear road constraints, which only considers the uncertainty of the road modeling, i.e., R_r. Through this operation, the nonlinear road constraint is applied progressively tightly.

4.4.3 Simulation Results

The simulations are carried out in a simulated square area of 5 km by 5 km as shown in Fig. 4.7. Within this area there are four BTSs, a, b, c and d. It is assumed that a vehicle equipped with a MS traveled along an arc route as an example to show the performance of the road-constrained approach. The road constraint (Eq. 4.50) can be specified to yield on the arc road and in discrete time as

$$r^2 = \big(x(k) - x_0\big)^2 + \big(y(k) - y_0\big)^2 \tag{4.56}$$

where r denotes the radius of the road arc and (x_0, y_0) is the two-dimensional coordinate of the arc's centre, both of which are known as $r = 2000$ m and $(x_0, y_0) = (1000\text{ m}, 3000\text{ m})$. The measurements update rate is $T = 0.48$ s. The standard deviation of the measurement noise is assumed to be $\sigma_d = 300$ m.

The vehicle executes a coordinated turn starting at (1000 m, 1000 m), and the initial velocity is 20 m/s and 0 m/s in x and y direction, respectively. The trajectory is generated by the curvilinear motion model (Eq. 3.11), which is called truth model since it represents the real trajectory for the simulations. The state vector $\mathbf{x}_t(k) = \begin{bmatrix} x(k) & y(k) & v(k) & \phi(k) \end{bmatrix}^T$ includes the target position in two dimensions, speed and heading. a_t and a_n denote tangential and normal accelerations, respectively, which are set to be $a_t = 0$ m/s^2, $a_n = 0.2$ m/s^2. The process noise $\mathbf{w}_t(k) = \begin{bmatrix} w_x(k) & w_y(k) & w_v(k) & w_\phi(k) \end{bmatrix}^T$ is assumed to be zero-mean white Gaussian noise

$$\mathbf{w}_t(k) \sim \mathcal{N}\big(\mathbf{0}, \mathbf{Q}_t(k)\big) \tag{4.57}$$

$$\mathbf{Q}_t(k) = \mathrm{diag}(\sigma_x^2, \sigma_y^2, \sigma_v^2, \sigma_\phi^2) \tag{4.58}$$

where σ_x, σ_y, σ_v, σ_ϕ are the standard deviations of the process noises set to be the values of 10^{-2} m, 10^{-2} m, 10^{-3} m/s and 10^{-4} rad, respectively.

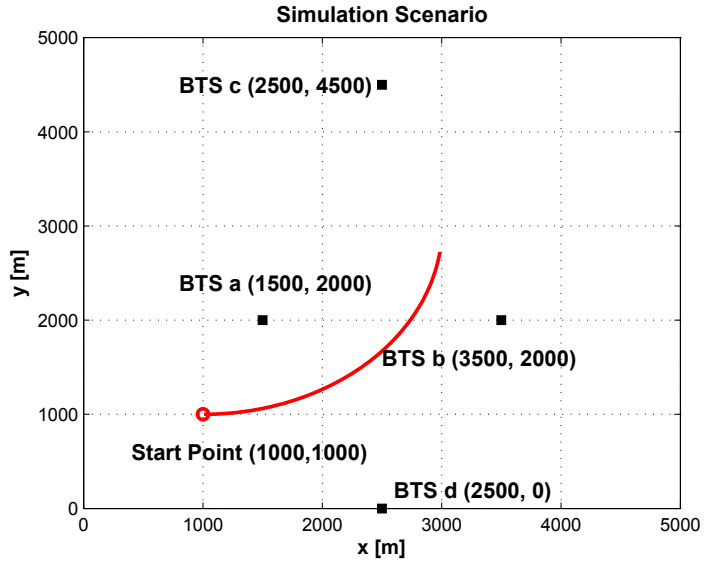

Figure 4.7: Simulation scenario

Design of the EKF

To track the trajectory shown in Fig. 4.7, the dynamic model can be described by a *nearly coordinated turn* (CT) model (see Section 3.1.4). The parameters for the EKF are chosen as follows: the standard deviation of the measurement noise is $\sigma_d = 300$ m; the standard deviation of the pseudo-measurement noise is $\sigma_r = (10 \text{ m})^2$; the standard deviations of the process noise are $\sigma_x = 10^{-4}$ m/s^2, $\sigma_y = 10^{-4}$ m/s^2, $\sigma_\omega = 10^{-6}$ rad/s^2. These designed values are chosen according to the prior knowledge and assumptions of the system, e.g., the measurement noise, the uncertainty of the road, and the trajectory. The initial state values $\hat{x}^+(0)$ and $\hat{y}^+(0)$ of the EKF are calculated by one point measurement [65], which uses a traditional least squares algorithm to achieve an initial position guess from three TOA measurements at time step $k = 0$. The initial values of velocity $\hat{\dot{x}}^+(0)$, $\hat{\dot{y}}^+(0)$ and turn rate $\hat{\omega}^+(0)$ are assumed to be zero-mean Gaussian random variables with an associated standard deviation equal to half of the known maximum state values. Thus, the initial state covariance matrix is set to $\mathbf{P}^+(0) = \text{diag}\left[(300 \text{ m})^2, (30 \text{ m/s})^2, (300 \text{ m})^2, (30 \text{ m/s})^2, (0.01 \text{ rad/s})^2\right]$.

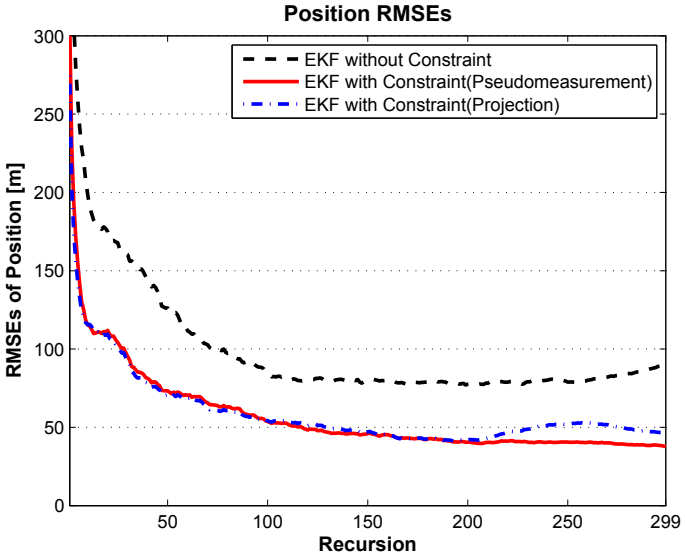

(a) Position RMSEs comparison

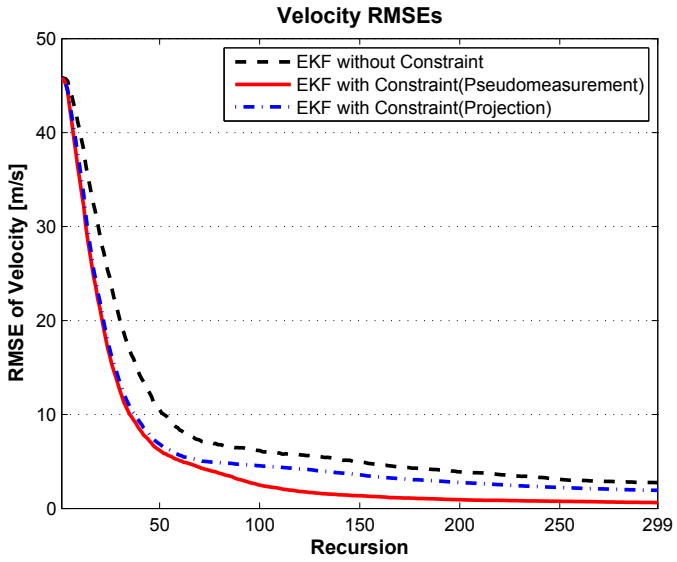

(b) Velocity RMSEs comparison

Figure 4.8: RMSE performance comparison (three BTSs)

Performance Comparisons of Different Approaches

The RMSE performance of EKFs without constraint, and with constraint on the base of three TOA measurements from BTS a, b and c, are shown

in Fig. 4.8. 500 Monte Carlo trials are run. It is observed that the results of the EKFs with constraint, no matter using pseudomeasurement or projection method, outperform that of the EKF without constraint. Especially at the initial phase the accuracy improvements are significant, which means that the estimates converge to the real values much quicker than those of the EKF without constraint. However, by comparing the performance of pseudomeasurement and projection methods, it is shown that the position RMSE of the two approaches are similar, but the pseudomeasurement approach has a smaller velocity RMSE than the projection approach.

Performance of Different Numbers of BTSs

In this part of simulations the performance of different approaches, when measurements from four BTSs of a, b, c and d, three BTSs of a, b and c, only two BTSs of a and b, or only one BTS of b are available, are compared. Same to the last simulation, 500 Monte Carlo simulations are run. The position RMSEs performance is shown in Fig. 4.9-Fig. 4.11.

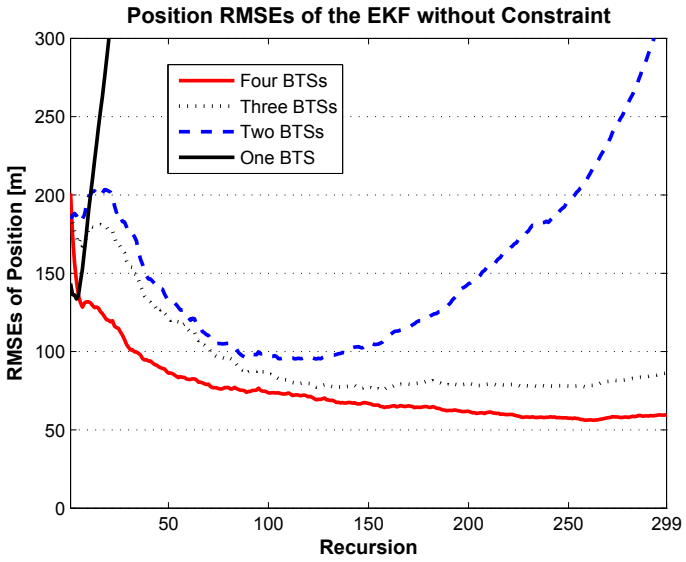

Figure 4.9: Position RMSEs of the EKF without constraint

For all of these three approaches, it is shown that the estimation performance in case of four measurements has the highest accuracy. For the EKF without constraint, the RMSEs in cases of only two measurements and only one measurement diverge. For the EKF with constraint using the projection approach, it is possible to get a position estimate in the case of two

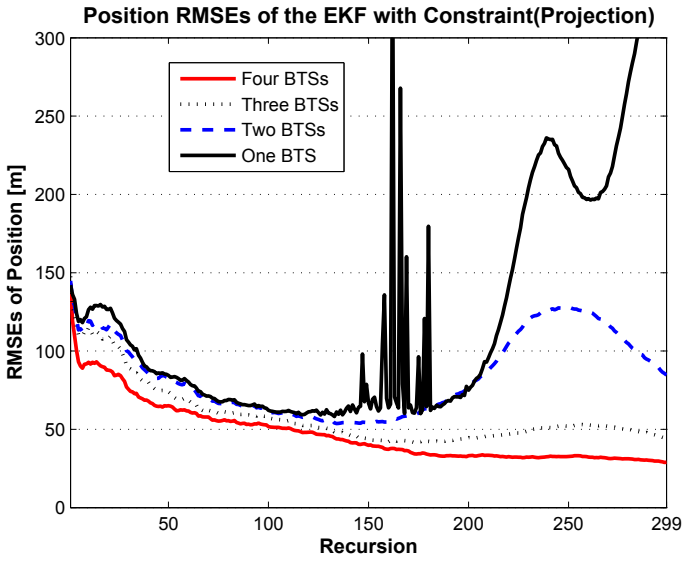

Figure 4.10: Position RMSEs of the EKF with constraint (projection approach)

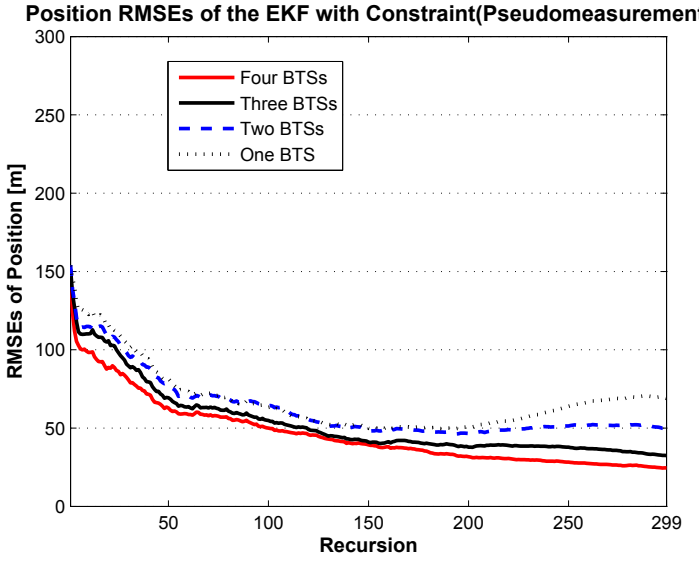

Figure 4.11: Position RMSEs of the EKF with constraint (pseudomeasurement approach)

measurements, but it diverges in the case of one measurement. It is noticed that the EKF with constraint using pseudomeasurement still converges

in the case of two measurements and can obtain an estimate in the case of one measurement. The difference of projection and pseudomeasurement approach is that the former one applies the normal EKF and then sequentially projects the unconstrained estimate into the constraint surface, but the pseudomeasurement approach augments the measurement model in the EKF by one pseudomeasurement equation, thus the necessary number of measurements for trilateration in two dimensions is reduced to two. Therefore, the estimator using pseudomeasurement to incorporate the road constraint can still provide stable and accurate estimates when only two measurements are available, and it is more robust than the projection approach.

4.5 Summary

In this chapter, we have investigated how to incorporate road constraints into the estimation process to improve the estimation accuracy. Firstly, the road information was introduced and the approaches of constrained state estimation were presented and compared. The pseudomeasurement approach has many advantages. It provides a convenient framework for incorporating constraints without greatly increasing the computational cost. The estimation performance will be improved since using the constraints removes some of the target dynamic uncertainty. In addition, it has less computational complexity to incorporate the constraints into the measurement model rather than into the state transition model, especially in the case of nonlinear constraints. We formulate the road constraint as a pseudomeasurement in the linear case and also in the nonlinear case. The EKF for the constrained system has also been explained. In particular, the nonlinear road constraint should be applied progressively tightly considering the linearization error.

The simulations verify that the road-constrained approach using pseudomeasurement significantly improves the estimation accuracy. Figures 4.6 and 4.9 - 4.11 show the tracking performance with different numbers of available BTSs. The constrained approach can obtain a good tracking accuracy of below 50 m even if there are only two BTSs available, whereas without the constraint two measurements can only provide position estimates of one to two hundred meters and which will diverge. Therefore, the constrained approach can reach the E112 accuracy goal of 10 m - 150 m in urban areas. Moreover, the hearability problem of the BTSs can be relaxed since only two BTSs are required for the constrained approach.

Chapter 5

An Adaptive Road-Constrained IMM Estimator

For the application of ground target tracking, the target should be regarded as a maneuvering target since the state to be estimated may change dramatically due to the restriction of terrain, road, traffic, and so on. In this chapter, we consider this target motion uncertainty problem in GSM environments. The maneuvering target tracking problem is formulated in Section 5.1. It is well known that *multiple model* (MM) estimation is a powerful approach for such a hybrid estimation problem. In Section 5.2 the *interacting multiple model* (IMM) estimator is analyzed and the estimation results of three different simulated scenarios are evaluated by the corresponding *posterior Cramér-Rao lower bound* (PCRLB) and compared with the single model method of using a *nearly constant velocity* (CV) model. The comparisons show that the IMM estimator reduces the estimation errors during the non-maneuvering period. However, a GSM positioning system based on current specifications faces many difficulties to yield accurate position estimate for ground target tracking. The additional information of the road network is very useful not only for restricting the target position inside the road but also for providing a potential constraint on the possible target motions. In Section 5.3, we propose an *adaptive road-constrained IMM* (ARC-IMM) estimator, in which the road constraint is incorporated into a *variable structure IMM* (VS-IMM) mechanism as a pseudomeasurement. The module set of the ARC-IMM, not only the dynamic model but also the road constraint, is updated adaptively according to the estimated target position and the road network. In particular, the selection of the dynamic models depends also

on the road constraint. The simulation results verify that the proposed approach significantly improves the estimation accuracy in comparison to an IMM estimator with directional noise, a standard IMM estimator and an EKF. A simulation study in the case of only two available measurements demonstrates the efficiency and robustness of the proposed approach.

5.1 Maneuvering Target Tracking

Different from air targets, ground targets may frequently accelerate, slow down, stop completely and turn depending on variable local conditions, e.g., terrain, road and traffic situations. Basically the target dynamics or motions are classified into two categories: *nonmaneuver motion*, which stands for the straight and level motion at a constant velocity, and *maneuver motion*, which includes all the other motions. The ground target motion has the unique nature of high maneuverability.

Kalman filters perform well if the target dynamics match the model, used in the filter, which assumes the dynamics to be well modeled. The traditional dynamic models which can describe the maneuver are CV model with relatively high process noise, *nearly constant acceleration* (CA) model, *coordinated turn* (CT) model, Singer model and so on [70]. But in most cases when a target maneuvers, the motion models turn to be uncertain and time varying. Therefore, the problem of maneuvering ground target tracking can be described by a hybrid system, which is usually modeled by the equations

$$\begin{aligned}\mathbf{x}(k+1)=&\mathbf{f}\big[k,\mathbf{x}(k),m(k+1)\big]\\&+\mathbf{g}\left[k,\mathbf{x}(k),m(k+1),\mathbf{w}\big[k,\mathbf{x}(k),m(k+1)\big]\right] \qquad (5.1)\\ \mathbf{z}(k)=&\mathbf{h}\big[k,\mathbf{x}(k),m(k)\big]+\mathbf{v}\big[k,\mathbf{x}(k),m(k)\big] \qquad (5.2)\end{aligned}$$

where $\mathbf{x}$ is the state vector, $\mathbf{z}$ is the noisy measurement vector, and $\mathbf{w}[\cdot\,]$ and $\mathbf{v}[\cdot\,]$ are the state-dependent mode-dependent process and measurement noises, which are assumed to be white Gaussian noises. The $\mathbf{f}[\cdot\,]$, $\mathbf{g}[\cdot\,]$ and $\mathbf{h}[\cdot\,]$ are nonlinear functions. $m(k)$ denotes the system mode at time k, i.e., a pattern of the target behavior, which is assumed to be among the possible r modes $m(k) \in \{M_j\}, j = 1, \ldots, r$ and it is assumed that the mode switching is a Markov chain with known mode transition probabilities

$$p_{ij} \triangleq P_{m(k)|m(k-1)}\left\{M_j|M_i\right\} \qquad (5.3)$$

It should be noted that here the mode transition probabilities are constant, which do not depend on time. As shown in Eqs. (5.1) and (5.2), the hybrid

system has both continuous uncertainties, i.e., the state, and discrete uncertainties, i.e., the mode. Thus, the hybrid estimation problem is to estimate the state and the mode based on the noisy measurements.

In order to solve such uncertainties, adaptive filters have been developed to detect maneuvers and adapt the filter to the target dynamics in real time and especially MM approaches have been proposed [69]. The MM estimation algorithms assume the system to be in a finite number of modes. The state estimate is computed under each possible current model by running a set of filters, and then the output of those filters are fused for an overall estimate by different ways.

5.2 Interacting Multiple Model Estimator

In recent years, MM methods have been generally considered as the mainstream approach for maneuvering target tracking under motion mode uncertainty [91], and IMM estimator is one of the most efficient MM estimators, which was firstly proposed by Blom and Bar-Shalom [65, 92]. Assuming a set of models as possible state modes, which is realized by running a bank of elemental filters in parallel, the state estimate is computed at time k in each filter using a different combination of the previous model-conditioned estimates, and the final state estimate is obtained by merging the results of all filters. Comparing with other different MM approaches which have acceptable tracking errors, the IMM algorithm has the best computational complexity [72]. The key difference of IMM approach is that at time k each filter is individually reinitialized using a different combination of the previous model-conditioned estimates, which is referred to as mixed initial condition.

5.2.1 Algorithm

Assuming that the system mode is in a finite set of possible motion models, the hybrid system (Eqs. 5.1 and 5.2) can be rewritten as:

$$\mathbf{x}(k+1) = \mathbf{f}_j\big[k, \mathbf{x}(k)\big] + \mathbf{g}_j\big[k, \mathbf{x}(k), \mathbf{w}_j(k)\big] \tag{5.4}$$

$$\mathbf{z}(k) = \mathbf{h}_j\big[k, \mathbf{x}(k)\big] + \mathbf{v}_j(k) \tag{5.5}$$

where $j = m(k)$ is in the model set $\{M_j\}, j = 1, \ldots, r$ and the mode transition probabilities are as Eq. (5.3). One cycle of the algorithm consists of the following (see Fig. 5.1):

Step 1: Calculation of the mixing probabilities. The probabilities that mode M_i was in effect at $k-1$ given that M_j is in effect at k conditioned

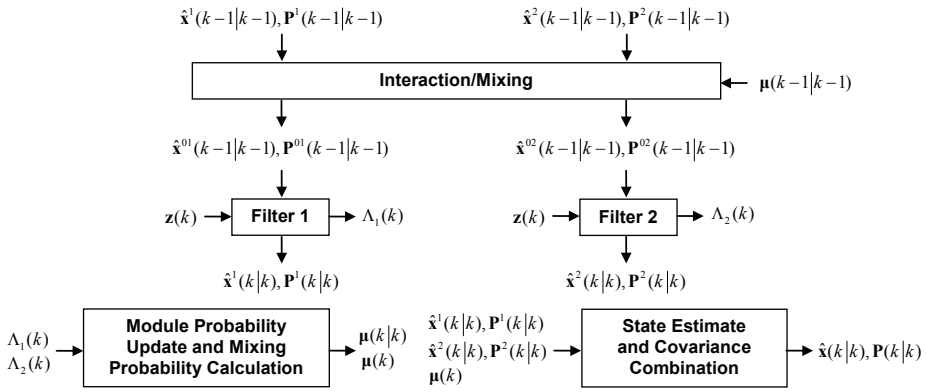

Figure 5.1: IMM algorithm consisting of two subfilters (one cycle)

on $\mathbf{z}(k-1)$ is derived applying the Bayes' theorem and the total probability theorem

$$\mu_{i|j}(k-1|k-1) \triangleq P_{m(k-1)|m(k),\mathbf{z}(k-1)}\left\{M_i|M_j,\mathbf{z}_{k-1}\right\} \tag{5.6}$$

$$= \frac{P_{m(k-1),m(k),\mathbf{z}(k-1)}\left\{M_i,M_j,\mathbf{z}_{k-1}\right\}}{P_{m(k),\mathbf{z}(k-1)}\left\{M_j,\mathbf{z}_{k-1}\right\}}$$

$$= \frac{P_{m(k)|m(k-1),\mathbf{z}(k-1)}\left\{M_j|M_i,\mathbf{z}_{k-1}\right\}P_{m(k-1)|\mathbf{z}(k-1)}\left\{M_i|\mathbf{z}_{k-1}\right\}P_{\mathbf{z}(k-1)}\left\{\mathbf{z}_{k-1}\right\}}{P_{m(k)|\mathbf{z}(k-1)}\left\{M_j|\mathbf{z}_{k-1}\right\}P_{\mathbf{z}(k-1)}\left\{\mathbf{z}_{k-1}\right\}}$$

$$= \frac{P_{m(k)|m(k-1),\mathbf{z}(k-1)}\left\{M_j|M_i,\mathbf{z}_{k-1}\right\}P_{m(k-1)|\mathbf{z}(k-1)}\left\{M_i|\mathbf{z}_{k-1}\right\}}{P_{m(k)|\mathbf{z}(k-1)}\left\{M_j|\mathbf{z}_{k-1}\right\}}$$

$$= \frac{P_{m(k)|m(k-1),\mathbf{z}(k-1)}\left\{M_j|M_i,\mathbf{z}_{k-1}\right\}P_{m(k-1)|\mathbf{z}(k-1)}\left\{M_i|\mathbf{z}_{k-1}\right\}}{\sum_{i=1}^{r}P_{m(k)|m(k-1),\mathbf{z}(k-1)}\left\{M_j|M_i,\mathbf{z}_{k-1}\right\}P_{m(k-1)|\mathbf{z}(k-1)}\left\{M_i|\mathbf{z}_{k-1}\right\}} \tag{5.7}$$

$$= \frac{1}{\bar{c}_j}p_{ij}\mu_i(k-1), i,j=1,\ldots,r \tag{5.8}$$

where $\mu_i(k-1)$ is the conditional probability about model i at time $k-1$, cf. Eq. (5.15), and $\bar{c}_j$ is the normalizing constants, which is

$$\bar{c}_j = \sum_{i=1}^{r} p_{ij}\mu_i(k-1), j=1,\ldots,r \tag{5.9}$$

Step 2: Calculation of the initial mixing condition for $j=1,\ldots,r$ filters. Starting with $\hat{\mathbf{x}}^i(k-1|k-1)$ one computes the mixed initial condition for the filter matched to $M_j(k)$ as

$$\hat{\mathbf{x}}^{0j}(k-1|k-1) = \sum_{i=1}^{r}\mu_{i|j}(k-1|k-1)\hat{\mathbf{x}}^i(k-1|k-1) \tag{5.10}$$

The corresponding covariance is

$$\begin{aligned}\mathbf{P}^{0j}(k-1|k-1)=&\sum_{i=1}^{r}\mu_{i|j}(k-1|k-1)\Big\{\mathbf{P}^{i}(k-1|k-1)\\&+\big[\hat{\mathbf{x}}^{i}(k-1|k-1)-\hat{\mathbf{x}}^{0j}(k-1|k-1)\big]\\&\cdot\big[\hat{\mathbf{x}}^{i}(k-1|k-1)-\hat{\mathbf{x}}^{0j}(k-1|k-1)\big]^{T}\Big\}\end{aligned}\tag{5.11}$$

Step 3: Mode-matched filtering for $j=1,\ldots,r$. The estimate (Eq. 5.10) and the covariance (Eq. 5.11) are used as input to each filter to yield $\hat{\mathbf{x}}^{j}(k|k)$ and $\mathbf{P}^{j}(k|k)$. The likelihood function corresponding to the j^{th} filter are computed as

$$\Lambda_j(k) \triangleq f_{\mathbf{z}(k)|\mathbf{Z}(k-1),m(k)}\{\boldsymbol{\zeta}_k,\boldsymbol{\rho}_{k-1},M_j\}\tag{5.12}$$

$$=\mathcal{N}\big[\mathbf{r}^{j}(k);\mathbf{0},\mathbf{S}^{j}(k)\big]\tag{5.13}$$

$$=(2\pi)^{-\frac{n}{2}}\|\mathbf{S}^{j}(k)\|^{-\frac{1}{2}}\exp\left\{-\frac{1}{2}\big[\mathbf{r}^{j}(k)\big]^{T}\big[\mathbf{S}^{j}(k)\big]^{-1}\mathbf{r}^{j}(k)\right\}\tag{5.14}$$

where $\mathbf{r}^{j}(k)=\mathbf{z}(k)-\mathbf{h}\big[\hat{\mathbf{x}}^{j}(k|k-1)\big]$ is the residual and $\mathbf{S}^{j}(k)$ is the residual covariance for filter j at time k.

Step 4: Mode probability update for $j=1,\ldots,r$.

$$\mu_j(k) \triangleq P_{m(k)|\mathbf{z}(k)}\big\{M_j|\mathbf{z}_k\big\}\tag{5.15}$$

$$=\frac{1}{c}\Lambda_j(k)\bar{c}_j\tag{5.16}$$

where c is the normalization constant

$$c=\sum_{j=1}^{r}\Lambda_j(k)\bar{c}_j\tag{5.17}$$

Step 5: Estimation and covariance combination. Combination of the model-conditioned estimate and covariance is done according to the mixture equations

$$\hat{\mathbf{x}}(k|k)=\sum_{j=1}^{r}\mu_j(k)\hat{\mathbf{x}}^{j}(k|k)\tag{5.18}$$

$$\begin{aligned}\mathbf{P}(k|k)=&\sum_{j=1}^{r}\mu_j(k)\Big\{\mathbf{P}^{j}(k|k)+\big[\hat{\mathbf{x}}^{j}(k|k)-\hat{\mathbf{x}}(k|k)\big]\\&\cdot\big[\hat{\mathbf{x}}^{j}(k|k)-\hat{\mathbf{x}}(k|k)\big]^{T}\Big\}\end{aligned}\tag{5.19}$$

Figure 5.1 shows one cycle of the IMM algorithm with two subfilters.

5.2.2 Extended Kalman Filter in Subfilters

For each subfilter in the IMM estimator, an EKF can be used. The most well-known representative dynamic models are CV model for nonmaneuver motion, and CA model and CT model for maneuver motions of accelerating and turning. These models are also the basic models for the IMM approach. All models have a generic state space model

$$\mathbf{x}(k+1) = \mathbf{F}\mathbf{x}(k) + \mathbf{G}\mathbf{w}(k) \tag{5.20}$$

where $\mathbf{x}$, $\mathbf{F}$, $\mathbf{G}$, and $\mathbf{w}$ have different forms for different models (see Section 3.1).

For simplicity, the measurements, $\mathbf{z} \in \Re^3$, are the distances between the BTSs and the MS according to the *time of arrival* (TOA) measurements received from three BTSs a, b, and c, whose position coordinates are (x_a, y_a), (x_b, y_b) and (x_c, y_c), respectively. We define

$$d_i = \sqrt{(x - x_i)^2 + (y - y_i)^2},\ i = a, b, c \tag{5.21}$$

Then the measurement model (Eq. 5.5) can be written as

$$\mathbf{z}(k) = \mathbf{h}[\mathbf{x}(k)] + \mathbf{v}(k) \tag{5.22}$$

$$\mathbf{h}[\mathbf{x}(k)] = \begin{bmatrix} d_a(k) \\ d_b(k) \\ d_c(k) \end{bmatrix} \tag{5.23}$$

where $\mathbf{h}[\mathbf{x}(k)]$ describes the nonlinear mapping of the states into the observation space. $\mathbf{v}(k)$ is measurement noise vector assumed to be zero-mean white Gaussian noise.

$$\mathbb{E}\left\{\mathbf{v}(k)\right\} = \mathbf{0}, \mathbb{E}\left\{\mathbf{v}(k) \cdot \mathbf{v}^T(j)\right\} = \mathbf{R} \cdot \delta(k - j) \tag{5.24}$$

$$\mathbf{R} = \mathrm{diag}(\sigma_d^2, \sigma_d^2, \sigma_d^2) \tag{5.25}$$

5.2.3 Simulation Results

Simulation Scenarios

The simulations are carried out in a simulated urban square area of 5 km × 5 km. Within this area there are three BTSs, a, b and c. It is assumed that a vehicle is equipped with a MS, and the trajectories are generated by the

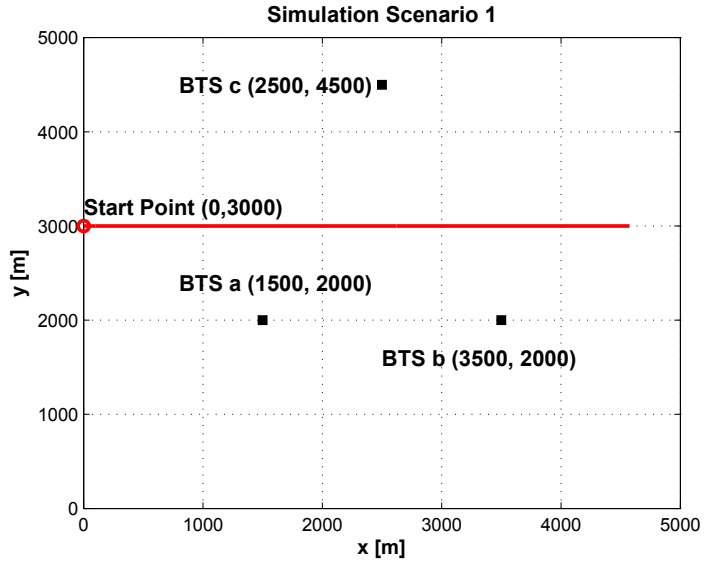

Figure 5.2: Simulation scenario 1

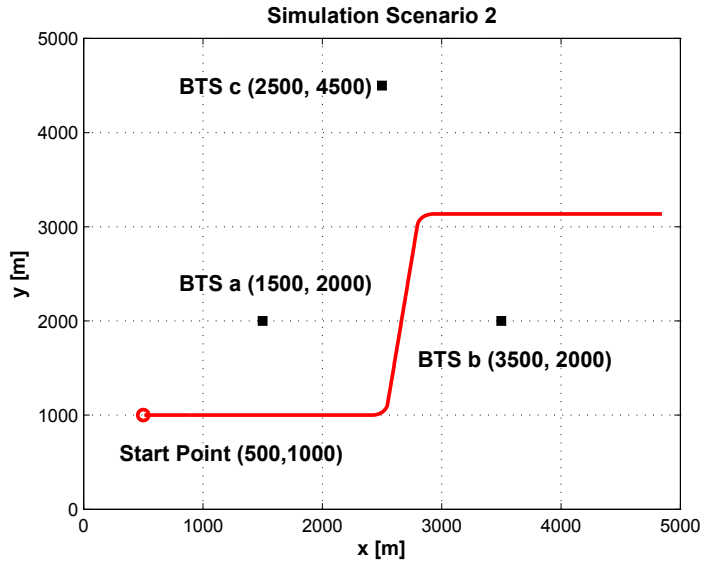

Figure 5.3: Simulation scenario 2

curvilinear motion model (see Section 3.1.5). Three different scenarios are simulated by setting different tangential accelerations a_t and normal accelerations a_n, as shown in Fig. 5.2-Fig. 5.4. In the first simulated scenario, the trajectory includes uniform motions and two segments of maneuvers with only

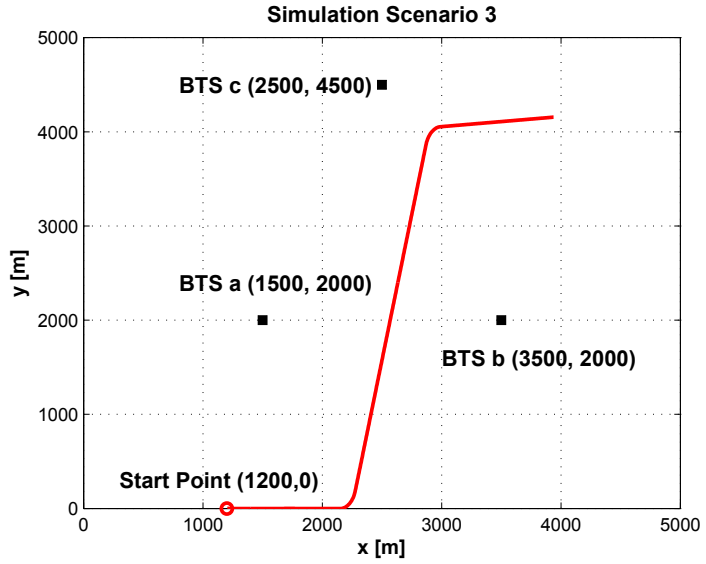

Figure 5.4: Simulation scenario 3

tangential accelerations. In the second one, the trajectory consists of uniform motions and two segments of maneuvers with only normal accelerations. The trajectory in the third scenario contains uniform motions and two segments of maneuvers with both tangential and normal accelerations. The values of a_t and a_n are shown in Table 5.1. They are set to be ± 3 m/s^2, which is about

Table 5.1: Values of a_t and a_n for different scenarios [m/s^2]

Samples	Scenario 1		Scenario 2		Scenario 3	
k	a_t	a_n	a_t	a_n	a_t	a_n
1-199	0	0	0	0	0	0
200-219	3	0	0	3	3	3
220-419	0	0	0	0	0	0
420-439	-3	0	0	-3	-3	-3
440-639	0	0	0	0	0	0

0.3 g. The positive and negative values for a_t mean accelerating and decelerating, whereas those for a_n denote left turn and right turn, respectively. The initial values of the position and velocity in two dimensions $\begin{bmatrix} x & \dot{x} & y & \dot{y} \end{bmatrix}^T$ for each trajectory are: scenario 1-$\begin{bmatrix} 0 \text{ m} & 5 \text{ m/s} & 3000 \text{ m} & 0 \text{ m/s} \end{bmatrix}^T$, scenario

2-$\begin{bmatrix}500\text{ m} & 20\text{ m/s} & 1000\text{ m} & 0\text{ m/s}\end{bmatrix}^T$ and $\begin{bmatrix}1200\text{ m} & 10\text{ m/s} & 0\text{ m} & 0\text{ m/s}\end{bmatrix}^T$ for scenario 3. The standard deviations of the process noise are set to be $\sigma_x = 10^{-4}$ m, $\sigma_y = 10^{-4}$ m, $\sigma_v = 10^{-5}$ m/s, $\sigma_\phi = 10^{-6}$ rad. The measurements are the distances between the BTSs and the MS according to the TOA received from three BTSs (Eqs. 5.22 and 5.23), respectively. The standard deviation of the measurement noise, which is assumed to be zero-mean white Gaussian noise, is $\sigma_d = 300$ m.

Design of IMM Estimator

There are three main steps for designing an IMM estimator: selection of model set, selection of process noise for each model, and selection of the Markov chain transition probabilities [71, 93].

(1) Selection of Model Set

Typically the models used in the IMM estimator include one CV model for uniform motion and one or more for the maneuver (e.g., CA or CT model). Both the estimation quality and the complexity should be considered. The main principle is to use the exact or approximate maneuver model set. It should be noted that increasing the number of the models will increase the computation loads, but it does not guarantee better performance [93]. Therefore, for the above three different simulated trajectories, we choose different IMM configurations in order to show the best performance of the IMM estimator.

- Scenario l: CV and CA models;
- Scenario 2: CV and CT models;
- Scenario 3: CV and CT models.

(2) Selection of Process Noises

The process noises are selected based on the expected disturbances and the similarity of the models with the real maneuvers. Since the first and second generated trajectories have small noises, and the models in the estimator match the real movement very well, the process noises of the filter should be set to be small values. In the third scenario, however, there is no exact model to describe the maneuver, so that one approximate model, CT model with high process noise, is used to cover the maneuver phase.

- Scenario l: CV model- the standard deviations of the acceleration noise in x and y directions are $\sigma_x = \sigma_y = 0.01$ m/s^2, CA model- the standard

deviations of the acceleration increment noise in x and y directions are $\sigma_x = \sigma_y = 0.01$ m/s^3;

- Scenario 2: CV model- $\sigma_x = \sigma_y = 0.01$ m/s^2, CT model- the standard deviations of the acceleration noise in x and y directions are $\sigma_x = \sigma_y = 0.01$ m/s^2 and noise for turn rate is $\sigma_\omega = 0.01$ rad/s^2;
- Scenario 3: CV model- $\sigma_x = \sigma_y = 0.01$ m/s^2, CT model- $\sigma_x = \sigma_y = 3$ m/s^2 and $\sigma_\omega = 1$ rad/s^2.

(3) Selection of Transition Probabilities Matrix

For each simulation scenario, we set the mode transition probability matrix and initial probability to the same values. The elements of the mode transition probability matrix (Eq. 5.3), which is a 2×2 matrix, are $p_{11} = 0.994$, $p_{12} = 0.006$, $p_{21} = 0.01$, $p_{22} = 0.99$, and the initial probability of the CV model is 0.9, while that of maneuver model, i.e., for scenario 1 CA model and for scenario 2 and scenario 3 CT model, is 0.1.

For each subfilter, an EKF is used. The TOA measurements for one point are used to initialize the EKF.

Results Comparison and Analysis

The RMSE performance of the IMM estimators for three scenarios are shown in Fig. 5.5-Fig. 5.7. All results are based on 500 Monte Carlo trials. We compare the RMSE with the corresponding PCRLB, which represens the theoretically best achievable estimation performance of a specific simulation scenario [73, 94]. The results are also compared with the RMSE performance of an EKF using only one CV model. It should be noted that for comparing the RMSE with the PCRLB, the PCRLB is calculated as the root of the PCRLB in x direction plus the PCRLB in y direction. The comparisons of the estimation errors are shown in Table 5.2.

- *Estimation errors during nonmaneuvering period:* Since the estimators have large errors at the beginning of the nonmaneuvering period, which is because that the estimators need some time to converge to the real state value, the average *uniform motion* (UM) position RMSEs and average UM velocity RMSEs in the Table 5.2 are calculated by the average over the samples 100-199, 320-419, and 540-639, when the estimation of each estimator already converged. In all three scenarios the IMM estimators reduce the estimation errors during the uniform motion comparing with the EKF of using only one model. For the scenario

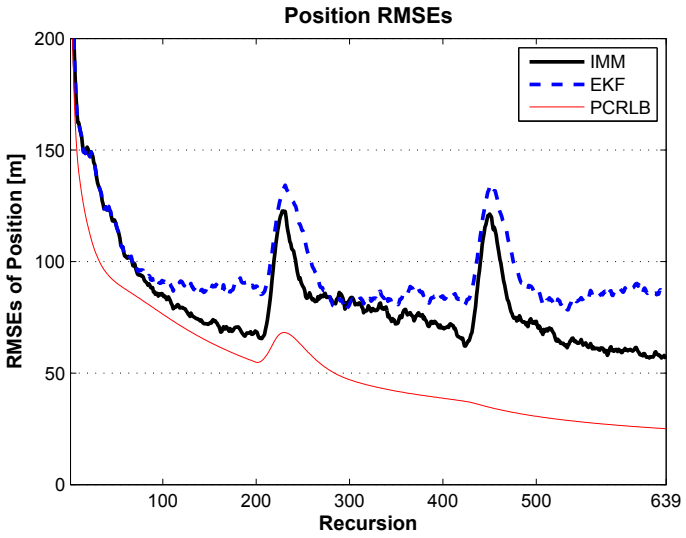

Figure 5.5: Position RMSEs against corresponding PCRLBs (scenario 1)

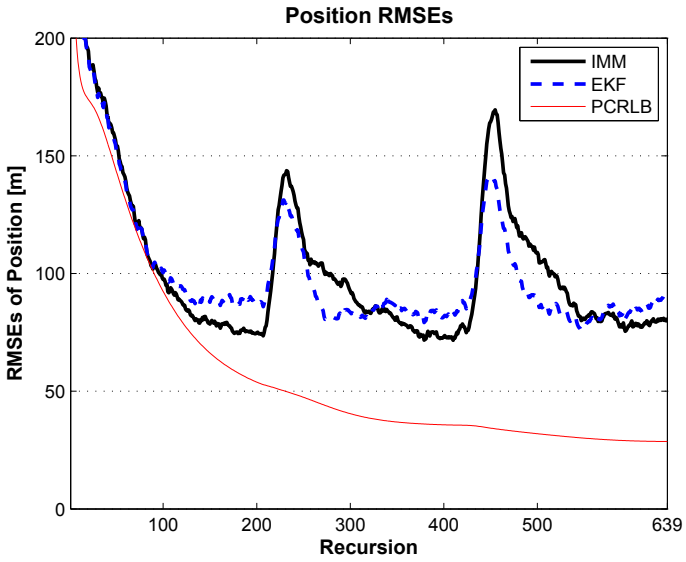

Figure 5.6: Position RMSEs against corresponding PCRLBs (scenario 2)

3, the IMM estimator has a 14.5 m smaller position RMSE and 1.6 m/s smaller velocity RMSE than the EKF estimator.

- *Peak errors during maneuvering:* For each scenario, the peak errors are taken at the samples when the errors of the IMM estimators achieve

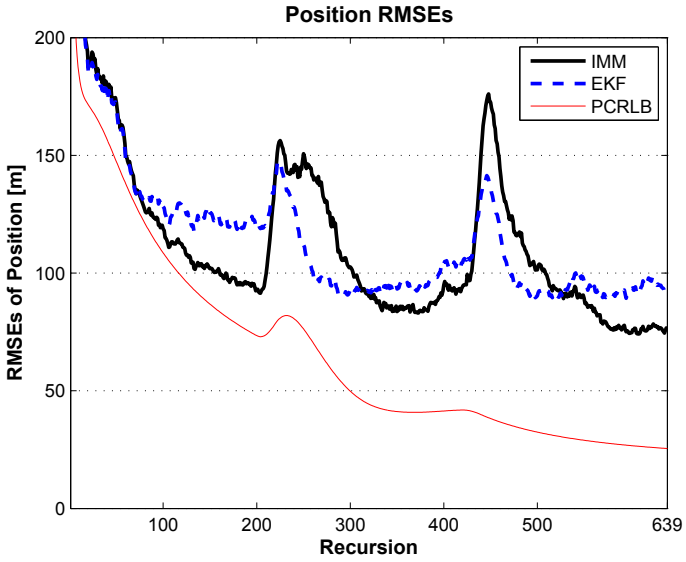

Figure 5.7: Position RMSEs against Corresponding PCRLBs (scenario 3)

Table 5.2: Estimation errors comparisons

	Scenario 1		Scenario 2		Scenario 3	
	EKF	IMM	EKF	IMM	EKF	IMM
Av. UM Position RMSE[5] [m]	86.5	69.4	86.2	79.8	104.5	90.0
Av. UM Velocity RMSE[5] [m/s]	5.3	4.1	5.4	4.9	7.9	6.3
Peak Position RMSE [m]	134.0	122.0	136.5	156.6	144.6	166.2
Peak Velocity RMSE [m/s]	25.4	25.3	23.8	24.7	30.6	33.5
Mode Detection Delay [sample]	-	34.5	-	40	-	30.5

[5]Av. stands for average

the peak, and they are the average of two maneuvers. For scenario 1, the IMM has a lower peak error, while for the other two scenarios, the IMM has a higher peak error than the EKF using one model.

- *Detection of the maneuver:* The mode detection delay is calculated as using the sample time, when the probability of maneuver mode is bigger than that of uniform motion, minus the sample time, when the maneuver actually happens. They are averaged over two maneuvers in each scenario. The delays are 30 samples to 40 samples (about 14 s to 20 s), e.g. the mode probability in scenario 3 is shown in Fig 5.8.

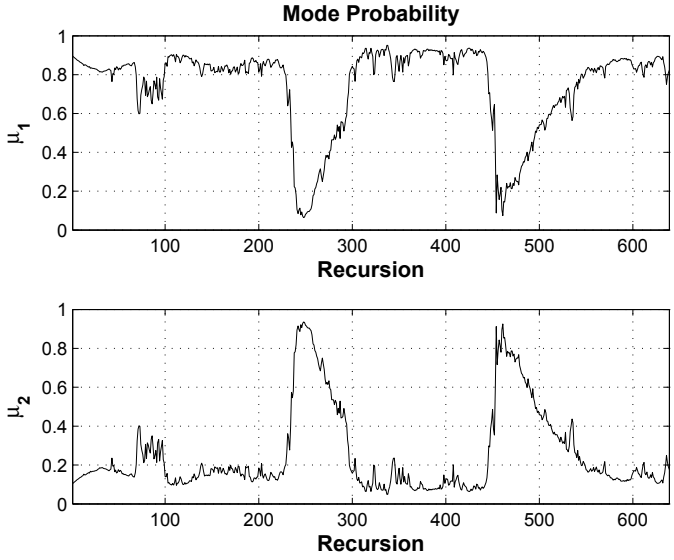

Figure 5.8: Mode probability (scenario 3)

As shown in the above comparisons, the IMM estimators achieve better accuracy during the nonmaneuvering period, but they have higher peak error when the target maneuvers. This is because that the mode detection is delayed. The possible reasons are high measurement noises and relatively low velocities for the application in GSM networks, which results in that the estimation of the acceleration in CA models and the turn rate in CT models converge to the real values slowly, and the nonmaneuver model (CV) and the maneuver model (CA or CT) can not be differentiated quickly.

5.3 An Adaptive Road-Constrained IMM Estimator

As discussed before, one of the natural characteristics for ground targets is the target motion uncertainty due to the change of terrain and road conditions. In recent years, MM methods have been generally considered as the mainstream approach for maneuvering target tracking under motion mode uncertainty, and the IMM estimator is one of the most efficient MM estimators, which has been considered in the last section. However, most of the work on the IMM estimators considers only fixed mode sets. This requires that the estimator carries as many modes as necessary to handle the varying target motion characteristics during the entire tracking period, which will

increase the computational load and may also degrade the estimation accuracy. It is possible to vary the set of models in the IMM estimator based on some criteria to yield better estimates, which results in VS-IMM [75, 95]. The road network is such a promising *a priori* information.

Although the road network will cause the high maneuverability of ground targets, it has the advantage of additional knowledge on the target state. There are already many approaches of incorporating the road information into the tracking algorithm. The main approaches include projection and pseudomeasurement approach, which were introduced in Chapter 4. Moreover, there are also many research efforts which have been done to incorporate the road information into MM schemes. In [75, 96] the road constraint was handled using the concept of directional process noise. The target dynamics was modeled in one-dimensional road coordinates and mapped onto the ground coordinate in [97]. The projection approach was applied within a VS-IMM filter in [98].

In Chapter 4, we expanded the pseudomeasurement approach for road-constrained target tracking in GSM networks, including straight roads and curved roads. The benefits were demonstrated. In this section, we will incorporate this road-constrained tracking approach into a VS-IMM mechanism, which results in an ARC-IMM estimator. In this approach, the module set, not only the dynamic model but also the road constraint as a pseudomeasurement, is updated adaptively according to the estimated position of the target and the road network information as the estimation process proceeds. In particular, the selection of the dynamic models also depends on the road constraint. Comparative studies with utilizing an IMM estimator with directional noise, a standard IMM estimator and an EKF verify that the proposed approach significantly improves the tracking accuracy. In addition, the performance when there are only two measurements available is also discussed.

5.3.1 Ground Target Tracking on the Road

Although the varying environmental conditions, e.g., road network, result in the high maneuverability of ground targets, they cause also another nature of the ground targets, i.e., constrained motion. As discussed in Chapter 4, the road constraint can be formulated as a fictitious measurement and rewritten by a pseudomeasurement model in discrete time

$$z_c(k) = h_c\big[\mathbf{x}(k)\big] + v_r(k) \tag{5.26}$$

where $z_c(k) = 0$, $h_c\big[\mathbf{x}(k)\big] = s\big(x(k), y(k)\big)$ representing the road model, and $v_r(k)$ is assumed to be zero-mean white Gaussian noise accounting for the uncertainty of the road constraint.

$$v_r(k) \sim \mathcal{N}\big(0, r_r(k)\big) \tag{5.27}$$
$$r_r(k) = \sigma_r^2 \tag{5.28}$$

Accordingly, the measurement model is augmented and an EKF can be utilized.

For simplicity, the measurements, $\mathbf{z} \in \Re^3$, are the distances between the BTSs and the MS according to the TOA received from three BTSs a, b, and c, whose position coordinates are (x_a, y_a), (x_b, y_b) and (x_c, y_c), respectively. The measurement model can be found in Eqs. (5.22) and (5.24).

5.3.2 ARC-IMM Algorithm

MM approaches can be divided into two categories: one with a fixed set of models, and one with a variable structure. As has been pointed out in [95], the fixed mode set approach is not realistic since more models have to be used to cover all the possible target motions, which adds to the computational load and also degrades the performance. Therefore, VS-IMM has been proposed to vary the set of models in the IMM estimator based on some criteria. E.g., the variations in the topography, which include targets entering and leaving roads, target motion at road junctions and target obscuration conditions, are considered to decide which models in the estimator are added or deleted at each revisit time [75].

In addition, the road network also conveys such information, that can be used to adaptively update the model set as the estimation process proceeds. Assuming that the road network can be modeled by a set of road segments $\{s_l\}, l = 1, \ldots, n$ and each s_l can be described by a straight line, arc, or low-order polynomial. At each time step, a neighboring road segment set of the target $\mathbf{S}(k) \triangleq \{s_o\} \in \{s_l\}, o = 1, \ldots, m$ can be obtained by examining the estimated target position and the road network. The road not only restricts the position of the target inside the road, but also has a potential constraint on the possible target motions corresponding to a specific road segment. E.g., on a straight road the target dynamic model might be a CV or a CA model, but cannot be a nearly CT model. Therefore, a road segment in the neighboring road segment set, which is selected from the whole set of the road network for the current position, has finite corresponding possible motion models.

The principle of the proposed ARC-IMM estimator is based on a VS-IMM mechanism, where the module set will be updated adaptively according to the latest position estimate and the road network information. In particular, the road constraint is incorporated into the measurement model as a pseudomeasurement, and the modules of the estimator at each time step not only have different dynamic models but also have different road constraints as pseudomeasurements, in which one or more dynamic models correspond to one road constraint. In the following, module M_j, i.e., mode in MM approaches, stands for the different filters in the ARC-IMM, which includes a pair of dynamic model and road constraint. And the set of modules is updated adaptively according to the road network.

Thus the hybrid system (Eqs. 5.1 and 5.2) can be written as

$$\mathbf{x}(k+1) = \mathbf{f}_p\big[k, \mathbf{x}(k)\big] + \mathbf{g}_p\big[k, \mathbf{x}(k), \mathbf{w}_p(k)\big] \tag{5.29}$$

$$\mathbf{z}_o(k) = \mathbf{h}_o\big[k, \mathbf{x}(k)\big] + \mathbf{v}_o(k) \tag{5.30}$$

where $\mathbf{z}_o(k)$ is the augmented measurement vector by the road constraint as a pseudomeasurement (Eq. 5.26), $\mathbf{z}_o(k) = \big[\mathbf{z}(k)^T \quad z_{s_o}(k)\big]^T$, $\mathbf{h}_o[\mathbf{x}(k)] = \Big[\mathbf{h}\big[\mathbf{x}(k)\big]^T \quad h_{s_o}\big[\mathbf{x}(k)\big]\Big]^T$, and $\mathbf{v}_o(k) = \big[\mathbf{v}(k)^T \quad v_{s_o}(k)\big]^T$, and the subscript s_o denotes the neighboring road segment at time k, and $o = 1, \ldots, m$. The subscript in the dynamic model p denotes the different motion models corresponding to each o^{th} road segment. The module of the target $M(k) \triangleq \{o, p\}$ is given by the combination of different road constraints and different target motions. Unlike the fixed set IMM estimator, the module set at time k, $\mathbf{M}(k) \triangleq \big\{M_j(k)\big\}, j = 1, \ldots, r$, and that at time $k-1$, $\mathbf{M}(k-1) \triangleq \big\{M_i(k-1)\big\}, i = 1, \ldots, s$, might be different. The module transition probability (Eq. 5.3) is modified as

$$p_{ij} \triangleq P_{m(k)|m(k-1)}\big\{M_j \in \mathbf{M}(k) | M_i \in \mathbf{M}(k-1)\big\} \tag{5.31}$$

where p_{ij} depends on the module set $\mathbf{M}(k-1)$ and $\mathbf{M}(k)$.

One cycle of the ARC-IMM algorithm consists of the following five steps as illustrated in Fig. 5.9:

Step 1: Module set update.

The module set at time k, $\mathbf{M}(k)$, is updated adaptively on the base of the latest estimated position, the neighboring road segments and corresponding possible target motions. Firstly, the neighboring road segment set is selected, which can be done by testing whether any segment of the road set $\{s_l\}$ lies within a certain neighborhood ellipse centered at the predicted position $\big(\hat{x}^-(k|k), \hat{y}^-(k|k)\big)$ [75]. Then the corresponding target dynamic models

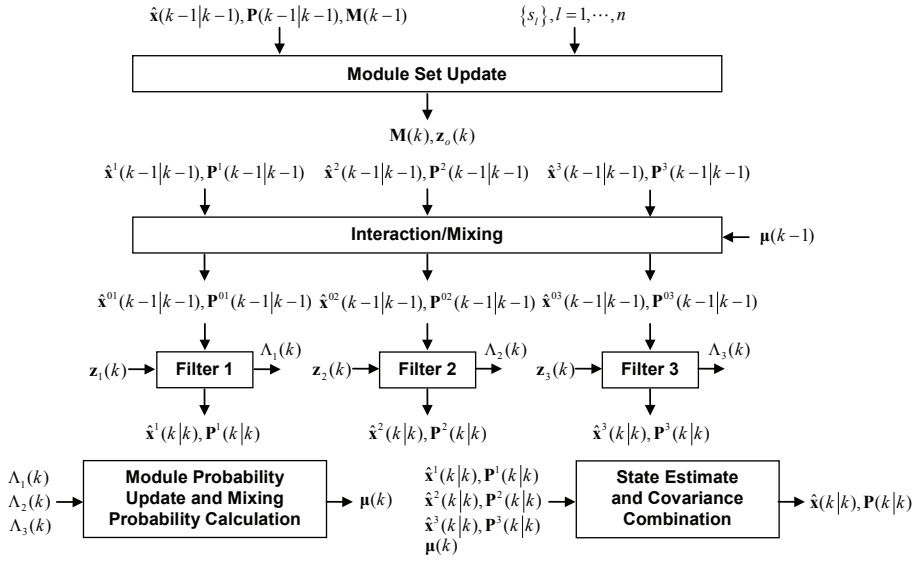

Figure 5.9: ARC-IMM estimator consisting of three subfilters (one cycle)

of each road segment are chosen according to the empirical knowledge. The modules of the estimator at one time step are illustrated in Fig. 5.10. There are two road segments in the neighboring road set, s_1 and s_2. For the straight road s_1, the target might move at constant velocity or constant acceleration, and for the arc road s_2, the target might do a coordinated turn. Therefore, three possible modules are chosen as shown in Fig. 5.10. In this step, the measurement model will be augmented by the road constraint pseudo-measurement from the selected neighboring road segments.

Step 2: Calculation of the initial mixing condition for $j = 1, \ldots, r$ filters.

The probabilities that module M_i was in effect at $k-1$ given that M_j is in effect at k conditioned on $\mathbf{z}(k-1)$ is

$$\mu_{i|j}(k-1|k-1) \triangleq P_{m(k-1)|m(k),\mathbf{z}(k-1)}\{M_i|M_j, \mathbf{z}_{k-1}\} \tag{5.32}$$

$$= \frac{1}{\bar{c}_j} p_{ij}\mu_i(k-1), M_i \in \mathbf{M}(k-1), M_j \in \mathbf{M}(k) \tag{5.33}$$

where $\mu_i(k-1)$ is the conditional probability about module i at time $k-1$, and $\bar{c}_j$ is the normalizing constants, which is

$$\bar{c}_j = \sum_{i=1}^{s} p_{ij}\mu_i(k-1), j = 1, \ldots, r \tag{5.34}$$

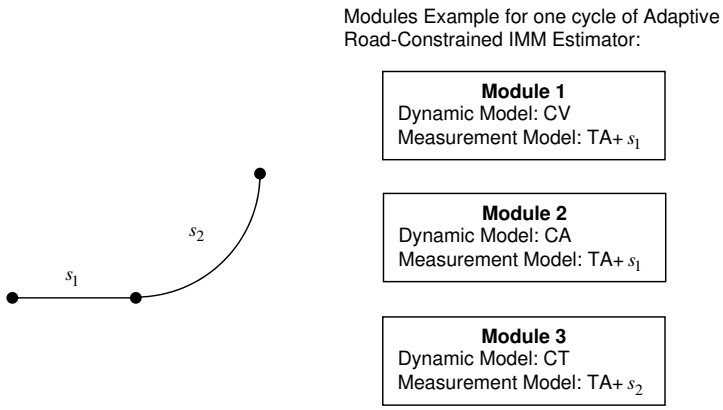

Figure 5.10: Modules example

Then starting with $\hat{\mathbf{x}}^i(k-1|k-1)$ one computes the mixed initial condition for the filter matched to $M_j(k)$ as

$$\hat{\mathbf{x}}^{0j}(k-1|k-1) = \sum_{i=1}^{s} \mu_{i|j}(k-1|k-1)\hat{\mathbf{x}}^i(k-1|k-1) \tag{5.35}$$

The corresponding covariance is

$$\begin{aligned}\mathbf{P}^{0j}(k-1|k-1) = \sum_{i=1}^{s} \mu_{i|j}(k-1|k-1)\Big\{&\mathbf{P}^i(k-1|k-1)\\ &+\big[\hat{\mathbf{x}}^i(k-1|k-1) - \hat{\mathbf{x}}^{0j}(k-1|k-1)\big]\\ &\cdot\big[\hat{\mathbf{x}}^i(k-1|k-1) - \hat{\mathbf{x}}^{0j}(k-1|k-1)\big]^T\Big\}\end{aligned} \tag{5.36}$$

Step 3: Module-matched filtering for $j = 1, \ldots, r$.

The estimate (Eq. 5.35) and the covariance (Eq. 5.36) are used as input to each filter, where the EKF can be used, to yield $\hat{\mathbf{x}}^j(k|k)$ and $\mathbf{P}^j(k|k)$. The EKF with road constraint as pseudomeasurement in linear and nonlinear case refers to Chapter 4. The likelihood functions corresponding to the r filters are computed as

$$\Lambda_j(k) = \mathcal{N}\big[\mathbf{r}^j(k); \mathbf{0}, \mathbf{S}^j(k)\big] \tag{5.37}$$

$$= (2\pi)^{-\frac{n}{2}} \|\mathbf{S}^j(k)\|^{-\frac{1}{2}} \exp\left\{-\frac{1}{2}\big[\mathbf{r}^j(k)\big]^T\big[\mathbf{S}^j(k)\big]^{-1}\mathbf{r}^j(k)\right\} \tag{5.38}$$

where $\mathbf{r}^j(k) = \mathbf{z}(k) - \mathbf{h}\big[\hat{\mathbf{x}}^j(k|k-1)\big]$ is the residual and $\mathbf{S}^j(k)$ is the residual covariance for filter j at time k. Note that the real measurement model $\mathbf{z}(k)$,

not the augmented measurement model $\mathbf{z}_o(k)$, is used to calculate the likelihood functions (Eq. 5.37) considering the different road segment functions for each modules, i.e., straight line, arc or polynomial function.

Step 4: Module probability update for $j = 1, \ldots, r$.

The module probability in effect at k is updated by

$$\mu_j(k) \triangleq P_{m(k)|\mathbf{z}(k)}\{M_j|\mathbf{z}_k\} \tag{5.39}$$

$$= \frac{1}{c}\Lambda_j(k)\bar{c}_j \tag{5.40}$$

where c is the normalization constant

$$c = \sum_{j=1}^{r} \Lambda_j(k)\bar{c}_j \tag{5.41}$$

Step 5: Estimation and covariance combination.

Combination of the module-conditioned estimate and covariance is done according to the mixture equations

$$\hat{\mathbf{x}}(k|k) = \sum_{j=1}^{r} \mu_j(k)\hat{\mathbf{x}}^j(k|k) \tag{5.42}$$

$$\mathbf{P}(k|k) = \sum_{j=1}^{r} \mu_j(k)\Big\{\mathbf{P}^j(k|k) + \big[\hat{\mathbf{x}}^j(k|k) - \hat{\mathbf{x}}(k|k)\big] \cdot \big[\hat{\mathbf{x}}^j(k|k) - \hat{\mathbf{x}}(k|k)\big]^T\Big\} \tag{5.43}$$

The above five steps are similar with the VS-IMM algorithm, but the road constraint is incorporated into the estimation as a pseudomeasurement and the structure of the module set is selected and updated considering the neighboring road segments and corresponding possible target motions.

5.3.3 Simulation Results

Simulation Scenario

The simulations are carried out in a simulated square area of 5 km by 5 km. Within this area there are three BTSs, a, b and c. As shown in Fig. 5.11, it is assumed that a vehicle equipped with a MS, whose position and velocity are going to be estimated using three TOA measurements from BTSs a, b and c, respectively, travels along a route D-E-F-G as an example to show the

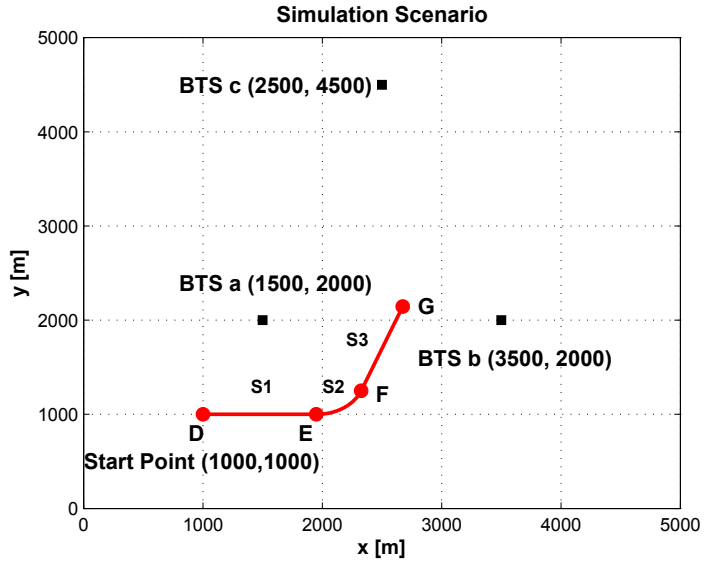

Figure 5.11: Simulation scenario

structure and performance of the proposed ARC-IMM Estimator. There are three road segments: s_1(D-E) is a straight road, s_2(E-F) is an arc road, and s_3(F-G) is also a straight road. It is assumed that these three road segments are modeled by a linear function or a circle function as

$$0 = \tan\theta \cdot x(k) - y(k) + c \tag{5.44}$$

$$r^2 = (x(k) - x_0)^2 + (y(k) - y_0)^2 \tag{5.45}$$

where $\tan\theta$ is the slope of the straight roads, c stands for the y-intercept of the straight roads, r denotes the radius of the arc road and (x_0, y_0) is the two-dimensional coordinate of the arc's centre, which are all known parameters. Therefore they can be written as pseudomeasurement models

$$z_{s_1}(k) = h_{s_1}[\mathbf{x}(k)] + v_{s_1}(k) \tag{5.46}$$

$$z_{s_2}(k) = h_{s_2}[\mathbf{x}(k)] + v_{s_2}(k) \tag{5.47}$$

$$z_{s_3}(k) = h_{s_3}[\mathbf{x}(k)] + v_{s_3}(k) \tag{5.48}$$

The measurement update rate is $T = 0.48$ s. The standard deviation of the measurement noise is assumed to be $\sigma_d = 300$ m.

It is assumed that the vehicle is moving on the road from D to G and the estimator starts working at position D: (1000 m, 1000 m) and at this time the velocity of the vehicle is 20 m/s and 0 m/s in x and y direction, respectively. Firstly the vehicle moves along the road s_1 at constant velocity,

then it executes a coordinated turn when it goes to the arc road s_2, and finally it has again constant velocity movement on the straight road s_3. The trajectory is generated by the curvilinear motion model. The tangential and normal accelerations a_t and a_n are set to be $a_t = 0$ m/s^2, $a_n = 0$ m/s^2 for the movement on s_1, $a_t = 0$ m/s^2, $a_n = 1$ m/s^2 for that on s_2, and $a_t = 0$ m/s^2, $a_n = 0$ m/s^2 for that on s_3. The process noise $\mathbf{w}_t(k) = \begin{bmatrix} w_x(k) & w_y(k) & w_v(k) & w_\phi(k) \end{bmatrix}^T$ is assumed to be zero-mean white Gaussian noise. The standard deviations of the process noise σ_x, σ_y, σ_v, σ_ϕ are set to be the values of 10^{-4} m, 10^{-4} m, 10^{-5} m/s and 10^{-6} rad, respectively.

Design of the ARC-IMM Estimator

For illustrating the module structure of the ARC-IMM estimator, it is assumed that in the period of traveling from D to G there are always three road segments in the neighboring road set $\mathbf{S}(k) = \{s_1, s_2, s_3\}$, i.e., the adaptive update of the module set is not considered in this example. Therefore, the ARC-IMM estimator consists of three modules during the movement from D to G, which are as follows:

- *Module 1*: The dynamic model is a CV Model, and the measurement model includes three TOA measurements plus the pseudomeasurement model of the road segment s_1 (Eq. 5.46). The standard deviations of the process noise, including acceleration in x and y directions, are set to be $\sigma_x = 1$ m/s^2, $\sigma_y = 1$ m/s^2. The standard deviation of the pseudomeasurement noise is $\sigma_r = 10$ m.

- *Module 2*: The dynamic model is a CT Model, and the measurement model includes three TOA measurements plus the pseudomeasurement model of the road segment s_2 (Eq. 5.47). The standard deviations of the process noise, including acceleration in x and y directions and the change of turn rate, are $\sigma_x = 10^{-2}$ m/s^2, $\sigma_y = 10^{-2}$ m/s^2, $\sigma_\omega = 10^{-4}$ rad/s^2. The standard deviation of the pseudomeasurement noise is $\sigma_r = (10 \text{ m})^2$.

- *Module 3*: The dynamic model is a CV Model, and the measurement model includes three TOA measurements plus the pseudomeasurement model of the road segment s_3 (Eq. 5.48). The standard deviations of the process noise are $\sigma_x = 1$ m/s^2, $\sigma_y = 1$ m/s^2, and the standard deviation of the pseudomeasurement noise is $\sigma_r = 10$ m.

The standard deviation of the measurement noise for all three modules is set to be $\sigma_d = 300$ m. The module transition probability matrix, which is a

3×3 matrix, is designed as follows

$$\mathbf{M}_1 = \begin{bmatrix} 0.99 & 0.005 & 0.005 \\ 0.01 & 0.98 & 0.01 \\ 0.005 & 0.005 & 0.99 \end{bmatrix} \tag{5.49}$$

The initial probability of each module is set to be 0.9 for module 1, and 0.05 for module 2 and 3, respectively. The initial state values $\hat{x}^+(0)$ and $\hat{y}^+(0)$ of the estimator are calculated by one point measurement [65], which uses a traditional least squares algorithm to achieve an initial position guess from three independent TOA measurements at time step $k = 0$. The initial values of the velocity $\hat{\dot{x}}^+(0)$, $\hat{\dot{y}}^+(0)$ are assumed to be zero-mean Gaussian random variables with an associated standard deviation equal to be half of the known maximum state values.

In order to evaluate the performance of the proposed approach, an IMM estimator with directional noise (IMM-DN), a standard IMM estimator, and a single model EKF estimator are also designed for the simulated scenario and the results are compared. The IMM-DN estimator comprises three models, one CV model for the road segment D-E, one CT model and one CV model for the road segment F-G. Since the target should have more uncertainty along the road than orthogonal to it, the variance of the corresponding process noise could be set as $\sigma_a = 10^{-2}$ m/s^2, $\sigma_o = 10^{-6}$ m/s^2, $\sigma_a^2 \gg \sigma_o^2$. Then they need to be converted into a covariance matrix in the X-Y coordinate system.

$$\mathbf{Q} = \begin{bmatrix} -cos\varphi & sin\varphi \\ sin\varphi & -cos\varphi \end{bmatrix} \begin{bmatrix} \sigma_a^2 & 0 \\ 0 & \sigma_o^2 \end{bmatrix} \begin{bmatrix} -cos\varphi & sin\varphi \\ sin\varphi & -cos\varphi \end{bmatrix} \tag{5.50}$$

where φ is the direction of the road segment D-E and F-G, respectively. The details of the directional noise design can be found in [75]. The mode transition probability matrix is the same with the ARC-IMM. The IMM estimator consists of two models, one CV model, in which the standard deviation of process noises $\sigma_{a_x} = 10^{-2}$ m/s^2, $\sigma_{a_y} = 10^{-2}$ m/s^2, and one CT model with process noises $\sigma_{a_x} = 10^{-2}$ m/s^2, $\sigma_{a_y} = 10^{-2}$ m/s^2, $\sigma_\omega = 10^{-4}$ rad/s^2. The mode transition probability matrix is assumed to be

$$\mathbf{M}_2 = \begin{bmatrix} 0.99 & 0.01 \\ 0.02 & 0.98 \end{bmatrix} \tag{5.51}$$

The initial probability is set to be 0.9 for CV model, 0.1 for CT model. The dynamic model of the EKF is CV model, and the standard deviations of process noises are set to be $\sigma_{a_x} = 3$ m/s^2, $\sigma_{a_y} = 3$ m/s^2, which are designed to be large enough to track both the uniform motion and maneuver motion.

Performance Comparisons

The state estimate results of the proposed ARC-IMM estimator, the IMM-DN estimator, the IMM estimator and the single model EKF estimator are shown in Fig. 5.12. It is observed that the performance of the ARC-IMM outperforms those of the other three approaches. The state estimates of the target yielded by the ARC-IMM are close to the real state values. In particular, at the initial phase the estimates converge to the real values much quicker than that of the other three approaches. When the target maneuvers, i.e., when the target turns on the road, the proposed estimator can better track the change of the state than the others.

To further evaluate the estimation performance, the RMSE performance is obtained from 1000 Monte Carlo simulations as shown in Fig. 5.13. The comparison of the RMSEs verifies that the ARC-IMM significantly improves the estimation accuracy. During the uniform motion the ARC-IMM yields about 30 m position RMSE reduction when comparing with the IMM and about 20 m in comparison to the EKF. The velocity RMSE is improved about 6 m/s over the IMM and about 3 m/s over the EKF. During the maneuver, the ARC-IMM has a peak error, but it decreases much faster than in the case of the other three estimators. By comparing the performance of IMM and EKF, it is shown that the IMM cannot improve the estimation accuracy over the EKF even though an additional maneuver model is included, which is because the IMM estimator converges slowly in this application with high measurement noises and relatively low velocities. The comparison of the results from the IMM-DN and the IMM estimator shows that the IMM with directional noise has only a slightly better performance during the nonmaneuver period.

Performance in the Case of Two Measurements

As discussed in Section 4.3.4, to uniquely determine a position in two dimensions using trilateration techniques, at least three base stations are required to solve the ambiguities. However, sometimes this condition cannot be satisfied in GSM networks. In this part of simulations the performance of different approaches, when there are only two measurements from two BTSs of a and b available, are compared. The RMSE performance based on 1000 Monte Carlo simulations is shown in Fig. 5.14. It is observed that the proposed ARC-IMM yields the highest accuracy, and the performances of the other three approaches are greatly degraded. In the case of only two measurements the measurement model in the IMM-DN, the IMM and the EKF is

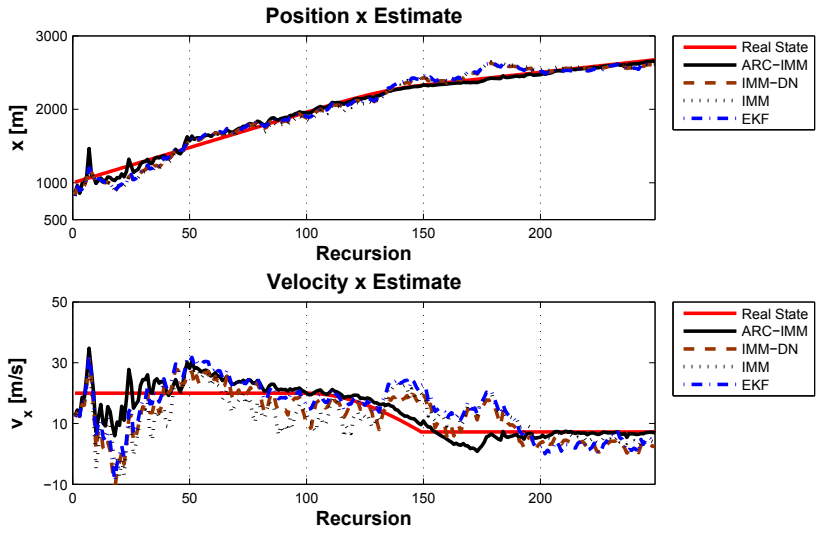

(a) State estimates in x direction

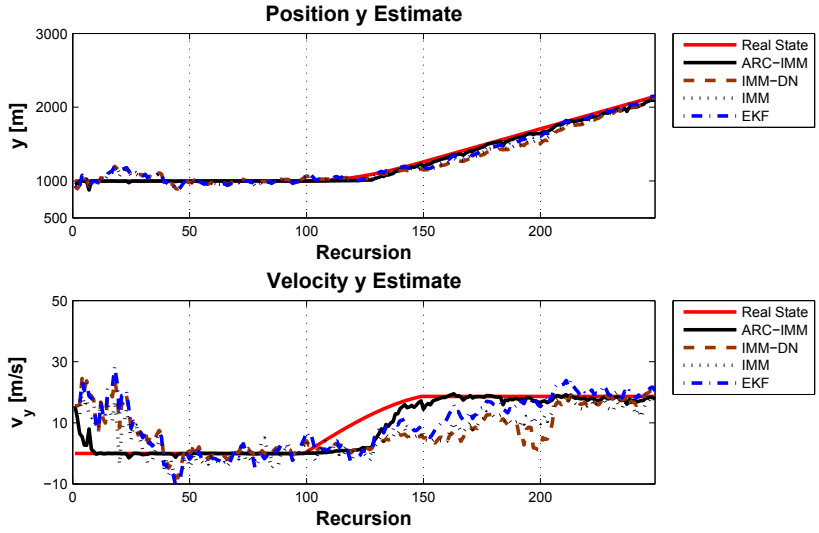

(b) State estimates in y direction

Figure 5.12: State estimates

only a two-dimensional vector, which results in increased estimation ambiguities. In the ARC-IMM, however, the incorporation of the road constraint as a pseudomeasurement augments the measurement model, thus the necessary number of measurements for trilateration in two dimensions is reduced to two. Therefore, the proposed ARC-IMM can still provide stable and accu-

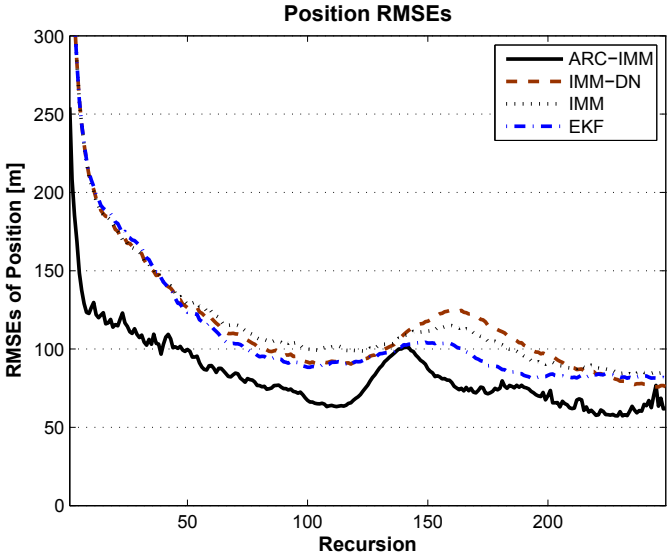

(a) Position RMSEs comparison

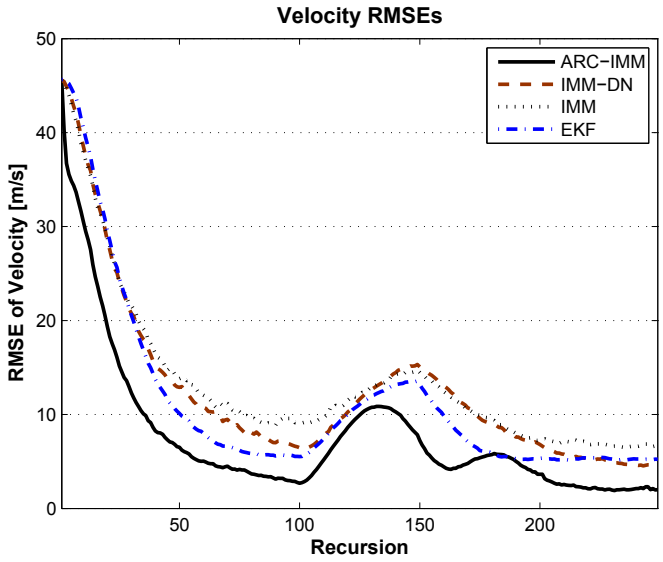

(b) Velocity RMSEs comparison

Figure 5.13: RMSE performance comparison (three measurements)

rate estimates when there are only two measurements available.

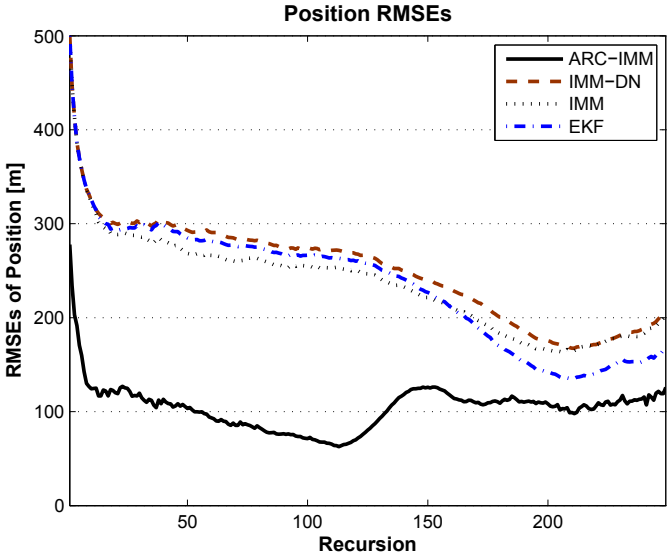

(a) Position RMSEs comparison

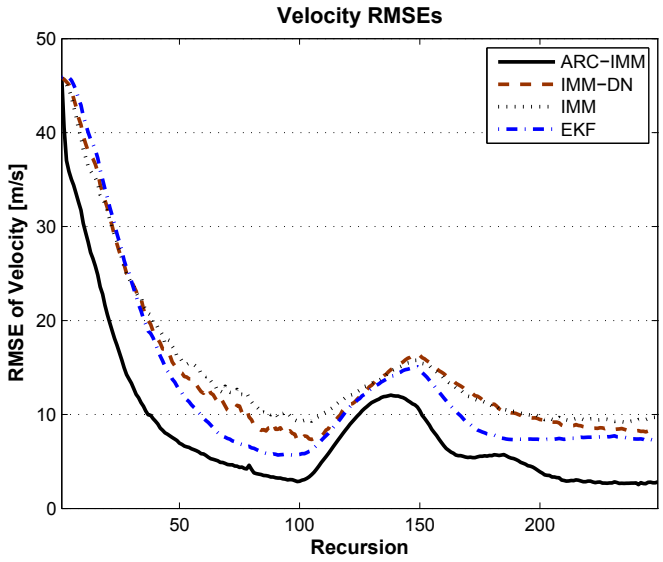

(b) Velocity RMSEs comparison

Figure 5.14: RMSE performance of only two measurements

5.4 Summary

In this chapter, the problem of motion uncertainty has been discussed. Firstly the IMM estimator has been applied. The simulation results show that the

IMM estimator can improve the estimation accuracy during the nonmaneuver period, but it has higher errors during the target maneuvers compared to the EKF estimator since it takes some time to shift to the correct motion model. Considering this difficulty, an ARC-IMM estimator to track the ground target in GSM networks has been proposed. The road constraint can be used not only to restrict the position of the target inside the road, but also as a criterion to select possible dynamic models. Similar to the VS-IMM estimator, the module set of the ARC-IMM is updated adaptively according to the estimated target position and the road network information. The difference is that in the ARC-IMM the road constraint is incorporated into the estimator as a pseudomeasurement, and the module is specified by the dynamic model and the road constraint together. In particular, the selection of the dynamic model also depends on the road constraint. The performance comparison verifies that the proposed ARC-IMM estimator is superior to an IMM with directional noise, a standard IMM estimator and a classic EKF estimator. The results in the situation of only two measurements available show the robustness and efficiency of the proposed approach.

Chapter 6

Conclusions and Outlook

6.1 Conclusions

This thesis presented data fusion solutions for ground target tracking in GSM networks. Since the communication signal is not designed for positioning purposes, it is difficult for a GSM positioning system relying on a single type of measurements under current specifications to provide accurate position estimates. Therefore, this work integrates the measurements from the GSM network and additional information applying estimation theory aiming at providing more accurate position estimates. The main contributions of this work are listed as follows:

1. A data fusion approach, which integrates two different types of measurements from GSM networks, TOA and RSS, using an EKF is proposed. The comparison results with the single measurement approach depicts that the data fusion approach can greatly improve the estimation accuracy. This contribution has been published in [99].

2. The PCRLB is derived for the proposed data fusion approach and the principle of the fusion, i.e., the information is additive, is clearly explained through the PCRLB. Moreover, the recursive equation of the PCRLB shows that the accuracy of the tracking using GSM networks is affected by the initial information, the process noise, the dynamics of the trajectory, the measurement noise, and the geometric relationship of the BTSs and the MS. Comparisons of PCRLBs, which are compatible with the comparisons of the estimation results using EKF, demonstrate the conclusion that the data fusion approach provides better accuracy and is more robust to the noisy measurements from a theoretical point of view. This contribution can be found in [94, 100].

3. The road information has been successfully incorporated into the estimation process as a pseudomeasurement. The simulation results concerning linear road segments and nonlinear road segments demonstrate the benefits of the proposed road-constrained approach. The estimation accuracy is greatly improved by the road information, and incorporating the road constraint reduces the condition for trilateration in two dimensions from three required BTSs to two BTSs. This contribution can be found in [101, 102].

4. An IMM estimator has been designed for the maneuvering target tracking in GSM networks under different maneuver scenarios. Moreover, an ARC-IMM estimator has been proposed to solve the motion mode uncertainty problem for tracking the ground target limited to the road network. The proposed approach incorporates the road information into a VS-IMM scheme so that the estimator can adaptively apply the road network information related into the current target position. The approach has been proven superior to a normal IMM estimator. This contribution can be found in [103, 104].

6.2 Outlook

There are several aspects for future work which can be done as a continuation work of this thesis:

- **NLOS**: The NLOS error is a critical issue for mobile positioning in a wireless communication environment. Due to reflection and diffraction, the radio signal may travel extra path lengths of the order of hundreds of meters and there might be no direct path from the BS to the MS. In such a situation, if the algorithm for LOS condition is directly utilized, the position estimates will greatly diverge from the true values. In this thesis, it is assumed that the NLOS bias error has been removed before the estimation by having the prior knowledge of the bias. However, in practice the statistics of the NLOS error are usually unknown or known in a limited way and the presence of NLOS is unpredictable. Therefore, the NLOS mitigation algorithm together with the estimation should be investigated.

- **ARC-IMM**: In this thesis an ARC-IMM estimator has been proposed and shown to be effective. The simulation is done using a limited area, which is 5 km by 5 km, and the simulated road network is simply consisting of three consecutive road segments. The estimator should be

examined in a wider area and more complicated road networks should be considered. Since the ARC-IMM estimator is an adaptive estimator with respect to the road network, the adaptive selection and the selection of the module set should be further studied to improve the efficiency of the proposed approach.

- **Road Constraint**: The road constraint is a very interesting topic since it is easily obtained from a digital map database and can be used to improve the positioning, especially in urban areas, where positioning using GPS and wireless communication networks will be greatly degraded due to dense buildings. The proposed approach can be examined in real environments to further demonstrate the benefits.

- **Data Fusion**: As the development of the *Global Navigation Satellite Systems* (GNSS) and navigation technologies, the data fusion of different positioning system should be under consideration. As shown in this thesis, the accuracy of the position estimate using the measurements from GSM networks is limited but the advantage is its ubiquity in different environments. The GNSS system provides much more accurate position information but will be greatly degraded in urban areas. Therefore, the integration of the navigation systems, e.g., GNSS and *Inertial Navigation System* (INS), and the positioning system using mobile communication networks can be considered for the ground vehicle navigation and tracking applications.

- **Real Experiments**: The work in this thesis focuses on the theoretical foundations of data fusion solutions and the proposed novel approaches are evaluated through Monte Carlo simulations. However, in practice, the communication channel is far more complicated than the assumptions in the thesis. The work should be further examined and improved by real data from field tests.

Appendix A

Some Useful Formulae for Vectors and Matrices

A.1 Derivatives of Vectors and Matrices

A.1.1 The Gradient of a Scalar Function $f(\mathbf{x})$

Let $f(\mathbf{x}) = f(x_1, x_2, \cdots, x_n)$ be a real valued scalar function of a n-vector $\mathbf{x}$, the *gradient* of $f(\cdot)$ with respect to $\mathbf{x}$ is defined as a $n \times 1$ vector

$$\nabla_{\mathbf{x}} = \left[\frac{\partial f(\mathbf{x})}{\partial x_1} \quad \frac{\partial f(\mathbf{x})}{\partial x_2} \quad \cdots \quad \frac{\partial f(\mathbf{x})}{\partial x_n}\right]^T \tag{A.1}$$

It should be noted that conventionally the *derivative* of $f(\mathbf{x})$ is defined as a row vector with dimension $1 \times n$.

$$\frac{\partial f(\mathbf{x})}{\partial \mathbf{x}} = \left[\frac{\partial f(\mathbf{x})}{\partial x_1} \quad \frac{\partial f(\mathbf{x})}{\partial x_2} \quad \cdots \quad \frac{\partial f(\mathbf{x})}{\partial x_n}\right] \tag{A.2}$$

A.1.2 The Gradient of a Vector-Valued Function $\mathbf{f}(\mathbf{x})$

Let $\mathbf{f}(\mathbf{x}) = \begin{bmatrix} f_1(\mathbf{x}) & f_2(\mathbf{x}) & \cdots & f_m(\mathbf{x}) \end{bmatrix}^T$ be a m-dimensional vector-valued function of a n-vector $\mathbf{x}$, the *gradient* of $\mathbf{f}(\cdot)$ with respect to $\mathbf{x}$ is defined as

a $n \times m$ matrix

$$\nabla_{\mathbf{x}} \mathbf{f}(\mathbf{x})^T = \begin{bmatrix} \frac{\partial f_1(\mathbf{x})}{\partial x_1} & \frac{\partial f_2(\mathbf{x})}{\partial x_1} & \cdots & \frac{\partial f_m(\mathbf{x})}{\partial x_1} \\ \frac{\partial f_1(\mathbf{x})}{\partial x_2} & \frac{\partial f_2(\mathbf{x})}{\partial x_2} & \cdots & \frac{\partial f_m(\mathbf{x})}{\partial x_2} \\ \vdots & \vdots & \ddots & \vdots \\ \frac{\partial f_1(\mathbf{x})}{\partial x_n} & \frac{\partial f_2(\mathbf{x})}{\partial x_n} & \cdots & \frac{\partial f_m(\mathbf{x})}{\partial x_n} \end{bmatrix} \tag{A.3}$$

The inverse of the above is the *Jacobian matrix*, which is a $m \times n$ matrix

$$\mathbf{F} \triangleq \frac{\partial \mathbf{f}(\mathbf{x})}{\partial \mathbf{x}} = \left[\nabla_{\mathbf{x}} \mathbf{f}(\mathbf{x})^T\right]^T = \begin{bmatrix} \frac{\partial f_1(\mathbf{x})}{\partial x_1} & \frac{\partial f_1(\mathbf{x})}{\partial x_2} & \cdots & \frac{\partial f_1(\mathbf{x})}{\partial x_n} \\ \frac{\partial f_2(\mathbf{x})}{\partial x_1} & \frac{\partial f_2(\mathbf{x})}{\partial x_2} & \cdots & \frac{\partial f_2(\mathbf{x})}{\partial x_n} \\ \vdots & \vdots & \ddots & \vdots \\ \frac{\partial f_m(\mathbf{x})}{\partial x_1} & \frac{\partial f_m(\mathbf{x})}{\partial x_2} & \cdots & \frac{\partial f_m(\mathbf{x})}{\partial x_n} \end{bmatrix} \tag{A.4}$$

A.1.3 The Hessian of a Scalar Function $f(\mathbf{x})$

The *Hessian* of the scalar function $f(\mathbf{x})$ with respect to the n-vector $\mathbf{x}$ is defined as a symmetric $n \times n$ matrix

$$\mathbf{F} \triangleq \frac{\partial^2 f(\mathbf{x})}{\partial \mathbf{x}^2} = \nabla_{\mathbf{x}} \nabla_{\mathbf{x}}^T f(\mathbf{x}) = \begin{bmatrix} \frac{\partial^2 f(\mathbf{x})}{\partial x_1 \partial x_1} & \frac{\partial^2 f(\mathbf{x})}{\partial x_1 \partial x_2} & \cdots & \frac{\partial^2 f(\mathbf{x})}{\partial x_1 \partial x_n} \\ \frac{\partial^2 f(\mathbf{x})}{\partial x_2 \partial x_1} & \frac{\partial^2 f(\mathbf{x})}{\partial x_2 \partial x_2} & \cdots & \frac{\partial^2 f(\mathbf{x})}{\partial x_2 \partial x_n} \\ \vdots & \vdots & \ddots & \vdots \\ \frac{\partial^2 f(\mathbf{x})}{\partial x_n \partial x_1} & \frac{\partial^2 f(\mathbf{x})}{\partial x_n \partial x_2} & \cdots & \frac{\partial^2 f(\mathbf{x})}{\partial x_n \partial x_n} \end{bmatrix} \tag{A.5}$$

A.2 The Inversion of a Partitioned Matrix

In general, the inversion of a partitioned matrix is given by

$$\begin{aligned}\mathbf{A}^{-1} &= \begin{bmatrix}\mathbf{A}_{11} & \mathbf{A}_{12}\\ \mathbf{A}_{21} & \mathbf{A}_{22}\end{bmatrix}^{-1}\\ &= \begin{bmatrix}\mathbf{A}_{11}^{-1}(\mathbf{I}+\mathbf{A}_{12}\mathbf{J}\mathbf{A}_{21}\mathbf{A}_{11}^{-1}) & -\mathbf{A}_{11}^{-1}\mathbf{A}_{12}\mathbf{J}\\ -\mathbf{J}\mathbf{A}_{21}\mathbf{A}_{11}^{-1} & \mathbf{J}\end{bmatrix}\end{aligned} \tag{A.6}$$

where

$$\mathbf{J} = (\mathbf{A}_{22} - \mathbf{A}_{21}\mathbf{A}_{11}^{-1}\mathbf{A}_{12})^{-1} \tag{A.7}$$

A.3 Matrix Inversion Lemma

The matrix inversion lemma is very useful for the derivation of the recursive equation of the least squares estimator and the linear estimation of dynamic systems.

$$(\mathbf{A}+\mathbf{B}\mathbf{C}\mathbf{B}^T)^{-1} = \mathbf{A}^{-1} - \mathbf{A}^{-1}\mathbf{B}(\mathbf{B}^T\mathbf{A}^{-1}\mathbf{B}+\mathbf{C}^{-1})^{-1}\mathbf{B}^T\mathbf{A}^{-1} \tag{A.8}$$

Appendix B

Posterior Cramér-Rao Lower Bound for Nonlinear Filtering with Additive Gaussian Noise

Given a nonlinear filtering problem with additive Gaussian noise

$$\mathbf{x}(k+1) = \mathbf{f}\big[\mathbf{x}(k)\big] + \mathbf{w}(k) \tag{B.1}$$

$$\mathbf{z}(k) = \mathbf{h}\big[\mathbf{x}(k)\big] + \mathbf{v}(k) \tag{B.2}$$

where $\mathbf{w}(k)$ and $\mathbf{v}(k)$ are zero-mean white Gaussian noises with invertible covariance matrix $\mathbf{Q}(k)$ and $\mathbf{R}(k)$, respectively.

$$\mathbb{E}\left\{\mathbf{w}(k)\right\} = 0, \mathbb{E}\left\{\mathbf{w}(k)\cdot\mathbf{w}(j)^T\right\} = \mathbf{Q}(k)\cdot\delta(k-j) \tag{B.3}$$

$$\mathbb{E}\left\{\mathbf{v}(k)\right\} = 0, \mathbb{E}\left\{\mathbf{v}(k)\cdot\mathbf{v}(j)^T\right\} = \mathbf{R}(k)\cdot\delta(k-j) \tag{B.4}$$

Further assume that the initial state $\mathbf{x}(0)$ has a known probability density function $f_{\mathbf{x}(0)}\big(\boldsymbol{\xi}_0\big)$. The dimension of the state vector $\mathbf{x}(k)$ is n. Let a capital symbol $\mathbf{X}(k) = \big[\mathbf{x}(0)^T \quad \mathbf{x}(1)^T \quad \cdots \quad \mathbf{x}(k)^T\big]^T$ represent the states in all time step and $\mathbf{Z}(k) = \big[\mathbf{z}(0)^T \quad \mathbf{z}(1)^T \quad \cdots \quad \mathbf{z}(k)^T\big]^T$ contain the measurements in all time step, then the joint probability distribution of $\big(\mathbf{X}(k), \mathbf{Z}(k)\big)$ is

$$f_{\mathbf{X}(k),\mathbf{Z}(k)}\big(\boldsymbol{\eta}_k, \boldsymbol{\rho}_k\big) = f_{\mathbf{x}(0)}\big(\boldsymbol{\xi}_0\big)\prod_{j=1}^{k} f_{\mathbf{z}(j)|\mathbf{x}(j)}\big(\boldsymbol{\zeta}_j|\boldsymbol{\xi}_j\big) \cdot\prod_{i=1}^{k} f_{\mathbf{x}(i)|\mathbf{x}(i-1)}\big(\boldsymbol{\xi}_i|\boldsymbol{\xi}_{i-1}\big) \tag{B.5}$$

Following Eq. (2.49), the FIM for PCRLB is calculated by the joint pdf. Let $\mathbf{J}\big(\mathbf{X}(k)\big)$ be the information matrix $(kn \times kn)$ of $\mathbf{X}(k)$ derived from the joint distribution (Eq. B.5). $\mathbf{X}(k)$ can be decomposed as $\begin{bmatrix}\mathbf{X}^T(k-1) & \mathbf{x}^T(k)\end{bmatrix}^T$. Then the information submatrix for $\mathbf{x}(k)$ at time step k, which is denoted as $\mathbf{J}(k)$, is given by the inversion of the $(n \times n)$ right-lower block of $\mathbf{J}\big(\mathbf{X}(k)\big)^{-1}$. Let

$$\mathbf{J}\big(\mathbf{X}(k)\big) = \begin{bmatrix}\mathbf{A}(k) & \mathbf{B}(k)\\ \mathbf{B}^T(k) & \mathbf{C}(k)\end{bmatrix} \tag{B.6}$$

$$\triangleq \begin{bmatrix}\mathbb{E}\left\{-\dfrac{\partial^2 \ln f(k)}{\partial \boldsymbol{\eta}_{k-1}\partial \boldsymbol{\eta}_{k-1}}\right\} & \mathbb{E}\left\{-\dfrac{\partial^2 \ln f(k)}{\partial \boldsymbol{\xi}_{k}\partial \boldsymbol{\eta}_{k-1}}\right\}\\ \mathbb{E}\left\{-\dfrac{\partial^2 \ln f(k)}{\partial \boldsymbol{\eta}_{k-1}\partial \boldsymbol{\xi}_{k}}\right\} & \mathbb{E}\left\{-\dfrac{\partial^2 \ln f(k)}{\partial \boldsymbol{\xi}_{k}\partial \boldsymbol{\xi}_{k}}\right\}\end{bmatrix} \tag{B.7}$$

where $f(k)$ denotes $f_{\mathbf{X}(k),\mathbf{Z}(k)}\big(\boldsymbol{\eta}_k, \boldsymbol{\rho}_k\big)$ for brevity. Using the formula of the inversion of a partitioned matrix (see Appendix A.2), $\mathbf{J}(k)$ is

$$\mathbf{J}(k) = \mathbf{C}(k) - \mathbf{B}^T(k)\mathbf{A}^{-1}(k)\mathbf{B}(k) \tag{B.8}$$

The matrix $\mathbf{J}^{-1}(k)$ provides a lower bound on the mean square error of estimating $\mathbf{x}(k)$.

Now it goes to the next step $k+1$, the joint probability function of $\mathbf{X}(k+1)$ and $\mathbf{Z}(k+1)$ can be written as

$$f(k+1) \triangleq f_{\mathbf{X}(k+1),\mathbf{Z}(k+1)}\big(\boldsymbol{\eta}_{k+1}, \boldsymbol{\rho}_{k+1}\big) \tag{B.9}$$

$$= f_{\mathbf{X}(k),\mathbf{Z}(k)}\big(\boldsymbol{\eta}_k, \boldsymbol{\rho}_k\big) \cdot f_{\mathbf{x}(k+1)|\mathbf{X}(k),\mathbf{Z}(k)}\big(\boldsymbol{\xi}_{k+1}|\boldsymbol{\eta}_k, \boldsymbol{\rho}_k\big)$$
$$\cdot f_{\mathbf{z}(k+1)|\mathbf{x}(k+1),\mathbf{X}(k),\mathbf{Z}(k)}\big(\boldsymbol{\zeta}_{k+1}|\boldsymbol{\xi}_{k+1}, \boldsymbol{\eta}_k, \boldsymbol{\rho}_k\big) \tag{B.10}$$

$$= f(k) \cdot f_{\mathbf{x}(k+1)|\mathbf{x}(k)}\big(\boldsymbol{\xi}_{k+1}|\boldsymbol{\xi}_k\big)$$
$$\cdot f_{\mathbf{z}(k+1)|\mathbf{x}(k+1)}\big(\boldsymbol{\zeta}_{k+1}|\boldsymbol{\xi}_{k+1}\big) \tag{B.11}$$

The posterior information matrix for $\mathbf{X}(k+1)$ can be written in block form as

$$\mathbf{J}\big(\mathbf{X}(k+1)\big) = \begin{bmatrix}\mathbf{A}(k) & \mathbf{B}(k) & \mathbf{0}\\ \mathbf{B}^T(k) & \mathbf{C}(k) + \mathbf{D}^{11}(k) & \mathbf{D}^{12}(k)\\ \mathbf{0} & \mathbf{D}^{21}(k) & \mathbf{D}^{22}(k)\end{bmatrix} \tag{B.12}$$

where

$$\mathbf{D}^{11}(k) = \mathbb{E}\left\{-\frac{\partial^2 \ln f_{\mathbf{x}(k+1)|\mathbf{x}(k)}\big(\boldsymbol{\xi}_{k+1}|\boldsymbol{\xi}_k\big)}{\partial \boldsymbol{\xi}_k \partial \boldsymbol{\xi}_k}\right\} \tag{B.13}$$

$$\mathbf{D}^{12}(k) = \mathbb{E}\left\{-\frac{\partial^2 \ln f_{\mathbf{x}(k+1)|\mathbf{x}(k)}\big(\boldsymbol{\xi}_{k+1}|\boldsymbol{\xi}_k\big)}{\partial\boldsymbol{\xi}_{k+1}\partial\boldsymbol{\xi}_k}\right\} \tag{B.14}$$

$$\mathbf{D}^{21}(k) = \mathbb{E}\left\{-\frac{\partial^2 \ln f_{\mathbf{x}(k+1)|\mathbf{x}(k)}\big(\boldsymbol{\xi}_{k+1}|\boldsymbol{\xi}_k\big)}{\partial\boldsymbol{\xi}_k\partial\boldsymbol{\xi}_{k+1}}\right\} = [\mathbf{D}^{\mathbf{12}}(k)]^T \tag{B.15}$$

$$\begin{aligned}\mathbf{D}^{22}(k) = \mathbb{E}&\left\{-\frac{\partial^2 \ln f_{\mathbf{x}(k+1)|\mathbf{x}(k)}\big(\boldsymbol{\xi}_{k+1}|\boldsymbol{\xi}_k\big)}{\partial\boldsymbol{\xi}_{k+1}\partial\boldsymbol{\xi}_{k+1}}\right\}\\ &+\mathbb{E}\left\{-\frac{\partial^2 \ln f_{\mathbf{z}(k+1)|\mathbf{x}(k+1)}\big(\boldsymbol{\zeta}_{k+1}|\boldsymbol{\xi}_{k+1}\big)}{\partial\boldsymbol{\xi}_{k+1}\partial\boldsymbol{\xi}_{k+1}}\right\}\end{aligned} \tag{B.16}$$

The information submatrix $\mathbf{J}(k+1)$ can be found as an inverse of the right-lower $n \times n$ submatrix of $\mathbf{J}^{-1}\big(\mathbf{X}(k+1)\big)$

$$\mathbf{J}(k+1) = \mathbf{D}^{22}(k) - \mathbf{D}^{21}(k)\big[\mathbf{J}(k) + \mathbf{D}^{11}(k)\big]^{-1}\mathbf{D}^{12}(k) \tag{B.17}$$

The initial information matrix $\mathbf{J}(0)$ can be calculated from *a priori* probability function $f_{\mathbf{x}(0)}\big(\boldsymbol{\xi}_0\big)$

$$\mathbf{J}(0) = \mathbb{E}\left\{-\frac{\partial^2 \ln f_{\mathbf{x}(0)}\big(\boldsymbol{\xi}_0\big)}{\partial\boldsymbol{\xi}_0\partial\boldsymbol{\xi}_0}\right\} \tag{B.18}$$

Using the assumption of additive Gaussian noise, Eqs. (B.3), (B.4), (B.13)-(B.16), are derived as

$$\mathbf{D}^{11}(k) = \mathbb{E}\left\{\mathbf{F}^T(k)\mathbf{Q}^{-1}(k)\mathbf{F}(k)\right\} \tag{B.19}$$

$$\mathbf{D}^{12}(k) = -\,\mathbb{E}\left\{\mathbf{F}^T(k)\right\}\mathbf{Q}^{-1}(k) \tag{B.20}$$

$$\mathbf{D}^{21}(k) = [\mathbf{D}^{\mathbf{12}}(k)]^T \tag{B.21}$$

$$\mathbf{D}^{22}(k) = \mathbf{Q}^{-1}(k) + \mathbb{E}\left\{\mathbf{H}^T(k+1)\mathbf{R}^{-1}(k+1)\mathbf{H}(k+1)\right\} \tag{B.22}$$

where $\mathbf{F}(k)$ is the Jacobian matrix of $\mathbf{f}(\cdot)$ in Eq. (B.2) with respect to the true values of $\mathbf{x}(k)$

$$\mathbf{F}(k) = \left.\frac{\partial\mathbf{f}\big[\mathbf{x}(k)\big]}{\partial\mathbf{x}(k)}\right|_{\mathbf{x}(k)} \tag{B.23}$$

Similarly, $\mathbf{H}(k+1)$ is the Jacobian matrix of $\mathbf{h}(\cdot)$ in Eq. (B.2) with respect to the true values of $\mathbf{x}(k+1)$

$$\mathbf{H}(k) = \left.\frac{\partial\mathbf{h}[\mathbf{x}(k+1)]}{\partial\mathbf{x}(k+1)}\right|_{\mathbf{x}(k+1)} \tag{B.24}$$

Substituting Eqs. (B.19)-(B.22) into Eq. (B.17) yields

$$\begin{aligned}\mathbf{J}(k+1) = \mathbf{Q}^{-1}(k) &+ \mathbb{E}\left\{\mathbf{H}^T(k+1)\mathbf{R}^{-1}(k+1)\mathbf{H}(k+1)\right\} \\ &- \left[\,\mathbb{E}\left\{\mathbf{F}^T(k)\right\}\mathbf{Q}^{-1}(k)\right]^T\left[\mathbf{J}(k) + \mathbb{E}\left\{\mathbf{F}^T(k)\right\}\mathbf{Q}^{-1}(k)\,\mathbb{E}\left\{\mathbf{F}(k)\right\}\right]^{-1} \\ &\cdot \mathbb{E}\left\{\mathbf{F}^T(k)\right\}\mathbf{Q}^{-1}(k) \end{aligned} \tag{B.25}$$

According to the matrix inversion lemma (see A.3), Eq. (B.25) can be written as

$$\begin{aligned}\mathbf{J}(k+1) = &\left[\mathbf{Q}^{-1}(k) + \mathbb{E}\left\{\mathbf{F}(k)\mathbf{J}(k)\mathbf{F}(k)\right\}^T\right]^{-1} \\ &+ \mathbb{E}\left\{\mathbf{H}^T(k+1)\mathbf{R}^{-1}(k+1)\mathbf{H}(k+1)\right\}\end{aligned} \tag{B.26}$$

where $\mathbf{J}(0)$ can be given by the inverse of the initial covariance matrix $\mathbf{P}(0)$.

Appendix C

Derivations for Constrained State Estimation

C.1 Maximum Conditional Probability Method for Projection Approach

The problem of constrained state estimation is a constrained minimization problem

$$\tilde{\mathbf{x}} = \arg\min_{\tilde{\mathbf{x}}}(\tilde{\mathbf{x}} - \bar{\bar{\mathbf{x}}})^T\mathbf{P}^{-1}(\tilde{\mathbf{x}} - \bar{\bar{\mathbf{x}}})) \text{ such that } \mathbf{D}\tilde{\mathbf{x}} = \mathbf{d} \tag{C.1}$$

where $\tilde{\mathbf{x}}(k)$ denotes the constrained state estimate, $\bar{\bar{\mathbf{x}}}$ depicts the conditional mean of the state, and $\mathbf{P}$ stands for the covariance matrix of the state estimation error. Constrained optimization problems can be solved using the Lagrange multiplier method. So a Lagrangian L can be formed

$$L = (\tilde{\mathbf{x}} - \bar{\bar{\mathbf{x}}})^T\mathbf{P}^{-1}(\tilde{\mathbf{x}} - \bar{\bar{\mathbf{x}}}) + 2\boldsymbol{\lambda}^T(\mathbf{D}\tilde{\mathbf{x}} - \mathbf{d}) \tag{C.2}$$

To obtain the optimization, we let the partial derivatives of the Lagrangian with respect to $\tilde{\mathbf{x}}$ and $\boldsymbol{\lambda}$ be equal to zero and solve them simultaneously.

$$\frac{\partial L}{\partial \tilde{\mathbf{x}}} = \mathbf{P}^{-1}(\tilde{\mathbf{x}} - \bar{\bar{\mathbf{x}}}) + \mathbf{D}^T\boldsymbol{\lambda} = \mathbf{0} \tag{C.3}$$

$$\frac{\partial L}{\partial \boldsymbol{\lambda}} = \mathbf{D}\tilde{\mathbf{x}} - \mathbf{d} = \mathbf{0} \tag{C.4}$$

Then

$$\boldsymbol{\lambda} = (\mathbf{D}\mathbf{P}\mathbf{D}^T)^{-1}(\mathbf{D}\bar{\bar{\mathbf{x}}} - \mathbf{d}) \tag{C.5}$$

$$\tilde{\mathbf{x}} = \bar{\bar{\mathbf{x}}} - \mathbf{P}\mathbf{D}^T(\mathbf{D}\mathbf{P}\mathbf{D}^T)^{-1}(\mathbf{D}\bar{\bar{\mathbf{x}}} - \mathbf{d}) \tag{C.6}$$

Since $\bar{\bar{\mathbf{x}}}$ is the unconstrained state estimate $\hat{\mathbf{x}}$ of the Kalman filter, the constrained state estimation is

$$\tilde{\mathbf{x}} = \hat{\mathbf{x}} - \mathbf{P}\mathbf{D}^T(\mathbf{D}\mathbf{P}\mathbf{D}^T)^{-1}(\mathbf{D}\hat{\mathbf{x}} - \mathbf{d}) \tag{C.7}$$

C.2 Mean Square Method for Projection Approach

The constrained state estimation problem can be solved from a mean square point of view.

$$\tilde{\mathbf{x}} = \arg\min_{\tilde{\mathbf{x}}} \mathbb{E}\left\{\|\mathbf{x} - \tilde{\mathbf{x}}\|^2 | \mathbf{z} = \mathbf{z}_0\right\} \text{ such that } \mathbf{D}\tilde{\mathbf{x}} = \mathbf{d} \tag{C.8}$$

The conditional expected value can be written as

$$\mathbb{E}\left\{\|\mathbf{x} - \tilde{\mathbf{x}}\|^2 | \mathbf{z} = \mathbf{z}_0\right\} = \int (\boldsymbol{\xi} - \tilde{\mathbf{x}})^T (\boldsymbol{\xi} - \tilde{\mathbf{x}}) f_{\mathbf{x}|\mathbf{z}}(\boldsymbol{\xi}|\mathbf{z}_0) d\boldsymbol{\xi} \tag{C.9}$$

$$= \int \boldsymbol{\xi}^T \boldsymbol{\xi} f_{\mathbf{x}|\mathbf{z}}(\boldsymbol{\xi}|\mathbf{z}_0) d\boldsymbol{\xi} - 2\tilde{\mathbf{x}} \int \boldsymbol{\xi} f_{\mathbf{x}|\mathbf{z}}(\boldsymbol{\xi}|\mathbf{z}_0) d\boldsymbol{\xi} + \tilde{\mathbf{x}}^T \tilde{\mathbf{x}} \tag{C.10}$$

Then a Lagrangian can be formed

$$L = \mathbb{E}\left\{\|\mathbf{x} - \tilde{\mathbf{x}}\|^2 | \mathbf{z} = \mathbf{z}_0\right\} + 2\boldsymbol{\lambda}^T(\mathbf{D}\tilde{\mathbf{x}} - \mathbf{d}) \tag{C.11}$$

$$= \int \boldsymbol{\xi}^T \boldsymbol{\xi} f_{\mathbf{x}|\mathbf{z}}(\boldsymbol{\xi}|\mathbf{z}_0) d\boldsymbol{\xi} - 2\tilde{\mathbf{x}} \int \boldsymbol{\xi} f_{\mathbf{x}|\mathbf{z}}(\boldsymbol{\xi}|\mathbf{z}_0) d\boldsymbol{\xi} + \tilde{\mathbf{x}}^T \tilde{\mathbf{x}} + 2\boldsymbol{\lambda}^T(\mathbf{D}\tilde{\mathbf{x}} - \mathbf{d}) \tag{C.12}$$

Assume that the Gaussian assumption holds for the unconstrained state estimate obtained from Kalman filter $\hat{\mathbf{x}}$, then

$$\hat{\mathbf{x}} = \mathbb{E}\left\{\mathbf{x} | \mathbf{z} = \mathbf{z}_0\right\} = \int \boldsymbol{\xi} f_{\mathbf{x}|\mathbf{z}}(\boldsymbol{\xi}|\mathbf{z}_0) d\boldsymbol{\xi} \tag{C.13}$$

Let the partial derivatives of the Lagrangian with respect to $\tilde{\mathbf{x}}$ and $\boldsymbol{\lambda}$ be equal to zero and solve them simultaneously.

$$\frac{\partial L}{\partial \tilde{\mathbf{x}}} = -2\hat{\mathbf{x}} + 2\tilde{\mathbf{x}} + 2\mathbf{D}^T\boldsymbol{\lambda} = \mathbf{0} \tag{C.14}$$

$$\frac{\partial L}{\partial \boldsymbol{\lambda}} = \mathbf{D}\tilde{\mathbf{x}} - \mathbf{d} = \mathbf{0} \tag{C.15}$$

Solving them gives

$$\boldsymbol{\lambda} = (\mathbf{D}\mathbf{D}^T)^{-1}(\mathbf{D}\bar{\mathbf{x}} - \mathbf{d}) \tag{C.16}$$

$$\tilde{\mathbf{x}} = \hat{\mathbf{x}} - \mathbf{D}^T(\mathbf{D}\mathbf{D}^T)^{-1}(\mathbf{D}\hat{\mathbf{x}} - \mathbf{d}) \tag{C.17}$$

C.3 Constrained Estimate in Terms of the Unconstrained Estimate Using Pseudo-measurement Approach

We would like to write the constrained estimate obtained by pseudomeasurement approach in terms of the unconstrained estimate. The system is

$$\mathbf{x}(k+1) = \mathbf{f}\big[\mathbf{x}(k)\big] + \mathbf{w}(k) \tag{C.18}$$
$$\mathbf{z}(k) = \mathbf{h}\big[\mathbf{x}(k)\big] + \mathbf{v}(k) \tag{C.19}$$

where the process noise $\mathbf{w}(k)$ and the measurement noise $\mathbf{v}(k)$ are assumed to be zero-mean white Gaussian noises.

$$\mathbf{w}(k) \sim \mathcal{N}\big(\mathbf{0}, \mathbf{Q}(k)\big) \tag{C.20}$$
$$\mathbf{v}(k) \sim \mathcal{N}\big(\mathbf{0}, \mathbf{R}(k)\big) \tag{C.21}$$

Then the unconstrained estimate using EKF is

Prediction:

$$\hat{\mathbf{x}}^-(k+1) = \mathbf{F}(k)\hat{\mathbf{x}}^+(k) \tag{C.22}$$
$$\mathbf{P}^-(k+1) = \mathbf{F}(k)\mathbf{P}^+(k)\mathbf{F}^T(k) + \mathbf{Q}(k) \tag{C.23}$$

Correction:

$$\mathbf{K}(k+1) = \mathbf{P}^-(k+1)\mathbf{H}^T(k+1) \cdot\big[\mathbf{H}(k+1)\mathbf{P}^-(k+1)\mathbf{H}^T(k+1) + \mathbf{R}(k+1)\big]^{-1} \tag{C.24}$$
$$\mathbf{r}(k+1) = \mathbf{z}(k+1) - \mathbf{h}\big[\hat{\mathbf{x}}^-(k+1)\big] \tag{C.25}$$
$$\hat{\mathbf{x}}^+(k+1) = \hat{\mathbf{x}}^-(k+1) + \mathbf{K}(k+1)\mathbf{r}(k+1) \tag{C.26}$$
$$\mathbf{P}^+(k+1) = \mathbf{P}^-(k+1) - \mathbf{K}(k+1)\mathbf{H}(k+1)\mathbf{P}^-(k+1) \tag{C.27}$$

Now suppose that the system has constraints on the state estimate, the augmented system by constraints can be written as

$$\mathbf{x}(k+1) = \mathbf{f}\big[\mathbf{x}(k)\big] + \mathbf{w}(k) \tag{C.28}$$
$$\mathbf{z}_a(k) = \mathbf{h}_a\big[\mathbf{x}(k)\big] + \mathbf{v}_a(k) \tag{C.29}$$

where $\mathbf{z}_a(k) = \begin{bmatrix}\mathbf{z}(k)^T & \mathbf{z}_c(k)^T\end{bmatrix}^T$, $\mathbf{h}_a[\mathbf{x}(k)] = \begin{bmatrix}\mathbf{h}\big[\mathbf{x}(k)\big]^T & \big[\mathbf{H}_c\mathbf{x}(k)\big]^T\end{bmatrix}^T$, and $\mathbf{v}_a(k) = \begin{bmatrix}\mathbf{v}(k)^T & \mathbf{v}_c(k)^T\end{bmatrix}^T$. The state transition function (Eq. C.28) is the

same as the system without constraints (Eq. C.18). Assume that the uncertainty of constraints is also a zero-mean white Gaussian noise, the augmented measurement noise is

$$\mathbf{v}_c(k) \sim \mathcal{N}\big(\mathbf{0}, \mathbf{R}_c(k)\big) \tag{C.30}$$
$$\mathbf{v}_a(k) \sim \mathcal{N}\big(\mathbf{0}, \mathbf{R}_a(k)\big) \tag{C.31}$$
$$\mathbf{R}_a(k) = \text{diag}\left[\mathbf{R}(k), \mathbf{R}_c(k)\right] \tag{C.32}$$

Thus the corresponding EKF equations are

Prediction:

$$\hat{\mathbf{x}}_a^-(k+1) = \mathbf{F}(k)\hat{\mathbf{x}}_a^+(k) \tag{C.33}$$
$$\mathbf{P}_a^-(k+1) = \mathbf{F}(k)\mathbf{P}_a^+(k)\mathbf{F}^T(k) + \mathbf{Q}(k) \tag{C.34}$$

Correction:

$$\mathbf{K}_a(k+1) = \mathbf{P}^-(k+1)\mathbf{H}_a^T(k+1) \cdot\Big[\mathbf{H}_a(k+1)\mathbf{P}^-(k+1)\mathbf{H}_a^T(k+1) + \mathbf{R}_a(k+1)\Big]^{-1} \tag{C.35}$$
$$\mathbf{r}_a(k+1) = \mathbf{z}_a(k+1) - \mathbf{h}_a\big[\hat{\mathbf{x}}^-(k+1)\big] \tag{C.36}$$
$$\hat{\mathbf{x}}_a^+(k+1) = \hat{\mathbf{x}}^-(k+1) + \mathbf{K}_a(k+1)\mathbf{r}_a(k+1) \tag{C.37}$$
$$\mathbf{P}_a^+(k+1) = \mathbf{P}^-(k+1) - \mathbf{K}_a(k+1)\mathbf{H}_a(k+1)\mathbf{P}^-(k+1) \tag{C.38}$$

If we start with a same previous estimate $\mathbf{x}_a^+(k) = \mathbf{x}^+(k)$ and error covariance matrix $\mathbf{P}_a^+(k) = \mathbf{P}^+(k)$ for both constrained and unconstrained system. Comparing Eq. (C.33) and Eq. (C.22), the predicted state estimate are the same.

$$\mathbf{x}_a^-(k+1) = \mathbf{x}^-(k+1) \tag{C.39}$$
$$\mathbf{P}_a^-(k+1) = \mathbf{P}^-(k+1) \tag{C.40}$$

Now we rewrite the correction part for the constrained system. Since the following derivation is all from step $(k+1)^-$ to $(k+1)^+$, we delete the time index for simplicity. The measurement residual is

$$\mathbf{r}_a = \begin{bmatrix} \mathbf{z} - \mathbf{h}[\hat{\mathbf{x}}^-] \\ \mathbf{z}_c - \mathbf{H}_c\hat{\mathbf{x}}^- \end{bmatrix} = \begin{bmatrix} \mathbf{r} \\ \mathbf{z}_c - \mathbf{H}_c\hat{\mathbf{x}}^- \end{bmatrix} \tag{C.41}$$

Let $\mathbf{S} = \mathbf{H}\mathbf{P}^-\mathbf{H}^T + \mathbf{R}$ represent the measurement residual covariance matrix, then the constrained measurement residual covariance matrix can be written

as

$$\mathbf{S}_a = \mathbf{H}_a\mathbf{P}^-\mathbf{H}_a^T + \mathbf{R}_a \tag{C.42}$$

$$= \begin{bmatrix}\mathbf{H}\\ \mathbf{H}_c\end{bmatrix}\mathbf{P}^-\begin{bmatrix}\mathbf{H} & \mathbf{H}_c\end{bmatrix} + \begin{bmatrix}\mathbf{R} & 0\\ 0 & \mathbf{R}_c\end{bmatrix} \tag{C.43}$$

$$= \begin{bmatrix}\mathbf{H}\mathbf{P}^-\mathbf{H}^T + \mathbf{R} & \mathbf{H}\mathbf{P}^-\mathbf{H}_c^T\\ \mathbf{H}_c\mathbf{P}^-\mathbf{H}^T & \mathbf{H}_c\mathbf{P}^-\mathbf{H}_c^T + \mathbf{R}_c\end{bmatrix} \tag{C.44}$$

$$= \begin{bmatrix}\mathbf{S} & \mathbf{H}\mathbf{P}^-\mathbf{H}_c^T\\ \mathbf{H}_c\mathbf{P}^-\mathbf{H}^T & \mathbf{H}_c\mathbf{P}^-\mathbf{H}_c^T + \mathbf{R}_c\end{bmatrix} \tag{C.45}$$

In order to obtain the inverse matrix of $\mathbf{S}_a(k+1)$, we denote it in a block matrix form

$$(\mathbf{S}_a)^{-1} = \begin{bmatrix}(\mathbf{S}_a)_a^{-1} & (\mathbf{S}_a)_b^{-1}\\ (\mathbf{S}_a)_c^{-1} & (\mathbf{S}_a)_d^{-1}\end{bmatrix} \tag{C.46}$$

Follow Appendix A.2,

$$\begin{aligned}(\mathbf{S}_a)_a^{-1} = \mathbf{S}^{-1} &+ \mathbf{S}^{-1}\mathbf{H}\mathbf{P}^-\mathbf{H}_c^T\\ &\cdot(\underbrace{\mathbf{H}_c\mathbf{P}^-\mathbf{H}_c^T + \mathbf{R}_c - \mathbf{H}_c\mathbf{P}^-\mathbf{H}^T\mathbf{S}^{-1}\mathbf{H}\mathbf{P}^-\mathbf{H}_c^T}_{\mathbf{J}})^{-1}\\ &\cdot\mathbf{H}_c\mathbf{P}^-\mathbf{H}^T\mathbf{S}^{-1}\end{aligned} \tag{C.47}$$

where

$$\mathbf{J} = \mathbf{H}_c\mathbf{P}^-\mathbf{H}_c^T + \mathbf{R}_c - \mathbf{H}_c\mathbf{P}^-\mathbf{H}^T\mathbf{S}^{-1}\mathbf{H}\mathbf{P}^-\mathbf{H}_c^T \tag{C.48}$$

$$= \mathbf{H}_c\mathbf{P}^-\mathbf{H}_c^T + \mathbf{R}_c - \mathbf{H}_c\mathbf{K}\mathbf{H}\mathbf{P}^-\mathbf{H}_c^T \tag{C.49}$$

$$= \mathbf{H}_c(\mathbf{I} - \mathbf{K}\mathbf{H})\mathbf{P}^-\mathbf{H}_c^T + \mathbf{R}_c \tag{C.50}$$

$$= \mathbf{H}_c\mathbf{P}^+\mathbf{H}_c^T + \mathbf{R}_c \tag{C.51}$$

Therefore,

$$\begin{aligned}(\mathbf{S}_a)_a^{-1} &= \mathbf{S}^{-1} + (\mathbf{P}^-\mathbf{H}^T\mathbf{S}^{-1})^T\mathbf{H}_c^T(\mathbf{H}_c\mathbf{P}^+\mathbf{H}_c^T + \mathbf{R}_c)^{-1}\\ &\quad\cdot\mathbf{H}_c\mathbf{P}^-\mathbf{H}^T\mathbf{S}^{-1} &\text{(C.52)}\\ &= \mathbf{S}^{-1} + \mathbf{K}^T\mathbf{H}_c^T(\mathbf{H}_c\mathbf{P}^+\mathbf{H}_c^T + \mathbf{R}_c)^{-1}\mathbf{H}_c\mathbf{K} &\text{(C.53)}\end{aligned}$$

Similarly,

$$(\mathbf{S}_a)_b^{-1} = -\mathbf{S}^{-1}\mathbf{H}\mathbf{P}^-\mathbf{H}_c^T(\underbrace{\mathbf{H}_c\mathbf{P}^-\mathbf{H}_c^T + \mathbf{R}_c - \mathbf{H}_c\mathbf{P}^-\mathbf{H}^T\mathbf{S}^{-1}\mathbf{H}\mathbf{P}^-\mathbf{H}_c^T}_{\mathbf{J}})^{-1} \tag{C.54}$$

$$= -\mathbf{S}^{-1}\mathbf{H}\mathbf{P}^-\mathbf{H}_c^T(\mathbf{H}_c\mathbf{P}^+\mathbf{H}_c^T + \mathbf{R}_c)^{-1} \tag{C.55}$$

$$= -\mathbf{K}^T\mathbf{H}_c^T(\mathbf{H}_c\mathbf{P}^+\mathbf{H}_c^T + \mathbf{R}_c)^{-1} \tag{C.56}$$

$$(\mathbf{S}_a)_c^{-1} = -(\underbrace{\mathbf{H}_c\mathbf{P}^-\mathbf{H}_c^T + \mathbf{R}_c - \mathbf{H}_c\mathbf{P}^-\mathbf{H}^T\mathbf{S}^{-1}\mathbf{H}\mathbf{P}^-\mathbf{H}_c^T}_{\mathbf{J}})^{-1}\mathbf{H}_c\mathbf{P}^-\mathbf{H}^T\mathbf{S}^{-1} \tag{C.57}$$

$$= -(\mathbf{H}_c\mathbf{P}^+\mathbf{H}_c^T + \mathbf{R}_c)^{-1}\mathbf{H}_c\mathbf{K} \tag{C.58}$$

$$(\mathbf{S}_a)_d^{-1} = (\underbrace{\mathbf{H}_c\mathbf{P}^-\mathbf{H}_c^T + \mathbf{R}_c - \mathbf{H}_c\mathbf{P}^-\mathbf{H}^T\mathbf{S}^{-1}\mathbf{H}\mathbf{P}^-\mathbf{H}_c^T}_{\mathbf{J}})^{-1} \tag{C.59}$$

$$= (\mathbf{H}_c\mathbf{P}^+\mathbf{H}_c^T + \mathbf{R}_c)^{-1} \tag{C.60}$$

After obtaining the measurement residual covariance matrix, we can derive the Kalman gain.

$$\mathbf{K}_a = \mathbf{P}^- \begin{bmatrix}\mathbf{H}^T & \mathbf{H}_c^T\end{bmatrix} \begin{bmatrix}(\mathbf{S}_a)_a^{-1} & (\mathbf{S}_a)_b^{-1} \\ (\mathbf{S}_a)_c^{-1} & (\mathbf{S}_a)_d^{-1}\end{bmatrix} \tag{C.61}$$

$$= \begin{bmatrix}\underbrace{\mathbf{P}^-\mathbf{H}^T(\mathbf{S}_a)_a^{-1} + \mathbf{P}^-\mathbf{H}_c^T(\mathbf{S}_a)_c^{-1}}_{(\mathbf{K}_a)_a} \\ \underbrace{\mathbf{P}^-\mathbf{H}^T(\mathbf{S}_a)_b^{-1} + \mathbf{P}^-\mathbf{H}_c^T(\mathbf{S}_a)_d^{-1}}_{(\mathbf{K}_a)_b}\end{bmatrix}^T \tag{C.62}$$

$$\begin{aligned}(\mathbf{K}_a)_a = \mathbf{P}^-\mathbf{H}^T\big[&\mathbf{S}^{-1} + \mathbf{K}^T\mathbf{H}_c^T(\mathbf{H}_c\mathbf{P}^+\mathbf{H}_c^T + \mathbf{R}_c)^{-1}\mathbf{H}_c\mathbf{K}\big] \\ &-\mathbf{P}^-\mathbf{H}_c^T(\mathbf{H}_c\mathbf{P}^+\mathbf{H}_c^T + \mathbf{R}_c)^{-1}\mathbf{H}_c\mathbf{K} \qquad \text{(C.63)} \\ = \mathbf{K} &+ (\mathbf{P}^-\mathbf{H}^T\mathbf{K}^T - \mathbf{P}^-)\mathbf{H}_c^T(\mathbf{H}_c\mathbf{P}^+\mathbf{H}_c^T + \mathbf{R}_c)^{-1}\mathbf{H}_c\mathbf{K} \qquad \text{(C.64)} \\ = \mathbf{K} &- \mathbf{P}^+\mathbf{H}_c^T(\mathbf{H}_c\mathbf{P}^+\mathbf{H}_c^T + \mathbf{R}_c)^{-1}\mathbf{H}_c\mathbf{K} \qquad \text{(C.65)}\end{aligned}$$

$$\begin{aligned}(\mathbf{K}_a)_b = &-\mathbf{P}^-\mathbf{H}^T\mathbf{K}^T\mathbf{H}_c^T(\mathbf{H}_c\mathbf{P}^+\mathbf{H}_c^T + \mathbf{R}_c)^{-1} \\ &+\mathbf{P}^-\mathbf{H}_c^T(\mathbf{H}_c\mathbf{P}^+\mathbf{H}_c^T + \mathbf{R}_c)^{-1} \qquad \text{(C.66)} \\ = &(-\mathbf{P}^-\mathbf{H}^T\mathbf{K}^T + \mathbf{P}^-)\mathbf{H}_c^T(\mathbf{H}_c\mathbf{P}^+\mathbf{H}_c^T + \mathbf{R}_c)^{-1} \qquad \text{(C.67)} \\ = &\mathbf{P}^+\mathbf{H}_c^T(\mathbf{H}_c\mathbf{P}^+\mathbf{H}_c^T + \mathbf{R}_c)^{-1} \qquad \text{(C.68)}\end{aligned}$$

Then the constrained state estimate is

$$\hat{\mathbf{x}}_a^+ = \hat{\mathbf{x}}_a^- + \begin{bmatrix}(\mathbf{K}_a)_a & (\mathbf{K}_a)_b\end{bmatrix} \begin{bmatrix}\mathbf{r} \\ \mathbf{r}_c\end{bmatrix} \tag{C.69}$$

$$= \hat{\mathbf{x}}^- + \big[\mathbf{K} - \mathbf{P}^+\mathbf{H}_c^T(\mathbf{H}_c\mathbf{P}^+\mathbf{H}_c^T + \mathbf{R}_c)^{-1}\mathbf{H}_c\mathbf{K}\big]\mathbf{r} + \mathbf{P}^+\mathbf{H}_c^T(\mathbf{H}_c\mathbf{P}^+\mathbf{H}_c^T + \mathbf{R}_c)^{-1}\mathbf{r}_c \tag{C.70}$$

$$= \hat{\mathbf{x}}^- + \mathbf{K}\mathbf{r} - \mathbf{P}^+\mathbf{H}_c^T(\mathbf{H}_c\mathbf{P}^+\mathbf{H}_c^T + \mathbf{R}_c)^{-1}\mathbf{H}_c\mathbf{K}\mathbf{r} + \mathbf{P}^+\mathbf{H}_c^T(\mathbf{H}_c\mathbf{P}^+\mathbf{H}_c^T + \mathbf{R}_c)^{-1}\mathbf{r}_c \tag{C.71}$$

$$= \hat{\mathbf{x}}^+ - \mathbf{P}^+\mathbf{H}_c^T(\mathbf{H}_c\mathbf{P}^+\mathbf{H}_c^T + \mathbf{R}_c)^{-1}\mathbf{H}_c(\hat{\mathbf{x}}^+ - \hat{\mathbf{x}}^-) + \mathbf{P}^+\mathbf{H}_c^T(\mathbf{H}_c\mathbf{P}^+\mathbf{H}_c^T + \mathbf{R}_c)^{-1}(\mathbf{z}_c - \mathbf{H}_c\hat{\mathbf{x}}^-) \tag{C.72}$$

$$= \hat{\mathbf{x}}^+ - \mathbf{P}^+\mathbf{H}_c^T(\mathbf{H}_c\mathbf{P}^+\mathbf{H}_c^T + \mathbf{R}_c)^{-1}(\mathbf{H}_c\hat{\mathbf{x}}^+ - \mathbf{z}_c) \tag{C.73}$$

The error covariance matrix of the constrained state estimate is

$$\mathbf{P}_a = \left(\mathbf{I} - \begin{bmatrix}(\mathbf{K}_a)_a & (\mathbf{K}_a)_b\end{bmatrix} \begin{bmatrix}\mathbf{H} \\ \mathbf{H}_c\end{bmatrix}\right)\mathbf{P}^- \tag{C.74}$$

$$= \big[\mathbf{I} - (\mathbf{K}_a)_a\mathbf{H} - (\mathbf{K}_a)_b\mathbf{H}_c\big]\mathbf{P}^- \tag{C.75}$$

$$= \big[\mathbf{I} - \mathbf{K}\mathbf{H} + \mathbf{P}^+\mathbf{H}_c^T(\mathbf{H}_c\mathbf{P}^+\mathbf{H}_c^T + \mathbf{R}_c)^{-1}\mathbf{H}_c\mathbf{K}\mathbf{H} - \mathbf{P}^+\mathbf{H}_c^T(\mathbf{H}_c\mathbf{P}^+\mathbf{H}_c^T + \mathbf{R}_c)^{-1}\mathbf{H}_c\big]\mathbf{P}^- \tag{C.76}$$

$$= (\mathbf{I} - \mathbf{K}\mathbf{H})\mathbf{P}^- - \mathbf{P}^+\mathbf{H}_c^T(\mathbf{H}_c\mathbf{P}^+\mathbf{H}_c^T + \mathbf{R}_c)^{-1}\mathbf{H}_c(\mathbf{I} - \mathbf{K}\mathbf{H})\mathbf{P}^- \tag{C.77}$$

$$= \mathbf{P}^+ - \mathbf{P}^+\mathbf{H}_c^T(\mathbf{H}_c\mathbf{P}^+\mathbf{H}_c^T + \mathbf{R}_c)^{-1}\mathbf{H}_c\mathbf{P}^+ \tag{C.78}$$

Bibliography

[1] FCC, "Third report and order," FCC 99-245, Oct. 1999.

[2] ——, "FCC amended report to congress on the development of E-911 phase II services by tier III service providers," www.fcc.gov/911/enhanced/, Apr. 2005.

[3] Coordinate Group on Access to Location Information by Emergency Services (CGALIES), "Report on implementation issues related to access to location information by emergency services (E112) in the European Union," www.telematica.de/cgalies, Feb. 2002.

[4] T. S. Rappaport, J. H. Reed, and B. D. Woerner, "Position location using wireless communications on highways of the future," *IEEE Communications Magazine*, vol. 34, no. 10, pp. 33–41, Oct. 1996.

[5] J. H. Reed, K. J. Krizman, B. D. Woerner, and T. S. Rappaport, "An overview of the challenges and progress in meeting the E-911 requirement for location service," *IEEE Communications Magazine*, vol. 36, no. 4, pp. 30–37, Apr. 1998.

[6] M. Vossiek, L. Wiebking, P. Gulden, J. Wieghardt, C. Hoffmann, and P. Heide, "Wireless local positioning," *IEEE Microwave Magazine*, vol. 4, no. 4, pp. 77–86, Dec. 2003.

[7] F. Gustafsson and F. Gunnarsson, "Mobile positioning using wireless networks: Possibilities and fundamental limitations based on available wireless network measurements," *IEEE Signal Processing Magazine*, vol. 22, no. 4, pp. 41–53, Jul. 2005.

[8] A. H. Sayed, A. Tarighat, and N. Khajehnouri, "Network-based wireless location: Challenges faced in developing techniques for accurate wireless location information," *IEEE Signal Processing Magazine*, vol. 22, no. 4, pp. 24–40, Jul. 2005.

[9] G. Sun, J. Chen, W. Guo, and K. J. R. Liu, "Signal processing techniques in network-aided positioning: A survey of state-of-the-art positioning designs," *IEEE Signal Processing Magazine*, vol. 22, no. 4, pp. 12–23, Jul. 2005.

[10] S. Gezici, "A survey on wireless position estimation," *Wireless Personal Communications, Springer Netherlands*, vol. 44, no. 3, pp. 263–282, Feb. 2008.

[11] V. Schwieger, "Positioning within the GSM network," in *Proc. of the 6th FIG Regional Conference*, San Jose, Costa Rica, Nov. 2007.

[12] J. J. Caffery and G. L. Stüber, "Overview of radiolocation in CDMA cellular systems," *IEEE Communications Magazine*, vol. 36, no. 4, pp. 38–45, Apr. 1998.

[13] J. J. Caffery, *Wireless Location in CDMA Cellular Radio Systems*. Kluwer Academic Publishers, 2000.

[14] C. Drane, M. Macnaughtan, and C. Scott, "Positioning GSM telephones," *IEEE Communications Magazine*, vol. 36, no. 4, pp. 46–54,59, Apr. 1998.

[15] Y. Zhao, "Standardization of mobile phone positioning for 3G systems," *IEEE Communications Magazine*, vol. 40, no. 7, pp. 108–116, Jul. 2002.

[16] SnapTrack, QUALCOMM, "Location technologies for GSM, GPRS, UMTS networks," White Paper, 2003.

[17] K. A. Grajski and E. Kirk, "Towards a mobile multimedia age - location-based services: A case study," *Wireless Personal Communications, Springer Netherlands*, vol. 26, no. 2-3, pp. 105–116, Sep. 2003.

[18] M. I. Silventoinen and T. Rantalainen, "Mobile station emergency locating in GSM," in *Proc. of IEEE International Conference on Personal Wireless Communications*, New Delhi, India, Feb. 1996, pp. 232–238.

[19] M. A. Spirito, S. Pöykkö, and O. Knuuttila, "Experimental performance of methods to estimate the location of legacy handsets in GSM," in *Proc. of 2001 IEEE 54th Vehicular Technology Conference: VTC2001-Fall*, Atlantic City, NJ, USA, Oct. 2001, pp. 2716–2720.

[20] J. Caffery and G. L. Stüber, "Subscriber location in CDMA cellular networks," *IEEE Transactions on Vehicular Technology*, vol. 47, no. 2, pp. 406–416, May 1998.

[21] M. Pent, M. A. Spirito, and E. Turco, "Method for positioning GSM mobile stations using absolute time delay measurements," *Electronics Letters*, vol. 33, no. 22, pp. 2019–2020, Nov. 1997.

[22] M. A. Spirito and A. G. Mattioli, "Preliminary experimental results of a GSM mobile phones positioning system based on timing advance," in *Proc. of 1999 IEEE 50th Vehicular Technology Conference: VTC1999-Fall*, Amersterdam, the Netherlands, Sep. 1999, pp. 2072–2076.

[23] K. W. Cheung, H. C. So, W. K. Ma, and Y. T. Chan, "Least squares algorithms for time-of-arrival-based mobile location," *IEEE Transactions on Signal Processing*, vol. 52, no. 4, pp. 1121–1128, Apr. 2004.

[24] M. A. Spirito and A. G. Mattioli, "On the hyperbolic positioning of GSM mobile stations," in *Proc. of 1998 URSI International Symposium on Signals, Systems, and Electronics (ISSSE'98)*, Pisa, Italy, Sep. 1998, pp. 173–177.

[25] M. A. Spirito, "Further results on GSM mobile station location," *Electronics Letters*, vol. 35, no. 11, pp. 867–869, May 1999.

[26] M. McGuire, K. N. Plataniotis, and A. N. Venetsanopoulos, "Estimating position of mobile terminals from path loss measurements with survey data," *Wireless Communications and Mobile Computing*, vol. 3, no. 1, pp. 51–62, Aug. 2002.

[27] ——, "Location of mobile terminals using time measurements and survey points," *IEEE Transactions on Vehicular Technology*, vol. 52, no. 4, pp. 999–1011, Jul. 2003.

[28] M. Hellebrandt, R. Mathar, and M. Scheibenbogen, "Estimating position and velocity of mobiles in a cellular radio network," *IEEE Transactions on Vehicular Technology*, vol. 46, no. 1, pp. 65–71, Feb. 1997.

[29] M. Hellebrandt and R. Mathar, "Location tracking of mobiles in cellular radio networks," *IEEE Transactions on Vehicular Technology*, vol. 48, no. 5, pp. 1558–1562, Sep. 1999.

[30] D.-B. Lin and R.-T. Juang, "Mobile location estimation based on differences of signal attenuations for GSM systems," *IEEE Transactions on Vehicular Technology*, vol. 54, no. 4, pp. 1447–1453, Jul. 2005.

[31] T. Kleine-Ostmann and A. E. Bell, "A data fusion architecture for enhanced position estimation in wireless networks," *IEEE Communications Letter*, vol. 5, no. 8, pp. 343–345, Aug. 2001.

[32] M. McGuire, K. N. Plataniotis, and A. N. Venetsanopoulos, "Data fusion of power and time measurements for mobile terminal location," *IEEE Transactions on Mobile Computing*, vol. 4, no. 2, pp. 142–153, Mar. 2005.

[33] L. Cong and W. Zhuang, "Hybrid TDOA/AOA mobile user location for wideband CDMA cellular systems," *IEEE Transactions on Wireless Communications*, vol. 1, no. 3, pp. 439–447, Jul. 2002.

[34] N. J. Thomas, D. G. M. Cruickshank, and D. I. Laurenson, "Performance of a TDOA-AOA hybrid mobile location system," in *Proc. of 3G Mobile Communication Technologies*, London, UK, Mar. 2001, pp. 216–220.

[35] M. A. Spirito, "Mobile station locatoin with heterogeneous data," in *Proc. of 2000 IEEE 52nd Vehicular Technology Conference: VTC2000-Fall*, Boston, MA, Sep. 2000, pp. 1583–1589.

[36] R.-T. Juang, D.-B. Lin, and H.-P. Lin, "Hybrid SADOA/TDOA location estimation scheme for wireless communication systems," in *Proc. of 2006 IEEE 63rd Vehicular Technology Conference: VTC2006-Spring*, Melbourne, Australia, May 2006, pp. 1053–1057.

[37] W. Pan, J. Wu, Z. Jiang, Y. Wang, and X. You, "Mobile position tracking by TDOA-Doppler hybrid estimation in mobile cellular system," in *Proc. of the IEEE International Conference on Communications (ICC) 2007*, Glasgow, Scotland, Jun. 2007, pp. 4670–4673.

[38] D. Catrein, M. Hellebrandt, R. Mathar, and M. P. Serrano, "Location tracking of mobiles: A smart filtering method and its use in practice," in *Proc. of 2004 IEEE 59th Vehicular Technology Conference: VTC2004-Spring*, Milan, Italy, May 2004, pp. 2677–2681.

[39] M. McGuire and K. N. Plataniotis, "Dynamic model-based filtering for mobile terminal location estimation," *IEEE Transactions on Vehicular Technology*, vol. 52, no. 4, pp. 1012–1031, Jul. 2003.

[40] Z. R. Zaidi and B. L. Mark, "Real-time mobility tracking algorithms for cellular network based on Kalman filtering," *IEEE Transactions on Mobile Computing*, vol. 4, no. 2, pp. 195–208, Mar. 2005.

[41] T. S. Rappaport, *Wireless Communications: Principles and Practice*. Prentice-Hall PTR, 1996.

[42] G. L. Stüber, *Principles of Mobile Communication*. Kluwer Academic Publishers, 1996.

[43] A. U. Planas, "Signal processing techniques for wireless locationing," Ph.D. dissertation, Technical University of Catalonia, Barcelona, Spain, 2006.

[44] Y. Qi, "Wireless geolocation in a non-line-of-sight environment," Ph.D. dissertation, Princeton University, US, 2003.

[45] M. A. Spirito, "On the accuracy of cellular mobile station location estimation," *IEEE Transactions on Vehicular Technology*, vol. 50, no. 3, pp. 674–685, May 2001.

[46] Y. Qi, H. Kobayashi, and H. Suda, "Analysis of wireless geolocation in a non-line-of-sight environment," *IEEE Transactions on Wireless Communications*, vol. 5, no. 3, pp. 672–681, Mar. 2006.

[47] ETSI-European Telecommunication Standard Institute, "European digital telecommunications system (phase 2); radio subsystem synchronization (GSM 05.10)," ETSI TC-SMG, Sep. 1995.

[48] C. Botteron, A. Host-Madsen, and M. Fattouche, "Effects of system and environment parameters on the performance of network-based mobile station position estimators," *IEEE Transactions on Vehicular Technology*, vol. 53, no. 1, pp. 163–180, Jan. 2004.

[49] A. Urruela, J. Sala, and J. Riba, "Average performance analysis of circular and hyperbolic geolocation," *IEEE Transactions on Vehicular Technology*, vol. 55, no. 1, pp. 52–66, Jan. 2006.

[50] F. Cesbron and R. Arnott, "Locating GSM mobiles using antenna array," *Electronics Letters*, vol. 34, no. 16, pp. 1539–1540, Aug. 1998.

[51] COST 231, "Digital mobile radio towards future generation systems," COST 231 Final Report, 1999.

[52] ETSI-European Telecommunication Standard Institute, "Digital cellular telecommunications system (phase 2+); radio network planning aspects (3GPP TR 43.030 version 5.0.0 release 5)," Jun. 2002.

[53] Y. Qi, H. Kobayashi, and H. Suda, "On time-of-arrival positioning in a multipath environment," *IEEE Transactions on Vehicular Technology*, vol. 55, no. 5, pp. 1516–1526, Sep. 2006.

[54] E. R. Játiva and J. Vidal, "First arrival detection for positioning in mobile channels," in *Proc. of 13th IEEE International Symposium on Personal, Indoor and Mobile Radio Communications (PIMRC)*, vol. 4, Sep. 2002, pp. 1540–1544.

[55] C. Botteron, A. Host-Madsen, and M. Fattouche, "Cramér-Rao bounds for the estimation of multipath parameters and mobiles' positions in asynchronous DS-CDMA systems," *IEEE Transactions on Signal Processing*, vol. 52, no. 4, pp. 862–874, Apr. 2004.

[56] H. Koorapaty, H. Grubeck, and M. Cedervall, "Effect of biased measurement errors on accuracy of position location methods," in *Proc. of Global Telecommunications Conference 1998 (GLOBECOM 98)*, Sydney, Australia, Nov. 1998, pp. 1497–1502.

[57] L. Cong and W. Zhuang, "Nonline-of sight error mitigation in mobile location," *IEEE Transactions on Wireless Communications*, vol. 4, no. 2, pp. 560–573, Mar. 2005.

[58] M. P. Wylie and J. Holtzman, "The non-line of sight problem in mobile location estimation," in *Proc. of IEEE International Conference on Universal Personal Communications*, Cambridge, MA, Sep. 1996, pp. 827–831.

[59] S. Al-Jazzar, J. Caffery, and H.-R. You, "Scattering-model-based methods for TOA location in NLOS environments," *IEEE Transactions on Vehicular Technology*, vol. 56, no. 2, pp. 583–593, Mar. 2007.

[60] M. P. Wylie-Green and S. S. Wang, "Robust range estimation in the presence of the non-line-of-sight error," in *Proc. of 2001 IEEE 54th Vehicular Technology Conference: VTC2001-Fall*, Atlantic City, USA, Oct. 2001, pp. 101–105.

[61] H. Miao, K. Yu, and M. J. Juntti, "Positioning for NLOS propagation: Algorithm derivations and Cramér-Rao bounds," *IEEE Transactions on Vehicular Technology*, vol. 56, no. 5, pp. 2568–2580, Sep. 2007.

[62] N. J. Thomas, "Techniques for mobile location estimation in UMTS," Ph.D. dissertation, The University of Edinburgh, 2001.

[63] K. Ramm, R. Czommer, and V. Schwieger, "Map-based positioning using mobile phones," in *Proc. on XXIII International FIG Congress*, Munich, Germany, Oct. 2006.

[64] S. M. Kay, *Fundamentals of Statistical Signal Processing: Estimation Theory*. Prentice-Hall, Inc., 1993.

[65] Y. Bar-Shalom, X. R. Li, and T. Kirubarajan, *Estimation with Applications to Tracking and Navigation*. John Wiley & Sons, Inc., 2001.

[66] N. Bergman, "Recursive bayesian estimation: Navigation and tracking applications," Ph.D. dissertation, Linkoping University, Sweden, 1999.

[67] S. Tekinay, E. Chao, and R. Richton, "Performance benchmarking for wireless location systems," *IEEE Communications Magazine*, vol. 36, no. 4, pp. 72–76, Apr. 1998.

[68] FCC, "Guidelines for testing and verifying the accuracy of wireless E911 location systems," OET BULLETIN No. 71, Apr. 2000.

[69] C.-Y. Chong, D. Garren, and T. P. Grayson, "Ground target tracking-a historical perspective," in *Proc. of IEEE Aerospace Conference*, vol. 3, Big Sky, MT, USA, Mar. 2000, pp. 433–448.

[70] X. R. Li and V. P. Jilkov, "Survey of maneuvering target tracking. part I: dynamic models," *IEEE Transactions on Aerospace and Electronic Systems*, vol. 39, no. 4, pp. 1333–1364, Oct. 2003.

[71] ——, "A survey of maneuvering target tracking: dynamic models," in *Proc. of SPIE Conference on Signal and Data Processing of Small Targets*, Orlando, USA, Apr. 2000.

[72] R. R. Pitre, V. P. Jilkov, and X. R. Li, "A comparative study of multiple-model algorithms for maneuvering target tracking," in *Proc. of 2005 SPIE Conference Signal Processing, Sensor Fusion, and Target Recognition XIV*, Orlando, USA, Mar. 2005.

[73] P. Tichavský, C. H. Muravchik, and A. Nehorai, "Posterior Cramér-Rao bounds for discrete-time nonlinear filtering," *IEEE Transactions on Signal Processing*, vol. 46, no. 5, pp. 1386–1396, 1998.

[74] Y. Zhao, *Vehicle Location and Navigation Systems*. Artech House, Inc, 1997.

[75] T.Kirubarajan, Y.Bar-Shalom, K. Pattipati, and I. Kadar, "Ground target tracking with variable structure IMM estimator," *IEEE Transactions on Aerospace and Electronic Systems*, vol. 36, no. 1, pp. 26–46, Jan. 2000.

[76] C.-C. Ke, J. G. Herrero, and J. Llinas, "Comparative analysis of alternative ground target tracking techniques," in *Proc. of the 3rd International Conference on Information Fusion*, Paris, France, Jul. 2000, pp. 503–510.

[77] C. Yang, M. Bakich, and E. Blasch, "Nonlinear constrained tracking of targets on roads," in *Proc. of the 8th International Conference on Information Fusion*, Philadelphia, PA, Jul. 2005.

[78] S. J. Julier and J. J. LaViola, "On Kalman filtering with nonlinear equality constraints," *IEEE Transactions on Signal Processing*, vol. 55, no. 6, pp. 2774–2784, Jun. 2007.

[79] Y. Cui and S. S. Ge, "Autonomous vehicle positioning with GPS in urban canyon environments," *IEEE Transactions on Robotics and Automation*, vol. 19, no. 1, pp. 15–25, Feb. 2003.

[80] M. Tahk and J. L. Speyer, "Target tracking problems subject to kinematic constraints," *IEEE Transactions on Automatic Control*, vol. 35, no. 3, pp. 324–326, Mar. 1990.

[81] A. Alouani and W. Blair, "Use of a kinematic constraint in tracking constant speed, maneuvering targets," *IEEE Transactions on Automatic Control*, vol. 38, no. 7, pp. 1107–1111, Jul. 1993.

[82] J. Geeter, H. Brussel, and J. D. Schutter, "A smoothly constrained Kalman filter," *IEEE Transactions on Pattern Analysis and Machine Intelligence*, vol. 19, no. 10, pp. 1171–1177, Oct. 1997.

[83] D. Simon and T. L. Chia, "Kalman filtering with state equality constraints," *IEEE Transactions on Aerospace and Electronic Systems*, vol. 38, no. 1, pp. 128–136, Jan. 2002.

[84] T. L. Chia, D. Simon, and H. J. Chizeck, "Kalman filtering with statistical state constraints," *Control and Intelligent Systems*, vol. 34, no. 1, pp. 73–79, 2006.

[85] C. Yang and E. Blasch, "Kalman filtering with nonlinear state constraints," in *Proc. of the 9th International Conference on Information Fusion*, Florence, Italy, Jul. 2006, pp. 1–8.

[86] D. Simon, *Optimal State Estimation: Kalman HInfinity, and Nonlinear Approaches*. John Wiley & Sons, 2006.

[87] S. Ko and R. R. Bitmead, "State estimation for linear systems with state equality constraints," *Automatica*, vol. 43, no. 8, pp. 1363–1368, Aug. 2007.

[88] G. Nachi, "Kalman filtering in the presence of state space equality constraints," in *Proc. of the 26th Chinese Control Conference*, Zhangjiajie, Hunan, China, Jul. 2007, pp. 107–113.

[89] C. Yang and E. Blasch, "Fusion of tracks with road constraints," *Journal of Advances in Information Fusion*, vol. 3, no. 1, pp. 14–32, Jun. 2008.

[90] A. Bessell, A. F. B. Ristic, X. Wang, and M. Arulampalam, "Error performance bounds for tracking a maneuvering target," in *Proc. of the 6th International Conference on Information Fusion*, Cairns, Queensland, Australia, Jul. 2003, pp. 903–910.

[91] X. R. Li and V. P. Jilkov, "Survey of maneuvering target tracking. part V: multiple-model methods," *IEEE Transactions on Aerospace and Electronic Systems*, vol. 41, no. 4, pp. 1255–1320, Oct. 2005.

[92] H. A. P. Blom and Y. Bar-Shalom, "The interacting multiple model algorithm for systems with markovian switching coefficients," *IEEE Transactions on Automatic Control*, vol. 33, no. 8, pp. 780–783, Aug. 1988.

[93] I. Simeonova and T. Semerdjiev, "About the specifics of the IMM algorithm design," in *Proc. of NM&A 2002 Conference*, Borovetz, 2002, pp. 329–336.

[94] M. Zhang, S. Knedlik, and O. Loffeld, "PCRB for positioning in GSM networks," in *Proc. of 2nd Workshop Multiple Sensor Data Fusion: Trends, Solutions, Applications, INFORMATIK 2006, Band 1*, Dresden, Germany, Oct. 2006, pp. 389–393.

[95] X. R. Li and Y. Bar-Shalom, "Multiple-model estimation with variable structure," *IEEE Transactions on Automatic Control*, vol. 41, no. 4, pp. 478–493, Apr. 1996.

[96] M. S. Arulampalam, N. Gordon, M. Orton, and B. Ristic, "A variable structure multiple model particle filter for GMTI tracking," in *Proc.*

of the 5th International Conference on Information Fusion, Annapolis, MD, Jul. 2002, pp. 927–934.

[97] M. Ulmke and W. Koch, "Road-map assisted ground moving target tracking," *IEEE Transactions on Aerospace and Electronic Systems*, vol. 42, no. 4, pp. 1264–1274, Oct. 2006.

[98] B. Pannetier, K. Benameur, V. Nimier, and M. Rombaut, "VS-IMM using road map information for a ground target tracking," in *Proc. of the 8th International Conference on Information Fusion*, Philadelphia, PA, Jul. 2005, pp. 24–31.

[99] M. Zhang, S. Knedlik, P. Ubolkosold, and O. Loffeld, "A data fusion approach for improved positioning in GSM networks," in *Proc. of IEEE/ION Position, Location, And Navigation Sympoisum (PLANS) 2006*, San Diego, USA, Apr. 2006, pp. 218–222.

[100] M. Zhang, S. Knedlik, and O. Loffeld, "Performance analysis of data fusion for ground target tracking using GSM networks," in *Proc. of 2009 12th International Conference on Information Fusion*, Seattle, Washington, USA, Jul. 2009, pp. 1092–1099.

[101] ——, "Road-Constrained target tracking in GSM networks," in *Proc. of IEEE International Symposium on Wireless Communication Systems 2007*, Trondheim, Norway, Oct. 2007, pp. 138–142.

[102] ——, "On nonlinear road-constrained target tracking in GSM networks," in *Proc. of 2008 IEEE 67th Vehicular Technology Conference: VTC2008-Spring*, Singapore, May 2008, pp. 2026–2030.

[103] ——, "IMM estimator for maneuvering target tracking in GSM networks," in *Proc. of 4th Workshop on Positioning, Navigation and Communication 2007 (WPNC'07)*, Hannover, Germany, Mar. 2007, pp. 135–140.

[104] ——, "An adaptive road-constrained IMM estimator for ground target tracking in GSM networks," in *Proc. of 2008 11th International Conference on Information Fusion*, Cologne, Germany, Jul. 2008, pp. 964–971.